Development of a cognitive and decision-based model for pedestrian dynamics

INAUGURAL-DISSERTATION

zur

Erlangung des Doktorgrades

der Mathematisch-Naturwissenschaftlichen Fakultät

der Universität zu Köln

vorgelegt von

Cornelia von Krüchten

aus Köln

2019

Abstract

Research on pedestrian dynamics is always an interplay between empirical and experimental observations and theoretical modelling and simulations. Thereby, pedestrian models are not only used for theoretically reproducing empirical data, but also to better analyse and understand the mechanisms and behavioural aspects that underlie pedestrian dynamics. The model approach that is presented in this work assumes pedestrian motion to result from cognitive and decision-based processes.

The model is set in continuous space, but discrete time and therefore belongs to a model class whose potential has been rarely investigated yet. However, compared to other model classes that are widely used in pedestrian dynamics, this approach is highly advantageous considering fidelity and simplicity in its structure. A pedestrian is considered as an autonomous entity that gains information on the surrounding by visual perception and anticipation. On this basis, the agent takes a decision on its movement for the next time step.

The main focus during the development of the approach was on modelling the interaction and collision avoidance with other agents. Particularly for the collision avoidance, stochastic procedures are used in order to consider uncertainties of human decisions explicitly which makes the modelling approach more realistic.

As simulation results show, the new approach is able to reproduce characteristic effects of pedestrian motion very well. For typical scenarios that have been used as test cases the simulated results fit well, at least qualitatively but often even

quantitatively, to experimental data. Especially, important macroscopic effects, particularly collective phenomena, are observed in the results that are reproduced by modelling individual interaction of a single pedestrian with others. During the development of the model its parameters were specifically adjusted for the single scenarios, considering the empirical data basis. In addition, several cognitive mechanisms were supplemented. By this means, it is possible to identify and understand the important intrinsic properties and motivations of a pedestrian. Furthermore, this provides the opportunity to gain insight into how cognitive and decision-based approaches can model pedestrian behaviour as realistically as possible.

Kurzzusammenfassung

Die Erforschung von Fußgängerdynamik ist stets ein Zusammenspiel aus empirischen und experimentellen Beobachtungen und theoretischer Modellierung und Simulationen. Dabei sind Modelle nicht nur eine theoretische Reproduktion empirischer Daten, sondern eine wichtige Informationsquelle, um die Mechanismen und Verhaltensweisen, die der Fußgängerdynamik zugrunde liegen, zu analysieren und zu verstehen. In dieser Arbeit wird ein neuer Modellansatz vorgestellt, der die Bewegungen von Fußgängern als Resultat kognitiver und entscheidungsbasierter Prozesse auffasst.

Das Modell ist raumkontinuierlich, aber zeitdiskret und gehört damit zu einer Modellklasse, deren Potential bisher wenig untersucht wurde, die aber im Vergleich mit den üblicherweise verwendeten Klassen große Vorteile in Bezug auf Genauigkeit und strukturelle Einfachheit hat. Ein Fußgänger wird als eine autonome Einheit betrachtet, die mittels visueller Wahrnehmung und Antizipation Informationen über ihre unmittelbare Umgebung sammelt, und auf dieser Grundlage über ihre Bewegung im nächsten Zeitschritt entscheidet.

Ein Hauptaugenmerk in der Modellentwicklung lag auf der Modellierung der Interaktion und Kollisionsvermeidung mit anderen Agenten. Unter anderem an dieser Stelle wird insbesondere auf stochastische Prozeduren zurückgegriffen, die die Unsicherheiten und Unwägbarkeiten menschlicher Entscheidungen berücksichtigen und dabei helfen, den Modellansatz realistischer zu machen.

Wie die Simulationsergebnisse zeigen, ist der neue Ansatz in der Lage, charakteristische Effekte der Fußgängerbewegungen mindestens qualitativ, oft sogar auch quantitativ sehr gut zu modellieren. Im Besonderen können wichtige makroskopische Effekte, speziell kollektive Phänomene, durch die Modellierung von individueller Wechselwirkung eines Einzelnen mit anderen Fußgängern gut reproduziert werden. Während der Modellentwicklung wurden die verwendeten Parameter im Hinblick auf die empirische Datengrundlage situationsspezifisch angepasst und weitere kognitive Prozeduren ergänzt. Damit können zum einen die ausschlaggebenden intrinsischen Eigenschaften und Motive eines Fußgängers besser identifiziert und verstanden werden, zum anderen Erkenntnisse darüber gewonnen werden, wie kognitive und entscheidungsbasierte Modelle realistisches Verhalten für Fußgänger bestmöglich wiedergeben können.

Contents

CHAPTER 1

Introduction

'Pedestrian dynamics': basically everybody has at least a general idea what is meant by this expression. On the one hand, walking is the most natural form of human locomotion and a vast majority of us is part of road traffic as a pedestrian routinely. On the other hand, crowd disasters are also part of the public awareness. Research on pedestrian dynamics therefore often focuses not on the investigation of the motion of single individuals, but pedestrians in large groups and their interaction with others and the environment.

But, is this physics? In physical systems, particles are often considered as passive entities, exposed to extrinsic impacts, described by observables. In contrast, a pedestrian his- / herself would probably claim decision-making independence for his / her walking behaviour. Large pedestrian groups, especially in the light of crowd disasters, are often publicly referred to as 'panicking' masses showing irrational and asocial behaviour (see Sec. 2.1). In fact, it is often claimed that including behavioural aspects in pedestrian models makes them realistic [1–5].

Physics-based models are nevertheless able to reproduce pedestrian motion realistically for different situations. From a physicist's point of view, a pedestrian crowd can be considered as interacting particles that can be described e.g. in analogy to classical fluid or gas mechanics [6–8]. Other approaches use statistical phys-

ics to represent crowds as many-body systems in non-equilibrium states exposed to stochastic processes [9–11]. Pedestrians can be regarded as driven by external forces similar to Newtonian mechanics [12] or by minimising potentials [13]. An important characteristic feature of crowds is the emergence of self-ordering or collective phenomena. Due to microscopic interactions, the system spontaneously shows macroscopic effects, like stop-and-go waves or lane formation in counterflow. Some of these phenomena are also observed in totally different systems: intermittent egress flows at bottlenecks were observed for pedestrians, sheep or granular material [14, 15]. Lane formation could also be found for self-driven particles and colloids, see e.g. [16–18]. In a simple model for self-driven particles, Vicsek et al. found cooperative motion and self-ordering [19]. They predicted a continuous phase transition from a homogeneous to an ordered state, which is also assumed in models for pedestrian lane formation [9, 20]. Since these systems involve particles that are not naturally assigned with psychological mechanisms, it is still reasonable to describe pedestrians (also) as a physical system, especially at high densities. It might be necessary to combine both aspects, physics and psychology, in order to yield an understanding of the underlying principles of pedestrian motion.

In this thesis, a new modelling approach for pedestrian dynamics is presented that is physics-based and captures a pedestrian as an actively deciding agent. It tries to gain insight into coherencies of pedestrian motion by reproducing realistic dynamics. A pedestrian's decision on its velocity, both direction and absolute value, is modelled using a simply structured set of rules. An agent has cognitive abilities like perception or decision-making which are used to navigate through the surrounding infrastructure and to respond to other pedestrians. The approach belongs to a model class that combines aspects of different approaches and that has been sparsely investigated yet. It shows realistic behaviour that fits well to empirical data for collision avoidance, single-file motion, evacuation scenarios and bidirectional flow. It reproduces collective phenomena like stop-and-go waves, lane formation or clogging at bottlenecks. During the optimisation process, the model provides insight into a pedestrian's intrinsic prioritisation and decision behaviour.

Pedestrian Dynamics

A pedestrian is 'a person moving on foot in a publicly accessible area' [21]. As simple as this seems to be, research on pedestrian dynamics comprises not only many different approaches, methods and models, but is also influenced by a wide variety of research fields like physics, psychology, sociology, mathematics, engineering or computer game development. Each of these can only consider certain aspects of all coherences that influence pedestrian walking behaviour (yet). In this chapter, a short overview over central aspects of pedestrian dynamics is given, followed by a more detailed description of mechanisms with particular importance for the new model approach presented in this thesis. If not stated otherwise, the overview is based mainly on [22–24].

2.1 Empirical and Experimental Observations

Much insight into pedestrian dynamics is gained by either controlled experiments or empirical observations. Beneath qualitative results, pedestrian walking behaviour can be described quantitatively. In this context, three quantities are of major importance: the pedestrian density ρ, velocity v and flow J. There are multiple

approaches how to define and measure pedestrian density and velocity which are more or less suitable for different scenarios. The pedestrian flow is given by the number of agents passing a fixed measurement area of width b [21, 24],

$$J = \rho v b \quad [1/\text{time}], \tag{2.1}$$

and is usually considered as a scalar quantity since the normal component of the velocity with respect to the measurement line is used. The HYDRODYNAMIC RE-LATION describes the specific pedestrian flow as the number of pedestrians passing the measurement area per unit time and width:

$$J_s = \rho v \quad [1/(\text{width} \cdot \text{time})]. \tag{2.2}$$

The correlation between these three basic quantities is expressed via the FUN-DAMENTAL DIAGRAM. It describes the relationship between flow or velocity and density and is, as its name implies, one of the most important observables in pedestrian dynamics. In modelling, it is often used for calibration or validation purposes or as input parameter [25]. Measured fundamental diagrams in part differ significantly [26], in addition their shape can depend on the specific scenario [21, 25, 26] or the measurement method [25, 27, 28]. However, all diagrams consistently show a decrease in the velocity for an increasing pedestrian density [26].

In general, the CAPACITY of a system is given by the maximum number of pedestrians which is able to sustain a certain action (e.g. walking, standing, crossing) within the facility [21]. In fundamental diagrams, the capacity is given by the maximum flow, and the corresponding system state is referred to as 'capacity state', the respective density as 'critical density'[1]. For density values below the critical density, the system is in the free-flow phase, where the pedestrians can move with their preferred velocities without congestion; for densities above the critical density, the system is in the congested state and the flow decreases with increasing density [29].

---

[1]In this case 'critical' does not necessarily refer to criticality in the physical sense.

One of the most interesting characteristics of pedestrian dynamics is the emergence of collective phenomena or behaviours which is also referred to as 'self-organisation' [25, 29, 30]. These phenomena are macroscopically observable behaviours caused by individual, microscopic dynamics. As distinguished from aggregate behaviour, collective motion arises from spatial or temporal synchronisation of the crowd members [21]. There are several typical collective behaviours that are repeatedly observed for walking pedestrians.

Jamming, Clogging and Arching

Jamming and clogging are phenomena observed at high densities. Jamming usually occurs if the inflow or the number of pedestrians in a system exceeds the system's capacity, for example at narrowings or in counterflow scenarios, such a scenario is shown in Fig. 2.1(a) for an evacuation through a narrow door. Clogging can occur in pedestrian groups with a high urge to enter a facility of limited capacity, e.g. exits. The pedestrians form short-lived structures around the exit which often have a semi-circular shape. Due to these arches the participants block each other and the flow is decreased or interrupted [21–24].

Bottleneck Flow and Evacuations

Bottlenecks, in general, are spatial structures with limited capacity, e.g. the door in an evacuation scenario or a narrowing in a corridor [22]. For high densities, they can cause the reduction of flow and emergence of jamming [21]. In bidirectional motion, oscillations of the direction of motion through a narrow bottleneck occur. To reduce the number of interactions, several pedestrians of the same direction of motion pass the bottleneck consecutively before the situation changes and a person with opposite direction is able to pass. This person is again followed by other pedestrians with the same direction so that the direction of motion within the bottleneck changes in an oscillatory way [22, 24, 25]. At narrowings in corridors several collective phenomena can be observed. If the inflow is large enough, jamming occurs and the pedestrians wait in a cluster in front of the bottleneck [33] (see Fig. 2.1(a)).

(a) Jamming in front of an exit (screenshot from [31])
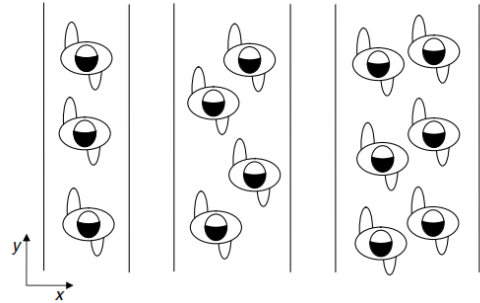
(b) Scheme of the zipper effect in corridors (from [32])

Figure 2.1: (a) Jamming in an evacuation scenario, the pedestrians wait in a dense group in front of the exit. (b) With an increasing width of a corridor the pedestrians increasingly walk in a zipper-like configuration and the flow increases approximately linearly.

Thereby, the density within the cluster usually does not depend on the width of the bottleneck, but decreases significantly within it [34]. The flow within the narrowing depends on its width. With increasing corridor width the pedestrians use the available space most efficiently by decreasing the interpersonal distance along the direction of motion while increasing the lateral distance. This behaviour is called 'zipper effect' (see Fig. 2.1(b)). It causes an almost linear increase of the maximum flow within the bottleneck with increasing corridor width [27]. At sufficiently high densities and desired velocities, clogging is observed at bottlenecks. The blockages lead to intermittent flows which show large time gaps between single pedestrians alternating with larger groups of pedestrians passing in a short space of time, so-called 'bursts' [15, 35, 36]. This is particularly important for evacuation scenarios in which the exit acts as a bottleneck for the egressing pedestrians. Muir et al. [37] showed for evacuations in airplanes that competitive behaviour can cause blockages of the exit and increase the egress times. The negative impact of

competitive behaviour on the total evacuation time is sometimes also referred to as 'faster-is-slower' effect [38]. Here, the competitiveness and higher urge to leave the room is interpreted as a higher desired velocity of the pedestrians ('faster') that causes increased evacuation times ('is slower').

Lane Formation

Lane formation in general describes the emergence of elongated clusters ('lanes') of pedestrians with the same walking direction along the direction of motion [21]. This self-ordering is often observed in bidirectional flow [25, 39–41] as shown in Fig. 2.2. By following other pedestrians with the same direction of motion, the number of interactions and collisions with oppositely walking agents is reduced [41]. This enhances comfort and smooth motion [25, 30]. As a result, the pedestrian flow is stabilised compared to the unordered system and the velocity of the agents increases [39, 40]. Lanes in bidirectional motion can be either stable, separating the system into, mostly two, regimes of opposite walking directions, or so-called dynamic multi-lanes [41]. Dynamic lanes can arise, decay or merge with other lanes, so that the number of lanes in the system varies in time. Lane formation requires a sufficiently high density and may depend on external components like boundary conditions or additional instructions, e.g. which side should be preferably chosen when evading an oppositely walking pedestrian [29].

Patterns in Intersecting Streams

At crossings and intersections, pedestrians show routes deviating from the supposed optimal or shortest route, e.g. short-lived roundabouts [22–24] or diagonal stripe formations [43]. They enhance the efficiency of the walking behaviour.

Density and Stop-and-Go Waves

Density waves are quasi-periodic changes of the density in space and time that are mostly observed in high-density scenarios. A typical example in pedestrian dynam-

Figure 2.2: Lane formation in bidirectional flow in a corridor. Pedestrians with black shirts are walking from left to right, participants with red shirts from right to left (screenshot from [42]).

ics are stop-and-go waves similar to those of vehicular traffic [22–24]. They can be observed in both empirical observations [44] and controlled experiments. Stop-and-go waves in pedestrian dynamics occur especially in one-dimensional single-file motion [27, 45–49]. Above a certain critical density, the formation of jams can be observed that separate the system into standing and moving pedestrians, whereby the density within the jams is increased compared to the rest of the system. This fluctuation in the density propagates in the opposite direction than the walking direction of the pedestrians. In vehicular traffic, the system separates into a jammed phase with standing cars and a free-flow phase with fast moving vehicles [23, 50]. In contrast, stop-and-go waves in pedestrian dynamics show separation into a standing and a slowly moving phase.

Collision Avoidance

Collision avoidance with static and moving obstacles is one of the basic interaction mechanisms of pedestrians and can, for example, be particularly observed at

intersections. It comprises adjustments of the walking speed and the direction of motion. Whether an agent slows down or evades the collision, can depend on multiple factors.

In laboratory experiments on crossing scenarios of two pedestrians (approaching each other at an angle of 90°), most collisions ($\sim 94\%$) are avoided because at least one of the agents changes its velocity [51]. In the majority of cases ($\sim 65\%$), one of the agents increases its speed, whereas the other one slows down. In other cases, both pedestrians either increase or decrease their speeds, or only one of the agents accelerates, whereas the opponent keeps its velocity. In contrast, Parisi et al. [52] observed that at crossings at 90° and 180° collisions in low-density situations were mainly avoided by adjusting the direction of motion. For higher densities, steering in encounters with 180° was less often and less distinct compared to crossings at 90°. Overall, the authors found that pedestrians are three times more likely to change their direction of motion than stop. Similar to that, the experimental results from Huber et al. [53] showed that adjustments of the speed were only used if the angle with the groups of participants and a crossing interferer was 45° or 90°, whereas changes in the walking directions were also observed for 130° and 180°. It is assumed that collision avoidance by adjusting the speed is used if the available space or time is restricted, while evading manoeuvres are applied more generally.

Psychology in Pedestrian Dynamics

In contrast to passive, non-autonomous particles, pedestrians can be considered as intelligent humans with a certain awareness about themselves. In terms of physics, a 'crowd' is mostly understood as a group of people who are on the same place at the same time. However, in the framework of the social identity theory a 'physical' crowd can involve one or more 'psychological' crowds [21]. Pedestrians within a psychological crowd understand themselves as part of a group and can distinguish between group members and others, while physical crowds describe pure aggregations of people. This self-categorisation can have an influence on the behaviour and interaction of the pedestrians [2–4].

There are several contributions which recommend the explicit incorporation of social and psychological aspects in pedestrian models in order to describe walking behaviour realistically [1, 3, 5, 54]. However, reliable experimental or empirical data are rare. Von Sivers et al. [2, 3] implemented previously observed social identity and helping behaviour in an terroristic incident which affected the overall evacuation time. In evacuation experiments, Garcimartin et al. [38] observed a negative influence of competitive behaviour on egress times, while Muir et al. [37] observed that competitiveness was disadvantageous in terms of evacuation times for small bottlenecks, but decreased the egress times for larger widths. Sieben et al. [5] aimed at capturing the influence of social norms and social psychology on the waiting behaviour of pedestrians in front of bottlenecks.

The public perception of pedestrian dynamics is probably highly connected to ideas of 'panic' or 'mass panic'. Thereby, one should consider that there is no consensus on the definition of the term 'panic'. In most cases it is understood as an irrational, asocial response to a potential threat or danger [55, 56]. However, panic in this view does not occur as often in pedestrian crowd incidents as assumed [55]. In fact, it has been observed that in states of fear, humans rather look for familiar persons and places than flee blindly [56, 57]. Showing this 'affiliate behaviour' [56], help and cooperation dominate in critical situations (see also [2, 3] and references therein).

2.2 Modelling Pedestrian Dynamics

As experiments and empirical studies on pedestrian dynamics are often difficult and for some situations even not possible for practical, ethical or financial reasons, simulation and modelling of pedestrian walking are two very important aspects of this research field. Over the years, lots of different model approaches have been developed and improved. Only in a recently developed glossary for pedestrian dynamics [21], 17 different sub-categories for pedestrian models were found. Therefore, the overview given in this section only describes a small subset in greater detail.

Classification of Pedestrian Models

Based on the modelled time scale, pedestrian models can focus on different levels of walking behaviours [22, 24, 58]. On a STRATEGIC LEVEL, a pedestrian decides on actions in the longer run, considering the superordinate goal. In contrast, decisions on the TACTICAL LEVEL are on short-term planning of the actions based on the current situations and comprises for example route choice behaviours. On the third, OPERATIONAL LEVEL, the actual walking dynamics is determined. These level distinguish themselves also by the degree of cognition and autonomy of the agents: whereas operational level models are often physics-based approaches and can represent pedestrians as simple particles, decisions on the tactical and strategical level require higher cognitive abilities and are therefore related to psychological and sociological effects. Models dealing with 'intelligence' often combine operational with tactical or even strategical decisions.

The majority of pedestrian models consider the operational level which is mainly determined by physics. They can be further classified based on the agents' autonomy [25] or underlying structure [22, 24] as described in the following.

Relying to the simulated length scale, pedestrian models can be macro-, meso- or microscopic. MACROSCOPIC MODELS describe the state of the system by global, averaged quantities like density or flow using conservation laws or continuity equations. Individual agents are indistinguishable [59]. Typical examples for macroscopic models are fluid or gas-kinetic models that treat the crowd of pedestrians analogously to a gas or fluid [6, 7, 60–63]. The crowd is considered as a continuum [8, 64, 65]. Models on a MESOSCOPIC scale consider the agents as individuals, but describe the system globally by probability distributions [21]. They are often also referred to as 'kinetic models' and can be used as intermediate step when deriving a macro- from a microscopic model [8, 43, 65, 66]. In MICROSCOPIC MODELS, pedestrians are described as distinguishable particles or agents whose state is characterised by microscopic variables like velocity or position. They can be further categorised [22, 24]: microscopic models can be HEURISTIC, if the dynamics is mainly determined by pedestrian interaction, or FIRST-PRINCIPLE MODELS where

the dynamics is characterised by pre-defined principles. With respect to the nature of the variables used in the models, they can either be DISCRETE or CONTINUOUS, depending on whether the values of the parameters are integers or arbitrary real numbers, respectively. In general, each combination of discrete and continuous quantities is possible. Moreover, model approaches can use STOCHASTIC elements which add uncertainties to the system. Whether it is used as probabilities for decision-making processes or as noise signals added to the system, the stochasticity can be regarded as 'intrinsic' or 'extrinsic'. In contrast, in DETERMINISTIC models the system state at a future time is fully pre-determined by the present state. With same initial conditions the time evolution of a deterministically modelled system will always be the same. These models neglect a lack of knowledge of underlying mechanisms in pedestrian dynamics which make the motion more unpredictable. Therefore, they are often regarded as less realistic than stochastic models.

Based on how the dynamics of the model is formulated, microscopic models can be categorised as acceleration-, velocity- or decision-based. ACCELERATION-BASED, also called force-based or second-order models, use analogies to Newtonian mechanics to describe the movement of the particles as determined by forces. In contrast, in VELOCITY-BASED models, the pedestrian's velocity (absolute value and direction) is directly determined based on the current state of the agents and the environment. They often use visual perception of the pedestrians to gain the information and rely on optimisation problems for interaction. RULE-BASED models are also called 'position-based' as they do not use any velocity- or acceleration-based formulation. In fact, the state of a pedestrian is determined by decisions which are modelled using a fixed set of rules. Two commonly used model classes are described hereinafter.

Social Force Models

In force- or acceleration-based models, the pedestrian is exposed to external and internal forces that determine its dynamics. In doing so, they rely on an analogy to Newtonian mechanics. These models are often fully continuous and deterministic

[67–69]. One of the most known acceleration-based models is the SOCIAL FORCE MODEL by Helbing and Molnár [12]. The dynamics of a pedestrian i is given by the equation of motion,

$$\frac{\mathrm{d}\boldsymbol{v}_i(t)}{\mathrm{d}t} = \boldsymbol{F}_i(t) = \boldsymbol{F}_i^{(\text{driv})} + \boldsymbol{F}_i^{(\text{soc})} + \boldsymbol{F}_i^{(\text{phys})}. \tag{2.3}$$

Here, the forces acting on the pedestrian can be summarised as the driving force $\boldsymbol{F}_i^{(\text{driv})}$, social forces $\boldsymbol{F}_i^{(\text{soc})}$ and physical forces $\boldsymbol{F}_i^{(\text{phys})}$. The driving force displays the pedestrian's aim to move with its desired velocity $\boldsymbol{v}_i^{(\text{des})}$ and to reach it within the relaxation time τ_i:

$$\boldsymbol{F}_i^{(\text{driv})} = \frac{\boldsymbol{v}_i^{(\text{des})} - \boldsymbol{v}_i}{\tau_i} \tag{2.4}$$

The social force $\boldsymbol{F}_i^{(\text{soc})}$ is the sum of all forces 'felt' by the agents exerted by others or elements of the environment like walls or obstacles. In terms of personal space and safety distance, social forces are usually repulsive, but can also include attractive components than depend on the relative distance or are used to model group cohesion [22, 24]. In centrifugal force models [70, 71], the repulsive force by other pedestrians additionally depends on the relative velocities of two interacting agents. Physical forces $\boldsymbol{F}_i^{(\text{phys})}$ are included for physical interactions like collisions, e.g. to prevent excessive overlapping.

Although social force models are commonly used for pedestrian dynamics, they show two inherent problems, first, with the underlying mechanical approach, second with the numerical calculation of the equation of motion.

While being related to Newtonian mechanics, social forces do not obey Newton's Third Law 'actio = reactio' [72, 73]. For example, an agent could exert a social force to another pedestrian which does not lie within the agent's vision and therefore cannot exert an opposite force of the same magnitude. In addition, the total force acting on a pedestrian is given by the superposition of driving, social and physical forces, see Eq. (2.3). Especially at high densities or for an increasing range of the forces, this can lead to unwanted backwards motion or unrealistically high velocities which exceed the desired speed [72, 73], or the occurrence of collisions

instead of stable jam formation [74]. Another characteristic for systems in Newtonian mechanics is the usage of inertia which is modelled as the mass of a pedestrian in force-based models (in Eq. (2.3), the mass m_i is not neglected, but set to 1). It is indicated, however, that inertia only plays a minor role in pedestrian dynamics since pedestrians are able to stop and accelerate almost immediately [75]. Inertia related 'overreactions' of the pedestrians lead to oscillations in the movement and collisions with others [73].

Köster et al. [76, 77] give a detailed description of the numerical problems of the social force model when solving the equation of motion which are mainly caused by discontinuities of the forces in Eq. (2.3). For example, the driving force $\boldsymbol{F}_i^{(\mathrm{driv})}$ is determined by the preferred velocity $\boldsymbol{v}_i^{(\mathrm{des})}$ which always points towards the agent's target,

$$\boldsymbol{v}_i^{(\mathrm{des})} = v_i^0 \frac{\boldsymbol{r}_{\mathrm{tar}} - \boldsymbol{r}_i}{|\boldsymbol{r}_{\mathrm{tar}} - \boldsymbol{r}_i|} \tag{2.5}$$

with the position of the target $\boldsymbol{r}_{\mathrm{tar}}$, the current position of pedestrian i, $\boldsymbol{r}_i$, and the desired absolute value of the speed, v_i^0. As can be seen from Eq. (2.5), the driving force has a singularity at the target position. When solving the equation of motion computationally, numerical schemes as the commonly used Euler scheme lose their accuracy and cannot converge. In order to solve the equation of motion, it is rewritten as difference equation discretising the time. This difference equations, however, result in oscillating solutions for trajectories in the vicinity of the target. Therefore the agent is not able to approach its goal but stays on a stable orbit around it with a constant speed. Decreasing the time step weakens this effect, but increases the computation time. Therefore, discontinuities in the equation of motion must be approached explicitly by mollification in order to obtain realistic results [76, 77].

Cellular Automaton Floor Field Models

Whereas social force models are mostly fully continuous, acceleration-based and deterministic, cellular automaton (CA) approaches are categorised on the other side

of the spectrum as fully discrete, stochastic and rule-based models. In CA models, time, space and state variables like the velocity are discrete [10, 11, 78]. The two-dimensional space is divided into, mostly square cells, whose size represents the space requirement of a pedestrian in a dense crowd, approximately $0.4\,\mathrm{m} \times 0.4\,\mathrm{m}$ [26]. The dynamics is performed in discrete time steps whose size is often associated with a pedestrian's reaction time between $0.1 - 0.3\,\mathrm{s}$. If a particle can move in every time step, $\Delta t = 0.3\,\mathrm{s}$ leads for this cell size to a velocity of $1.3\,\mathrm{m/s}$ which is consistent with a pedestrian's free flow speed [10]. Pedestrians are represented as particles which obey the exclusion principle: a cell can only be occupied by one particle at the same time. The dynamics is determined by probabilities for the transition of a particle towards a cell within its neighbourhood. In most cases, the velocity of the particles is restricted to one cell per time step. Usually, two different neighbourhood concepts are used: the von Neumann neighbourhood comprises the four cells to the front, back, left and right, whereas the Moore neighbourhood additionally includes the diagonal cells.

After few simple approaches to apply CA models on pedestrian dynamics, e.g. [9, 79], Burstedde et al. [11] proposed an extended version of a CA model which is now commonly used in pedestrian research, the FLOOR FIELD MODEL.

In order to approach the long-ranged interactions between pedestrians, the authors resort to a concept of chemotaxis as observed e.g. for ants. By means of floor fields, these long-ranged interactions can be transformed to short-ranged, local ones, which decreases the computational effort significantly. A pedestrian that moves away from a specific cell (i, j) leaves some kind of 'markers' which can be felt and traced by other agents. The information on these markers is stored in the so-called DYNAMIC FLOOR FIELD D_{ij}. The dynamic floor field is influenced by the pedestrians and determines the transition probabilities of the cells. It can be understood as a virtual trace left by the agents. Additional to the influence of the particles, the dynamic floor field changes in time by decay and diffusion and therefore has its own dynamics. Besides the interaction with other pedestrians, the agent tries to walk into its preferred direction. This information is provided by the MATRIX OF

PREFERENCE which gives the transition probabilities for the neighbouring cells of an agent considering e.g. the desired direction or the average velocity of the system. Thereby, each particle has its own 3×3 matrix of preference for each time step. This approach can be improved when considering an additional floor field, the STATIC FLOOR FIELD S_{ij}, which represents information on the environment and preferred direction [10]. It is usually equal for all agents and constant in time and gives the shortest way from the cell to the destination. Using this floor field, the matrix of preference can be omitted. Considering both floor fields, the final transition probability p_{ij} for a cell (i, j) is given by

$$p_{ij} = N \exp\left(k_S S_{ij}\right) \exp\left(k_D D_{ij}\right) \left(1 - n_{ij}\right) \zeta_{ij}. \qquad (2.6)$$

N is the normalisation constant, S_{ij} and D_{ij} the values for the static and dynamic floor field, respectively, which are considered for the probability by a respective coupling constant k_S and k_D. The obstacle number ζ_{ij} is zero for cells that are forbidden due to the environmental components like walls, and otherwise equal to one. The occupation number is $n_{ij} = 1$ for occupied cells, and $n_{ij} = 0$ for empty ones.

Based on the discrete time, the system update is usually performed in parallel. In this case, conflicts can occur whenever two or more particles have the same target cell. They can be solved in each time step [11] or approached more complexly using a friction parameter μ which gives the probability that none of the particles is allowed to move to the target cell and the conflict remains unsolved [80]. Accordingly, with probability $1 - \mu$ one of the agents is chosen randomly and moves to the target. It can be shown that friction helps at the description of clogging at bottlenecks. Beneath a single parameter, also friction functions can be used which also consider the number of particles involved in the conflict [81].

The spatial discretisation of CA models leads to some internal problems. More complex geometries with structures incommensurate with the size of a cell may not be representable in full detail, and microscopic assessment of trajectories or other locally measured quantities is not easily possible [10]. When using a Moore

neighbourhood, where diagonal motion is allowed, the total distance covered in one time step can be higher compared to straight motion to the front / back or to the left / right [82–84]. Therefore, the effective velocities vary depending on the chosen direction. This can be diminished when using the matrix of preference or smaller cells. Smaller cells, however, lead to new problems considering the resolution of conflicts.

Application of Models

In general, reproducing collective phenomena in pedestrian motion is a commonly used way to assess the performance of a model. Over the years, different types of collective motion were observed in simulated results. Pedestrian models are able to reproduce oscillatory changes of the direction of motion at bottlenecks [85–87] as well as intermittent flows in evacuation and bottleneck scenarios by clogs and bursts [15, 35, 88–92]. Also the empirically observed detours at intersections and crossings are found in simulation results [8, 43, 87].

The fundamental diagram is one of the most essential quantities in pedestrian motion and often used for calibration purposes [78]. However, it is a non-trivial problem to obtain realistic fundamental diagrams in pedestrian models. For example, the original social force model [12] seems not to be able to reproduce a fundamental diagram either in unidirectional flow in a corridor [93], or in one-dimensional single-file motion [94, 95]. Realistic results are only obtained with additional concepts and adjustments [93, 96]. Even for a simple CA floor field model, a good fit of the fundamental diagram to experimental data requires velocities larger than one cell per time step or an additional 'politeness factor' [78]. How well it fits often also depends on the measurement method [13, 78]. Velocity-based and heuristic models can reproduce fundamental diagrams mainly qualitatively [97–102].

Stop-and-go waves, especially for one-dimensional motion can also not be simulated by classical social force models [103, 104]. They were observed only in models that explicitly adjust the agent's velocity [45, 47, 102] or that add additional noise or small inhomogeneities to the modelled system [105, 106].

When simulating bidirectional flow in corridors, several model approaches reproduce stable lanes that cause a separation of the system or dynamically varying lanes. In either case, the walking behaviour of the agents is improved [107–112]. However, many model approaches have to cope with total blockages of the corridor, also referred to as 'gridlock', 'jamming' or 'freezing' state, these states are usually very stable and persist until the end of the simulation [9, 11, 29, 112–118]. As no such behaviour is found in reality, it must be an artefact of the model approaches.

2.3 Concepts Included in the Model

Social force models and CA floor field models are 'extremal examples' of model classes. Both approaches have advantages and drawbacks, which can significantly influence the simulation results. Therefore, the model presented in this work aims at a hybrid approach which includes aspects from several model classes in order to obtain optimal results. Characteristic features of this approach are:

- Continuous space and discrete time: there are no spatial artefacts as in CA approaches and no numerical artefacts as in force-based models. The approach uses the time-discrete and space-continuous Stochastic Headway Dependent Velocity model [102, 119, 120] as a basis.

- Introduction of cognitive abilities: the pedestrian has visual perception, anticipation, decision-making and navigation.

- Velocity adaptation based on the perceived environment: the agent decides actively on its speed by recognising and assessing the current situation. The concept of a 'distance-to-collision' is used as basis of decision-making.

- Stochasticity instead of optimisation problems: the pedestrians are not assumed to decide optimally for every time step, the behaviour is more uncertain.

Many of these concepts are also applied in different models. They mostly consider cognitive or perceptual abilities of the agents.

The SHDV Model

The Stochastic Headway Dependent Velocity (SHDV) model was developed in 2014 by C. Eilhardt and A. Schadschneider and acts as a basis for this new approach. Extended into two dimensions in this thesis, the SHDV model was originally developed in order to reproduce and analyse phase separation at high densities in pedestrian single-file motion. The following description relies on [102, 119, 120]. Combining aspects from acceleration-, velocity and rule-based models, the SHDV model is defined in discrete time and continuous, one-dimensional space. The length of the time steps, $\Delta t = 0.3\,\mathrm{s}$, represents a pedestrian's reaction time. Pedestrians are represented by point-like agents whose velocity v_i (for pedestrian i) is determined in each time step as a function of their distance headway h_i, $v_i = v(h_i)$ with

$$v(h) = \begin{cases} 0\,\mathrm{m/s} & : h \leq d, \\ \alpha(h-d) + v_{\min} & : d < h < d_c, \\ v_{\max} & : d_c \leq h. \end{cases} \qquad (2.7)$$

If the headway h is below a certain lower threshold d, the pedestrian does not move in the next time step. Above this threshold, the velocity v increases linearly with the headway, where α gives the slope of the function, and $v_{\min}$ is the agents' minimum velocity. When reaching a second threshold d_c, the velocity is cut and set to the free-flow velocity $v_{\max}$. The parameters are calibrated and validated and set to $\alpha = 0.5\,1/\mathrm{s}$, $d = 0.4\,\mathrm{m}$, $v_{\min} = 0.1\,\mathrm{m/s}$ and $v_{\max} = 1.2\,\mathrm{m/s}$. The fifth parameter is given by $d_c = d + \frac{1}{\alpha}(v_{\max} - v_{\min}) = 2.6\,\mathrm{m}$. The values for d and Δt were chosen accordingly to comparable values in floor field CA models, whereas α is drawn as a linear approximation from the optimal velocity function given by [121, 122].
In addition, the SHDV model involves a slow-to-start rule which states that agents who have had zero speed in the previous time step stand still in the next step with

a stopping probability $p_0 = 0.5$. This concept is adopted from vehicular traffic. It is crucial for reproducing stop-and-go waves as it reduces the outflow out of a jam significantly and stabilises it thereby.

Continuous Space and Discrete Time

As combination of the advantages of CA and social force models, continuous space and discrete time provide a framework that is simple to implement while preventing spatial artefacts. However, only few models rely on this concept. For the SHDV model, Eilhardt and Schadschneider use continuous, one-dimensional space and discrete time as described above [102, 119, 120]. In two dimensions, Teknomo et al. [123] draw on 'difference equations' instead of differential equations while using continuous space, and Baglietto et al. [124] describe an automaton model in which the agents move in continuous space while the dynamics is updated in time steps of $\Delta t = 0.5$ s. Fang et al. [125] model the step length and frequency of an agent continuously, but with discrete time. In a real-coded CA model, velocity and position for the next time step can be arbitrarily chosen, and the agents are repositioned afterwards on an underlying grid [83].

Other models that, in principle, use continuous space with discrete time steps, provide an individual discretisation for each pedestrian according either to step length [13] or a discrete choice set of possible directions and velocities, mostly within a visual field [89, 100, 126]. In doing so, the entire room is regarded as being continuous, whereas a single pedestrian cannot have arbitrary positions and velocities in one time step.

Visual Field

Visual fields as spatial representation of an agent's visual perception are mostly used in models that rely on cognitive abilities of pedestrians. In almost every case, a visual field is given as a circular segment centred at the pedestrian's position providing a certain range and extent. Values found for visual angles are 120°

[97, 127, 128], 135° [129], 150° [130–132], 170° [100, 130][2], 200° [114] and 360° [134]. Accordingly, the maximum visual distance ranges from 2 m [135] to 10 m [131]. Sometimes, the visual field is distributed into different angular or radial segments in order to represent the decision-process of the agents and bounds all possible positions [100, 130].

Decision-Making

Decision-making is a crucial aspect of the simulation of autonomous agents. Until now, few different approaches are used. First, decisions are represented by discrete choice models [101, 136, 137]. The dynamics of a pedestrian is modelled as sequence of single decisions. Out of discrete alternatives the agent chooses the one which optimises a certain cost, discomfort or utility function. Second, fuzzy logic tools are used in order to describe pedestrian decisions [100, 138]. They reduce the decision base to several elementary quantities which are itself assessed using discrete, 'fuzzy' categories. According to these input factors, an optimised output describes the pedestrian's next decision while walking. Rahmati and Talebpour [129] use game theory in order to simulate a pedestrian's decision and its strategies for decision-making according to the current situation. Another mathematical approach is presented by Hrabák et al. [139] who model a Markov decision process describing the probability for a certain sequence of decisions based on conditional probabilities of actions and system responses.

Collision Avoidance

Collision avoidance procedures differ significantly between several agent-based models. However, some concepts rely on the same basic idea. Similar to the social force approach, collision avoidance can be implemented by repulsive mechanisms applying when physical contacts occur [101, 124, 131]. Especially for decision-based models, pedestrians avoid collisions by optimising certain quantities like walking

---

[2]If this value is used, the work of Costella [133] is often cited, which itself states a span of the visual field of 150°-160°.

distance or number of speed changes [127], kinetic energy [126] or potentials [13], headway [140] or some specific cost function [100]. The optimised values are drawn from discrete sets for possible directions and / or velocities.

Time-to-Collision and Distance-to-Collision

Especially the time-to-collision (TTC) is an often used concept in the investigation of the environment in pedestrian models. Generally, the TTC is used in either of two ways: first, the time until a potential collision with another agent is estimated based on a linear interpolation of the current motion of both agents and then used to rank the imminence and importance of single collisions [111, 126, 132, 141]. Second, a fixed value for the TTC is used in order to maintain a certain safety distance to other agents while walking [101, 131, 142].

In [97], the perceived TTC is transferred into a 'mental distance-to-collision' which is then used in the further course. However, compared to the TTC, the distance-to-collision (DTC) is not as frequently used.

Anticipation

Many of the anticipation concepts are highly connected with the time-to-collision. Here, anticipation means determining future positions of itself and another pedestrian assuming straight motion of both participants, which can be used to assess the TTC or DTC [126, 127, 130, 135]. Other models use anticipation floor fields in order to assess which cells in a CA model might be occupied in the next time steps [109, 113, 143]. The transition probabilities are then decreased accordingly to the anticipated occupation.

Velocity Adaptation

In terms of collision avoidance, it is often necessary for a pedestrian to adjust its velocity according to the surrounding situation. A first example was given at the beginning of this section. Similar to the SHDV model, the velocity is often

determined as function of the (interpersonal) distance or headway [47, 70, 124, 144], especially in so-called optimal velocity models for pedestrian and vehicular traffic [86, 99, 112, 121, 122]. Similarly, the speed can also be given in dependence of the surrounding density [82, 88]. The specific value of the speed is either determined continuously by given equations or drawn from a discrete set of choice in order to optimise the walking behaviour by this decision.

Route Choice and Wayfinding

If a pedestrian is assigned a certain degree of cognition and decision-making abilities, the navigation through more complex geometries becomes important. Then, models must include certain aspects of the tactical level, mainly route choice or wayfinding behaviour. There are several approaches how to model a pedestrian's way through its environment, most of them aim at large buildings and more complex geometries. They include a wide variety of factors as efficiency, personal abilities and preferences, external stimuli (signage, illumination, instructions) and environmental conditions (smoke, heat, fire) [145, 146]. In most of these cases, networks are used in order to parametrise the actual room. Pedestrians are lead from node to node via network edges. Visibility graphs [134, 136, 147] try to capture the regions of the environment which are visible from a certain position and lead the agents by connecting these areas consecutively, see Fig. 2.3(a). Another common concept is cognitive maps that are mental representations of the spatial conditions of a pedestrian that represent global and local knowledge about the environment [148–152]. Other networks are directly connected to the geometry and surrounding paths [153–156].

Besides the global route choice for entire complex geometries, navigation can be crucial even on a much shorter scale. Leading pedestrians around a corner requires consideration on route choice and wayfinding in order to prevent unrealistic trajectories or large jams at the corners. This problem can occur in all situations with corners, like evacuation or bottleneck scenarios. To solve it, either the desired velocity can be adjusted not to lead directly to the shortest path but to provide

(a) Visibility graph approach (from [134]) (b) Guiding line approach (from [73])
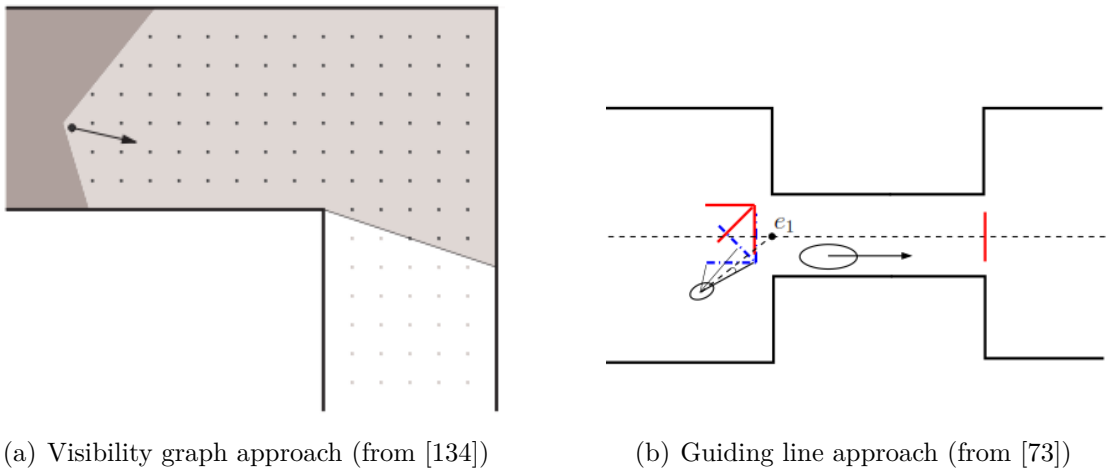
Figure 2.3: Route choice and wayfinding: (a) In the visibility graph approach, space is represented as a grid. Only 'visible' grid points are possible to be chosen by the agent as next position [134]; (b) Guiding line segments are used in [72, 73] to determine an agent's preferred velocity. The pedestrian targets the closest point on one of the lines (blue, red) consecutively to 'steer' around the corner.

a smooth motion [72] (shown in Fig. 2.3(b)), or the underlying static or dynamic floor field has to be changed accordingly [157, 158]. Tsai et al. [159] even change their vision-based navigation field manually in order to prevent unrealistic motion.

The Model

In the light of the wide variety of models for pedestrian dynamics careful consideration must be given to how a new model approach fits into the wide spectrum of pedestrian models and where it distinguishes itself. The development of the model in this work focused on the formulation of an approach that is as simple as possible but able to reproduce a pedestrian's decision process as realistically as possible. In this chapter, the basic principles and components of the model are described.

3.1 Concept, Classification and Structure

The approach presented in this work combines aspects from different model classes in order to obtain realistic results while using a simple structure. It aims at gaining insight into pedestrian walking behaviour during the model development process. Therefore, a pedestrian is modelled not as a passive particle whose motion is fully determined externally by forces or potentials, but as an autonomous, self-acting agent that uses cognitive abilities. In doing so, the model approach is intended to capture intrinsic properties and motivations of a pedestrian.

3.1.1 Concept of the Model

One of the key points of this model is that the system is set in continuous space and discrete time. While most other models are either fully discrete or continuous, this approach combines both. Despite of cellular automaton approaches, which are discrete in time and space, discrete time steps are not often used in pedestrian models. This approach therefore belongs to a model class which has been implemented rarely so far and whose potential has not been fully investigated yet. It unites advantages of decision- and force-based approaches: because of the discrete time like in cellular automaton models, the model can be formulated in a simple, discrete structure instead of differential equations whose solving would cause numerical artefacts. Moreover, the approach uses continuous space like many velocity- or force-based models in order to prevent artefacts that come along with spatial discretisation. In doing so, the walking behaviour of pedestrians can be represented as a sequence of single actions described by rules which every agent performs in each time step while keeping a high fidelity in terms of position and velocity.

The basic idea of this model approach is to reproduce a pedestrian's decision on its velocity for the next time step. Thereby, it explicitly uses cognitive abilities like perception, cognition or anticipation. A pedestrian is regarded as an agent that proactively decides based on information on the environment. Thus, it is intended to gain more insight into the priorities and components influencing a pedestrian's walking behaviour.

This approach uses the SHDV model [102, 119, 120] as a basis. It is also formulated in continuous space and discrete time and was developed for one-dimensional single-file motion. It models the one-dimensional velocity of pedestrians as a function of their headway and is used to determine the absolute value of the pedestrians' speed. The new model extends the SHDV model into two dimensions by adding an angular component. The determination of the direction of motion is the main part of the model and includes motion within the environment and mechanisms for collision avoidance.

Stochasticity is another essential aspect of this model approach. Used in all stages

of the decision process, it shall help at reproducing pedestrian walking behaviour in a realistic way. Stochastic elements represent uncertainties of human decisions and underlying psychological mechanisms one might not be able to simulate explicitly.

3.1.2 Classification of the Model

The criteria to describe and classify the model approach are taken from [22, 24] and presented in Sec. 2.2.

Since the model combines different aspects from several model classes it cannot always be clearly assigned to a specific model category. It mainly simulates pedestrian behaviour at the operational level as it models the concrete decision on the velocity for the next time step. However, because of the explicitly used cognitive mechanisms, it partially requires planning on a tactical level, e.g. by using intermediate targets for way finding. Hence, the approach can be regarded as an agent-based-model or multi-agent system.

The focus during the determination of the direction of motion is on the interaction with the environment. Therefore, the model fits in the class of heuristic models. It is a microscopic approach and includes features of velocity-based models as it simulates the determination of the pedestrian's velocity with collision avoidance behaviour and visual perception. However, one of the main aspects of the model is its rule-based structure realised by discrete time steps which is a pivotal property of decision- or rule-based models. In terms of mathematical formulation, the presented model belongs to the latter class. Its dual nature using both continuous space and discrete time combines benefits from both first- and zeroth-order models. Moreover, the model has a high fidelity as it approaches the decision process of a walking pedestrian as realistic as possible.

3.1.3 The Structure

Discretisation in time is one of the basic characteristics of this model approach. Time progresses in constant steps, $t \rightarrow t + \Delta t$, which is realised by using a parallel

update procedure. Each pedestrian's state is updated simultaneously, which means that all agents act and move at the same time.

The model describes the process a pedestrian runs through in every time step in order to determine its velocity for the next step. Starting from the pedestrian's current situation, this process consists of three phases: perception, decision-making and movement (see Fig. 3.1). Moreover, the decision process relies on two main components: motion within the environment and the interaction with other pedestrians. They are considered separately at first and combined at a later stage in the decision phase. In this section, the model structure is described for the overall context. A more detailed explanation is given in the subsequent sections.

In each time step, the initial situation for the process is the current state of a pedestrian i who has an individual target and a visual field. During the perception phase, the agent uses the visual field to detect the infrastructure, represented by walls, and other pedestrians. Walls are basically one-dimensional objects in space that a pedestrian is not allowed to cross. They confine the geometry the agents move in by separating accessible from non-accessible areas. The information on walls is combined with the individual target to orientate within the room, whereas the information on other agents is used to find the own position within the group of pedestrians. In the decision phase the agent, based on what has been perceived, determines two directions for reaching the target and avoiding collisions with other pedestrians, respectively. In a second step, one of these angles is chosen as direction of motion. Third, the pedestrian calculates the corresponding speed. During the last phase, the new position of the pedestrian is determined according to the velocity determined before.

This procedure is undergone by every pedestrian for each time step. The parallel update requires that the perception phase and the determination of the direction of motion is finalised for every pedestrian before the positions (and all other characteristics) are updated. In general, perception, decision and movement phase build on one another and must be performed in this order. During the decision phase, the determination of the target and the interaction angle are done independently
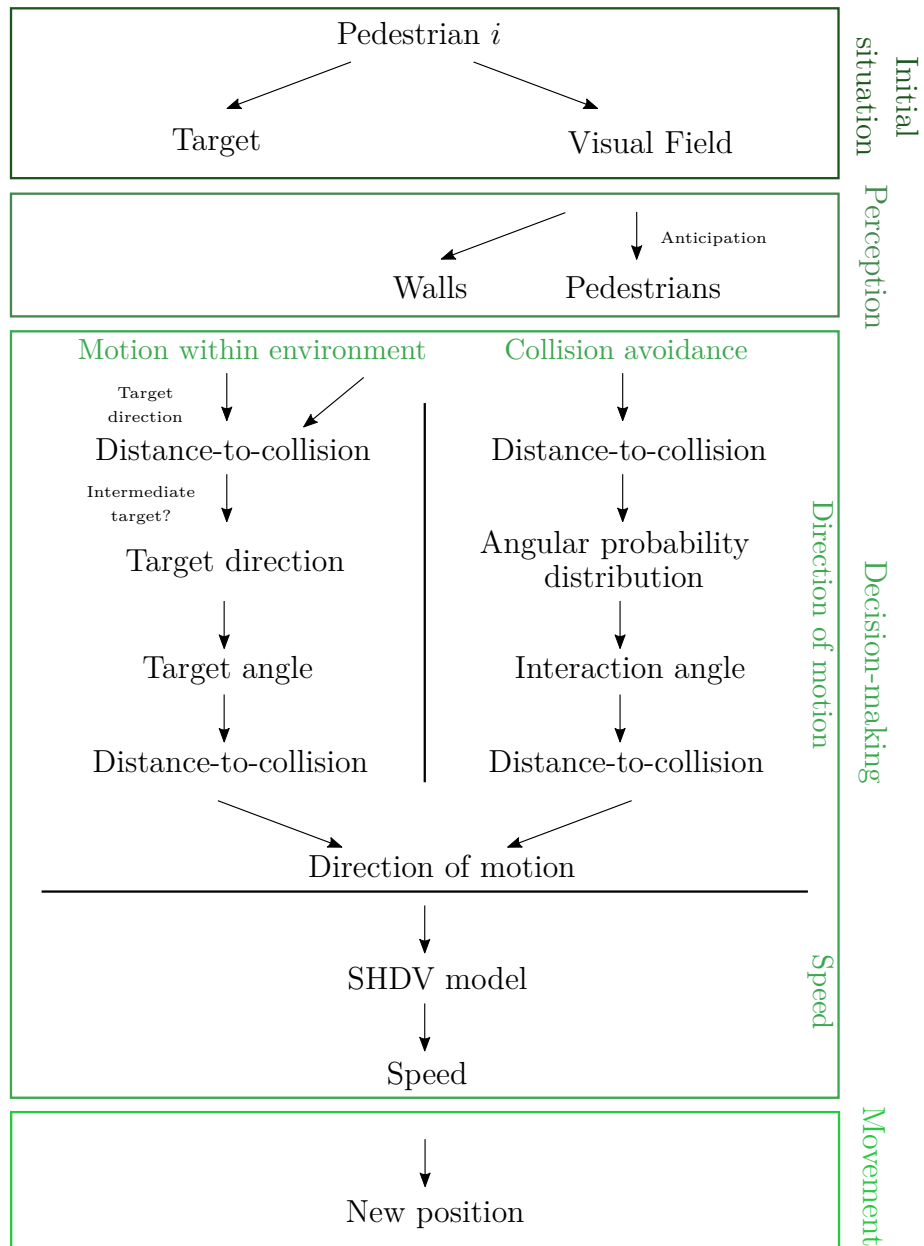
Figure 3.1: An update step is based on the pedestrians' current position and consists of three phases: perception of the environment and other pedestrians, decision-making on the direction of motion and the velocity and movement.

from each other and can be performed in an arbitrary order. In case the agent does not perceive any other pedestrians, the decision of the interaction angle and the final direction of motion can be omitted, and the motion is fully determined by the target direction.

3.2 The Model Components

The system that is described by the model consists of the environment or infrastructure and the agents moving therein. Both elements are the foundation for the entire dynamics. They are described by specific characteristics that are always constant in time for the infrastructure[1], but can be time-dependent for pedestrians. These characteristics are described in the following.

3.2.1 The Environment

In this model, the environment is solely build by walls representing areas that are not accessible and confining the available space for the pedestrians. A wall is as a one-dimensional object characterised by its orientation $o_\mathrm{W} = \omega\pi$, $\omega \in [0,1)$, position p_W and length l_W (see Fig. 3.2). For simplicity reasons, the orientation is, for the time being, either $o_\mathrm{W} = 0$ (horizontal, case '0') or $o_\mathrm{W} = \frac{\pi}{2}$ (vertical, '1'). Being extended in y-direction, the position of a vertical wall is then given by a coordinate in x-direction and vice versa for the horizontal case. The length of a wall results from the difference between a maximum and minimum value along the other direction, i.e. $l_\mathrm{W}^0 = x_\mathrm{max} - x_\mathrm{min}$ for a horizontal, $l_\mathrm{W}^1 = y_\mathrm{max} - y_\mathrm{min}$ for a vertical wall. Complex geometries are constructed by aligning several walls. An exit is represented by a gap between two walls, supplemented with respective target coordinates of the pedestrians. Some kinds of geometries necessitate further orientation aids, e.g. if the exit cannot directly be seen from some positions in the room. In this case the set of walls is complemented by intermediate targets. These targets are

---

[1]In general, also walls with time-dependent properties could be possible, e.g. including a door that opens or closes.
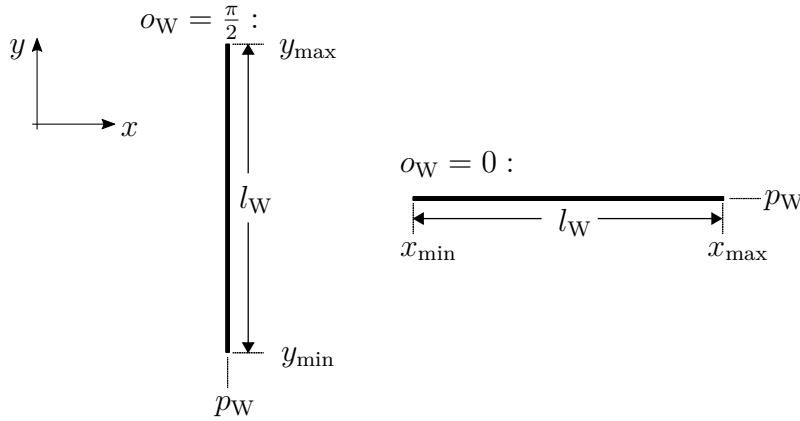
Figure 3.2: Definition of wall parameters: depending on the wall's orientation o_W the position p_W is a coordinate in x- or y-direction. y_min, y_max and x_min, x_max determine the length of a vertical or horizontal wall, respectively.

fixed positions in the room that are globally set and used to guide the pedestrians through complex geometries. How to place them depends strongly on the respective scenario and belongs to the research field of route choice or wayfinding behaviour.

3.2.2 The Agent

In pedestrian modelling, a pedestrian is often also referred to as 'particle' or 'agent'. While sometimes meaning the same, both terms could imply different conceptions of a pedestrian and the level of cognition. A particle may move passively responding to external forces or potentials, whereas an agent may decide on the movement in a more autonomous way. Since this model explicitly uses the cognition and perception of a pedestrian to determine the dynamics, the latter approach is more suitable and the terms 'pedestrian' and 'agent' are used synonymously.

A pedestrian is represented by a circle of radius r and characterised by a set of parameters as defined in Fig. 3.3(a). The identification number i is fixed and helps at identifying individual agents. The position of a pedestrian is described by the coordinates $x_i(t)$ and $y_i(t)$ which give the centre of the circle. Each pedestrian is assigned an individual goal represented by the target position $\left(x_{\mathrm{t},i}(t, x_i, y_i),\right.$
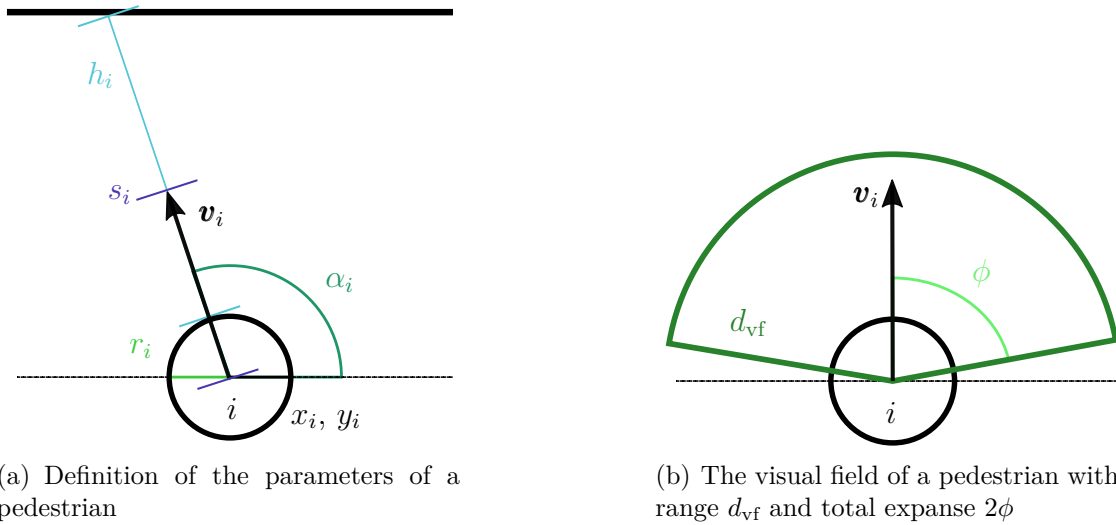
(a) Definition of the parameters of a pedestrian

(b) The visual field of a pedestrian with range d_{vf} and total expanse 2ϕ

Figure 3.3: (a) A pedestrian is described by its radius r_i, coordinates x_i, y_i, velocity $\boldsymbol{v_i}$ (speed s_i and direction α_i) and headway h_i. (b) The visual field is centred around the agent's velocity.

$y_{\mathrm{t},i}(t, x_i, y_i)$) which may depend on time and the current position of the pedestrian. The headway $h_i(t)$ denotes the free path or distance-to-collision in walking direction. A pedestrian's velocity $\boldsymbol{v}_i(t)$ is described by its absolute value $s_i(t)$, which is also referred to as 'speed' hereinafter, and the direction of motion $\alpha_i(t)$. The angle $\alpha_i(t)$ is defined in the mathematical direction of rotation with respect to the x-axis. Moreover, each agent has a visual field as outlined in Fig. 3.3(b). It expands in a shape of a circular segment with an opening angle 2ϕ and radius d_{vf} and is symmetrically set around the pedestrian's current direction of motion. In general, the number of pedestrians in the scenario is represented as N.

3.3 The Perception Phase

In the first phase, a pedestrian uses the visual field to gather information on the environment. At that stage, the infrastructure and the presence of other pedestrians are processed separately. Only walls or pedestrians that lie within the field are

detected and considered in the further course. Similar to the approach used in the work of Zhou et al. [100], objects within the visual field cover a certain angular range which depends on the relative distance and orientation to the perceiving pedestrian. During the perception phase this range is determined. Therewith, it can be assessed whether a given direction leads towards an obstacle by examining if it lies within a range of the visual field that is covered by a wall or another pedestrian.

3.3.1 Perception of Walls

The situation of an agent perceiving a wall is exemplarily shown in Fig. 3.4. A wall is detected by a pedestrian if it is in the visual range. Therefore, two criteria have to be met. First, the minimal distance d between the pedestrian's position and the wall has to be less or equal to the maximum visual range d_{vf} under consideration of the agent's body extension. Second, the wall has to cover a certain area of the visual field. For that, one determines the two angles β_1 and β_2 under which the edge of the visual field cuts the wall assuming it to be infinitely long. The actual finite length of the wall is not of importance at this stage, but is considered when determining the distance between a pedestrian and a wall in an arbitrary direction. Once one of these viewing angles lies within the visual field, the wall is detected. If both angles are outside of the visual range, the wall is not seen by the agent. It should be noted that the angles are given with respect to the x-axis. Therefore, their derivation relies on simple trigonometric considerations. The detailed calculations are shown in Sec. B.1.1 in the Appendix. If $d \leq d_{\text{vf}}$, the final results for the viewing angles for a horizontal (case 0) and a vertical (case 1) wall, respectively, are given by

$$
\begin{aligned}
\beta_1^0 &= \arcsin\left(\frac{p_{\text{W}} - y_i}{d_{\text{vf}}}\right), & \beta_2^0 &= \pi - \arcsin\left(\frac{p_{\text{W}} - y_i}{d_{\text{vf}}}\right); \\
\beta_1^1 &= \arccos\left(\frac{p_{\text{W}} - x_i}{d_{\text{vf}}}\right), & \beta_2^1 &= 2\pi - \arccos\left(\frac{p_{\text{W}} - x_i}{d_{\text{vf}}}\right).
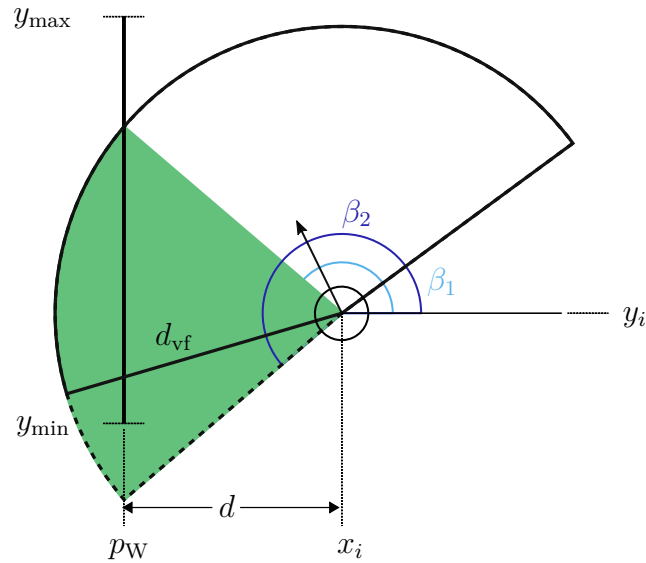\end{aligned}
\tag{3.1}
$$

Figure 3.4: Perceiving a wall means to determine the angular range that is covered by the wall (green area), if the minimal distance d to the wall is less or equal than the maximum visual range d_{vf}. This range is bonded by the angles β_1 and β_2 which are calculated during the perception phase.

3.3.2 Perception of Pedestrians

For the perception of other pedestrians similar criteria as for the perception of walls are applied. An agent can detect another pedestrian if the latter is 'in sight', that means that the distance between the pedestrian and the perceiving agent is less or equal to the maximum visual range, and if it covers a certain range of the visual field. Therefore, the distance between the agents, the angle under which the other pedestrian is perceived ('perception angle') and the corresponding coverage of the visual field are determined during the perception phase.

Different from the perception of the environment, an agent uses anticipation while perceiving other pedestrians. They are assumed to walk linearly based on the direction of motion and speed of the previous time step. Thereby, the relative velocity of two agents becomes more important. The anticipated position of an

arbitrary pedestrian i at time $t + \Delta t$ is given by

$$x_i^{\mathrm{a}}(t + \Delta t) = x_i(t) + s_i(t) \cos\left(\alpha_i(t)\right) \Delta t, \qquad (3.2)$$

$$y_i^{\mathrm{a}}(t + \Delta t) = y_i(t) + s_i(t) \sin\left(\alpha_i(t)\right) \Delta t. \qquad (3.3)$$

In a first step the distance d_n between a perceiving agent i and another pedestrian n $(n = 1, \ldots, N; n \neq i)$ is calculated under consideration of the body extension of both pedestrians. In order to assess the relative movement of both agents the anticipated position of the perceived pedestrian is used:

$$d_n = \sqrt{\left(x_i - x_n^{\mathrm{a}}\right)^2 + \left(y_i - y_n^{\mathrm{a}}\right)^2} - 2r. \qquad (3.4)$$

If the pedestrian n is in sight, $d_n \leq d_{\mathrm{vf}}$, the perception angle α_n is determined in a second step. It is defined as the angle that is enclosed by the connecting line between both agents and the x-axis (see Fig. 3.5(a)). For that, the expression for an angle enclosed by the connecting line between two arbitrary points in space and the x-axis is used as it is derived in Section B.1.2. In this case, the anticipated position is used for the perceived pedestrian. By doing so, the perceiving agent is able to determine its new state based on its anticipation of the current situation. Therefore it follows for the perception angle:

$$\alpha_n\left(x_i, x_n^{\mathrm{a}}, y_i, y_n^{\mathrm{a}}\right) = \begin{cases} 0 & : x_i < x_n^{\mathrm{a}}, y_i = y_n \\[4pt] \pi & : x_i > x_n^{\mathrm{a}}, y_i = y_n \\[4pt] \frac{\pi}{2} & : x_i = x_n^{\mathrm{a}}, y_i < y_n \\[4pt] \frac{3\pi}{2} & : x_i = x_n^{\mathrm{a}}, y_i > y_n \\[4pt] \arctan\left(\frac{y_n^{\mathrm{a}} - y_i}{x_n^{\mathrm{a}} - x_i}\right) & : x_i < x_n^{\mathrm{a}}, y_i < y_n^{\mathrm{a}} \\[4pt] \pi - \arctan\left(\frac{y_n^{\mathrm{a}} - y_i}{x_i - x_n^{\mathrm{a}}}\right) & : x_i > x_n^{\mathrm{a}}, y_i < y_n^{\mathrm{a}} \\[4pt] \pi + \arctan\left(\frac{y_i - y_n^{\mathrm{a}}}{x_i - x_n^{\mathrm{a}}}\right) & : x_i > x_n^{\mathrm{a}}, y_i > y_n^{\mathrm{a}} \\[4pt] 2\pi - \arctan\left(\frac{y_i - y_n^{\mathrm{a}}}{x_n^{\mathrm{a}} - x_i}\right) & : x_i < x_n^{\mathrm{a}}, y_i > y_n^{\mathrm{a}} \end{cases} \qquad (3.5)$$
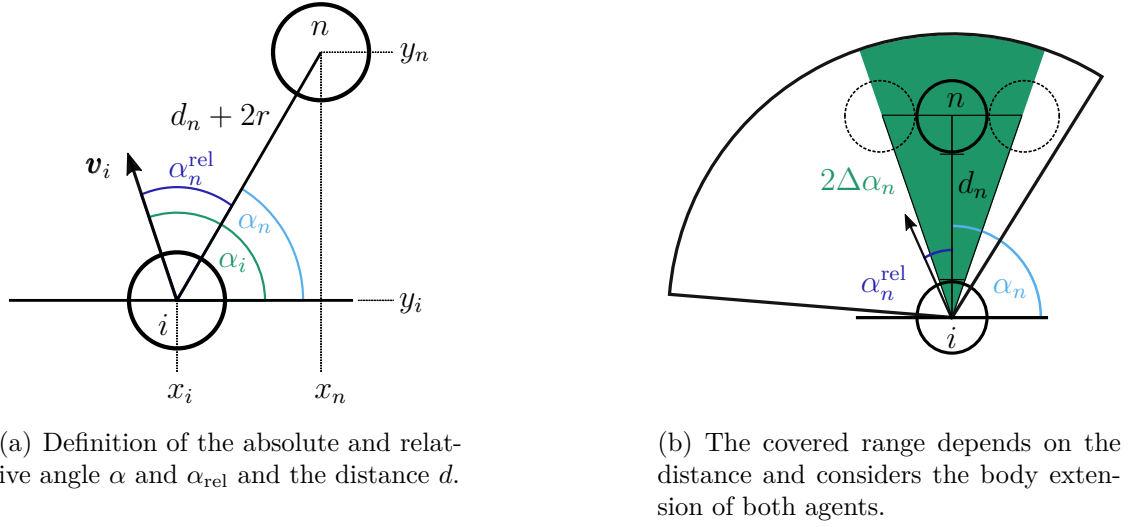
(a) Definition of the absolute and relative angle α and α_{rel} and the distance d.

(b) The covered range depends on the distance and considers the body extension of both agents.

Figure 3.5: When perceiving another pedestrian the agent determines the distance, both absolute and relative angle and the covered area of the visual field.

For calculations in the further course it is needed that the perception angle α_n is given relatively to the direction of motion α_i of the perceiving agent. This relative angle α_n^{rel} (see Fig. 3.5(a)) is a signed quantity, representing the relative position of the other pedestrian by the sign of the angle. According to the mathematical direction of rotation, pedestrians with a negative relative perception angle are located to the right of the perceiving agent, whereas the relative perception angle towards pedestrians on the left is positive. Hence, its absolute value satisfies $|\alpha_n^{\mathrm{rel}}| \in [0, \pi]$. The transformation between the absolute angle α_n and the relative perception angle α_n^{rel} with respect to the direction of motion α_i is given by

$$
\alpha_n^{\mathrm{rel}} = \begin{cases} \alpha_n - \alpha_i + 2\pi & : |\alpha_n - \alpha_i| > \pi, \quad \alpha_n - \alpha_i < 0, \\ \alpha_n - \alpha_i - 2\pi & : |\alpha_n - \alpha_i| > \pi, \quad \alpha_n - \alpha_i > 0, \\ \alpha_n - \alpha_i & : \text{else}. \end{cases}
\tag{3.6}
$$

The complete derivation can be found in the Appendix, Sec. B.1.3.

As described above, a pedestrian is detected if it covers a certain range of the visual

field. For that, the body extension of the perceived pedestrian as well as the perceiving agent has to be considered explicitly as schematically shown in Fig. 3.5(b): the angular range that would lead to a collision of the agent's body with the other pedestrian is shown by the green-coloured area. Neglecting the curvature of the circle that represents the pedestrian, it is determined as

$$2\Delta\alpha_n = 2\arctan\left(\frac{2r}{d_n}\right),\tag{3.7}$$

for a full derivation, see Sec. B.1.4 in the Appendix. A pedestrian n is perceived if the angle under which it is detected lies within the visual field or if the area which is covered by its presence extends into the visual field, i.e., if one of the following conditions is fulfilled:

$$\begin{aligned} &|\alpha_n^{\mathrm{rel}}| \leq \phi, \\ \vee\quad &\left[\alpha_n^{\mathrm{rel}} < -\phi \quad \wedge \quad (\alpha_n + \Delta\alpha_n) > -\phi\right], \\ \vee\quad &\left[\alpha_n^{\mathrm{rel}} > \phi \quad \wedge \quad (\alpha_n - \Delta\alpha_n) < \phi\right]. \end{aligned}\tag{3.8}$$

In conclusion, an agent determines the distance d, the angle under which the other pedestrian is perceived absolutely, α_n, as well as relatively, α_n^{rel}, and the covered angular range $\alpha_n^{\mathrm{rel}} \pm \Delta\alpha_n$ during the perception phase. All quantities are used in the further course for collision avoidance.

3.4 The Decision Phase

In the second phase the decision on the velocity is taken which can be regarded as the main part of the modelled process. Based on the information gathered in the previous perception phase, four single decisions are made: the decision on the preferred target direction, on the angle used for collision avoidance, the choice which of these two angles is used as final direction of motion and the determination of the speed. All decisions are based on the distance-to-collision which is the head-

way or free path into a given direction. It represents a pedestrian's desire to reach the individual goals in an undisturbed way. Therefore, directions providing larger distances-to-collisions are preferred. The speed is determined by the SHDV model using the distance-to-collision into the direction of motion as an input parameter. In contrast to other decision-based models, the distance-to-collision is used instead of the time-to-collision. The time-to-collision focusses more on the relative motion of two agents. However, for low or zero speeds of two pedestrians, the time-to-collision diverges. In contrast, the distance-to-collision is finite even for low velocities and 'uncouples' the own motion from the movement of the others. It enables the agent to gain an overview of the current overall situation. The relative motion of the agents is easily considered using anticipation of their future movement during the perception phase. Therefore, using the distance- instead of the time-to-collision facilitates the transition from the SHDV model to the new approach and reduces the basis of decision-making to one quantity.

3.4.1 Motion within the Environment: Decision on Target Angle

In the first instance, the pedestrian decides which direction should be chosen in order to reach the target. The agent uses its current position $(x_i(t), y_i(t))$, its assigned target coordinates $(x_{t,i}(t, x_i, y_i), y_{t,i}(t, x_i, y_i))$ and the information on the infrastructure that was gathered during the perception phase to orientate within the room and to determine the final target angle α_t^{fin}.

First, the pedestrian determines the current target angle α_t which gives the angle towards the target with respect to the current position of the pedestrian. As shown in Fig. 3.6, it is defined as the angle enclosed by the connecting line between the agent's current and the target position and the x-axis. Therefore, it is given by the same expressions as used before when calculating the absolute perception angle of a pedestrian, Eq. (3.5), replacing the perceived pedestrian's coordinates (x_n^a, y_n^a) by the target coordinates $(x_{t,i}, y_{t,i})$ (for a derivation see Sec. B.1.2).

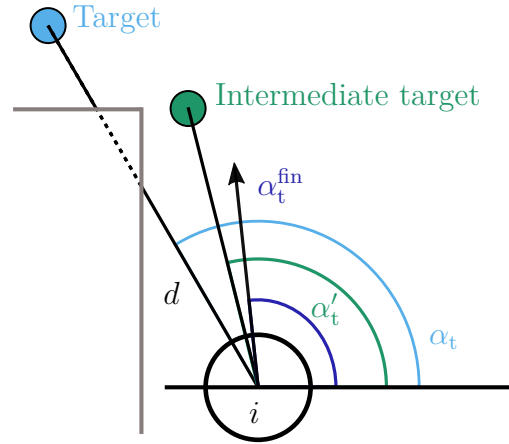Having determined the target direction α_t, the pedestrian refers to the information

Figure 3.6: Definition of the target direction α_{t}, the direction towards an intermediate target α_{t}' and the final target angle $\alpha_{\text{t}}^{\text{fin}}$.

on the infrastructure that was gathered during the perception phase. The agent determines the distance-to-collision d to any perceived wall in the room in target direction which is simply given by the minimum distance comparing all walls. The distance between a pedestrian and a wall in an arbitrary direction depends on the relative position and orientation of the pedestrian and the chosen direction with respect to the wall. For every particular situation it has to be determined whether the target angle α_{t} points towards the wall and would lead to a collision (under consideration of the agent's body extension) before it is possible to calculate the minimal distance. For reasons of clarity the derivation of the distance-to-collision towards walls is omitted at this point and it is referred to the corresponding Sec. B.2.1 in the Appendix.

As mentioned above, the distance-to-collision is the quantity the pedestrian's decision relies on. In case of the movement within the room, the distance-to-collision is used to assess whether the target could be directly reached or if it is screened by a wall. If d is smaller than a certain threshold, the target is not in direct sight with respect to the agent's current situation, as indicated in Fig. 3.6. In this case, the pedestrian has to use intermediate targets in order to navigate through the room. These additional target positions are globally set and constant in time and

can be used by all pedestrians. They should act as a tool for steering as long as the actual individual target is not in sight. Hence, if the distance-to-collision in target direction shows that it is hidden, the pedestrian uses the intermediate target that is closest to its current position instead. Analogously to the actual target, the agent determines a new direction α'_t towards the intermediate target.

Independently of the usage of intermediate targets, the further process is the same. The final target angle α_t^{fin} is calculated using a Gaussian distribution with the (intermediate) target direction α_t (α'_t) as mean. This additional step is done since a pedestrian is not assumed to always take the optimal route. The stochastic element allows for modelling an uncertainty that covers non-optimal or unclear decisions. In addition, the normally distributed deviation of the pedestrian from the perfect route may also represent the effects of body swaying which arise from the changing strain on the two legs.

Overall, the probability for an arbitrary angle a to be chosen as the final target direction is given by

$$p\left(a\right) = \frac{1}{\sqrt{2\pi\sigma^2}} \exp\left[-\frac{(a - \alpha_t)}{2\sigma^2}\right], \tag{3.9}$$

where the variance σ represents how large the uncertainty of the pedestrian's decision is. After this first decision in this phase, the pedestrian has obtained a target direction which is normally distributed around the optimal (intermediate) target angle α_t (α'_t). If there is no other pedestrian within the visual field, the collision avoidance decision is omitted and the target angle is set as final direction of motion for the next time step. The distance-to-collision in this direction (regarding walls) is then used as the new headway of pedestrian i:

$$\alpha_i\left(t + \Delta t\right) = \alpha_t^{\text{fin}}, \tag{3.10}$$

$$h_i\left(t + \Delta t\right) = d\left(\alpha_t^{\text{fin}}\right). \tag{3.11}$$

3.4.2 Collision Avoidance: Interaction Angle

Unaffected by the first decision, the pedestrian determines the direction for collision avoidance in a second step. The concept is based on a simple idea: angles within the visual field that are covered due to the presence of other agents are less preferable to be chosen as direction of motion than uncovered angles. Furthermore, the likelihood for an agent to walk into a certain direction decreases all the more the closer a pedestrian stands in this direction. The distance-to-collision towards pedestrians into an arbitrary direction therefore acts as a measure for the imminence of a collision and probability of this direction (see Fig. 3.7). Based on this information the angle for collision avoidance, also called 'interaction angle', can be calculated. The distance-to-collision $d(a)$ of an arbitrary angle a to all pedestrians is given by

$$d(a) = \begin{cases} \min\limits_{n} d_n & : \alpha_n^{\text{rel}} - \Delta\alpha_n \leq a \leq \alpha_n^{\text{rel}} + \Delta\alpha_n, \\ d_{\text{vf}} & : \text{else}. \end{cases} \tag{3.12}$$

In this case, the direction a is given relatively to the direction of motion α_i of the acting agent. If it points towards an area covered by another agent n, the respective distance-to-collision is equal to the relative distance to this agent as defined in Eq. (3.4). In case this area is covered by multiple agents, the final distance-to-collision is set as the minimum of the relative distances to all these agents. In turn, if a points at an angular range where no pedestrian has been perceived before, the distance-to-collision is only limited by the maximum visual range d_{vf}. A detailed description on how the distance-to-collision towards pedestrians for arbitrary angles is obtained can be found in the Appendix, Sec. B.2.2.

The distance-to-collision d_n to a pedestrian n is, excluding overlaps, a positive quantity. In addition, for all perceived pedestrians their relative distance to the perceiving agent is less or equal the maximum visual range, $d_n \leq d_{\text{vf}}$. Therefore, it holds that

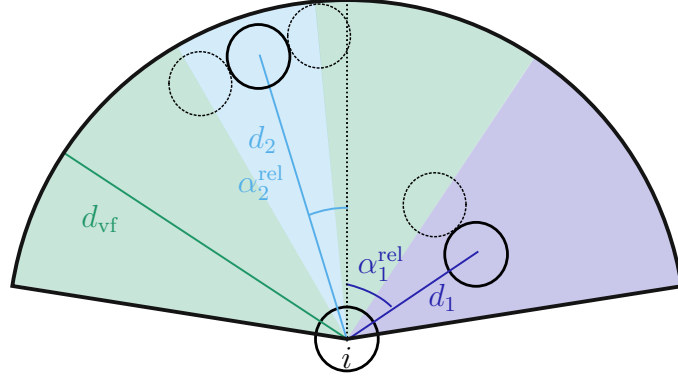$$\frac{d_n}{d_{\text{vf}}} \in [0, 1]. \tag{3.13}$$

Figure 3.7: The distance-to-collision is used to describe the likelihood of a given direction to be chosen as direction of motion: angles within free regions (green-shaded areas) are preferred over covered ranges (blue-shaded). The smaller the distance-to-collision for a given direction is, the less likely an agent will decide to go there.

This can be taken as a measure for the likelihood of a given direction a. Based on this, a probability distribution $p(a)$ for the angle a can be defined as

$$p(a) = \begin{cases} \frac{1}{c}\frac{d(a)}{d_{\mathrm{vf}}} & : |a| \leq \phi, \\ 0 & : \text{else} \end{cases} \tag{3.14}$$

with normalisation constant

$$c = \int_{-\phi}^{\phi} p(a)\,\mathrm{d}a. \tag{3.15}$$

For angular ranges that are covered by another agent, the probability is reduced correspondingly to the respective distance-to-collision d_n while it is maximum for all not-covered areas. Free areas and ranges where other pedestrians only stand far off are favoured over directions that would lead to more imminent collisions. It should be noted that $p(a)$ is only finite for directions within the visual field since the pedestrians outside are not perceived. The distribution displays the angular distribution of distances-to-collisions and can be used for calculating the final interaction angle α_{ia}. How to determine the normalisation constant c and to calculate

the angle from the probability distribution is described in the Appendix, Sec. B.3. The stochasticity that is inherent in this procedure represents again the uncertainty of human decisions. Even if it is unlikely, it is not impossible for a pedestrian to choose a disadvantageous direction during the collision avoidance process for whatever reasons. This is covered by modelling the decision process in this way. At the end of the second decision process the pedestrian has determined a direction that may help to avoid collisions with other agents in the next time step, according to the distribution and relative position of the pedestrians in the visual field.

3.4.3 Choice of the Direction of Motion

In the third decision, the agent combines the motion within the environment and within the crowd. The decisions so far have led to two independent angles α_t^{fin}, α_{ia} for reaching the target and avoiding collisions. In this step, the agent decides which one of these is chosen as final direction of motion. Again, the distance-to-collision d into both directions acts as the basis for this decision and is given as the minimum distance considering both walls and pedestrians:

$$d\left(\alpha_{\text{t, ia}}\right) = \begin{cases} d^{\text{w}}\left(\alpha_{\text{t, ia}}\right) & : d^{\text{w}} < d^{\text{p}}, \\ d^{\text{p}}\left(\alpha_{\text{t, ia}}\right) & : \text{else.} \end{cases} \tag{3.16}$$

with $d\left(\alpha_{\text{t, ia}}\right)$ the final distance-to-collision in target and interaction direction, respectively, d^{w} the distance-to-collision regarding walls and d^{p} the distance to any pedestrian in this direction. A more detailed description on how to calculate the distance towards a pedestrian for arbitrary angles is given in the Appendix, B.2.2. In order to model a pedestrian's urge to walk in an undisturbed way, the final direction of motion for the next time step is chosen to be the angle whose corresponding distance-to-collision is larger,

$$\alpha_i\left(t + \Delta t\right) = \begin{cases} \alpha_t^{\text{fin}} & : d\left(\alpha_t^{\text{fin}}\right) > d\left(\alpha_{\text{ia}}\right), \\ \alpha_{\text{ia}} & : \text{else.} \end{cases} \tag{3.17}$$

The headway $h_i\,(t + \Delta t)$ for the next time step is then the corresponding distance-to-collision of the final direction of motion,

$$h_i\,(t + \Delta t) = d\,(\alpha_i\,(t + \Delta t))\,.\tag{3.18}$$

3.4.4 Determination of Speed

Having determined the direction of motion for the next time step, the agent i has to calculate the speed s_i, the absolute value of the velocity, to complete the decision process. Here, the SHDV model [102, 119, 120] is used (see also Sec. 2.3). It defines a pedestrian's speed as a linear function of its headway. In this model, the distance-to-collision $h_i = h_i\,(t + \Delta t)$ for the chosen direction of motion is used as the input parameter:

$$s_i\,(t + \Delta t) = \begin{cases} 0\,\mathrm{m/s} & : h_i \leq d_\mathrm{S}, \\ \alpha_\mathrm{S}\,(h_i - d_\mathrm{S}) + v_\mathrm{min} & : d_\mathrm{S} < h_i < d_c, \\ v_\mathrm{max} & : d_c \leq h_i. \end{cases}\tag{3.19}$$

As in the original model, the speed is zero below a lower threshold d_S, increases linearly with h_i above this threshold and reaches the free-flow velocity v_max if h_i is equal to or greater than an upper threshold d_c. Additionally, the slow-to-start rule is included: if a pedestrian has had speed zero in the previous time step, it keeps this velocity with a probability p_0, otherwise the speed determined by Eq. (3.19) is accepted. This mechanism is crucial for the emergence of stop-and-go waves as it stabilises spontaneous jams by reducing the outflow of the pedestrians.

The determination of the speed is the fourth decision and terminates the decision phase.

3.5 The Movement Phase

The movement phase ends the modelled process which is now collision-free. Based on the direction of motion $\alpha_i\,(t + \Delta t)$ and the corresponding speed $s_i\,(t + \Delta t)$, the

position of pedestrian i for the next time step $t + \Delta t$ is calculated:

$$x_i \left(t + \Delta t\right) = x_i(t) + \cos\left(a_i \left(t + \Delta t\right)\right) s_i \left(t + \Delta t\right) \Delta t$$
$$y_i \left(t + \Delta t\right) = y_i(t) + \sin\left(a_i \left(t + \Delta t\right)\right) s_i \left(t + \Delta t\right) \Delta t. \tag{3.20}$$

In addition, if the situation requires, e.g. for motion in systems with periodic boundary conditions, the target coordinates are updated correspondingly to the new positions or orientations.

The procedure presented above describes the basic idea of the model. As it will be shown in Ch. 4, the decision process and the model parameters have to be adjusted for the particular scenario in order to obtain realistic results. In particular, the decision on the final direction of motion depends on the simulated situation. Moreover, additional concepts like body rotation must be included especially for evacuation (Sec. 4.3) and bidirectional flow (Sec. 4.4).

Modelling Results

In this chapter, the new model approach is applied to typical scenarios of pedestrian dynamics in order to validate the model dynamics and calibrate the model parameters. By comparison to experimental data, it should be assessed whether the model is able to reproduce realistic pedestrian behaviour qualitatively and quantitatively. Optimising the parameters and the dynamics of the model may give insight into the cognitive and decision-making mechanisms of walking pedestrians. The considered scenarios include simple collision avoidance in one-on-one situations, single-file motion, evacuations and bidirectional motion in a corridor.

Several model parameters are set globally and valid for every scenario that is simulated. This involves the radius of a pedestrian, $r = 0.15\,\mathrm{m}$, and the range $d_{\mathrm{vf}} = 8.0\,\mathrm{m}$ and expanse $2\phi = 170°$ of the visual field. These parameters are equal for all agents and constant in time.

4.1 Collision Avoidance Behaviour

In order to assess the mechanisms for collision avoidance implemented in the model different one-on-one situations were considered. Here, up to two pedestrians act

and react to each other without any influence by the environment or another group of agents. In this section four scenarios are described: a pedestrian heading up to a standing agent ('Standing'), two pedestrians approaching one another ('Walking'), two agents that cross each other's path while walking diagonally through the room ('Diagonal') and, finally, two agents that walk next to each other in opposite directions ('Next'). All scenarios are set in a square room of $20\,\text{m} \times 20\,\text{m}$ in which the pedestrians are placed in such that the main encounter of the agents occurs in the middle of the room. Therefore, any influence of the walls on the agents' collision avoidance behaviour should be excluded. The main direction of motion of the pedestrians in the different scenarios is preset by the choice of target coordinates for every agent.

At the beginning, the remaining parameters in the model are set to the values used in the original SHDV model [102, 119, 120], i.e. $\Delta t = 0.3\,\text{s}$, $\alpha_\text{S} = 0.5\,1/\text{s}$, $v_\text{min} = 0.1\,\text{m/s}$, $v_\text{max} = 1.2\,\text{m/s}$ and $p_0 = 0.5$. However, since the SHDV model considers point-like particles rather than extended circular pedestrians like this model, the lower threshold d_s of the SHDV model is reduced according to the pedestrians' radius: $d'_\text{s} = d_\text{s} - 2r = 0.4\,\text{m} - 2 \cdot 0.15\,\text{m} = 0.1\,\text{m}$. In doing so, the distance between the centres of two pedestrians corresponds to the distance as it is measured in the original SHDV model.

Fig. 4.1(a) shows three realisations of the first scenario, 'Standing', in which an agent encounters a pedestrian standing in the middle of the room (lilac-coloured circle). The agent walks bottom up from the starting point $(10.0\,\text{m}, 1.0\,\text{m})$ towards the target at $(10.0\,\text{m}, 19.0\,\text{m})$. The resulting trajectories for the different runs are shown by the blue and green lines. For all three runs, they partially display large fluctuations in the direction of motion. In this regime the walking pedestrian has detected its opponent and uses the collision avoidance procedure. Due to the stochastic nature of this mechanism, the trajectories show many changes in the direction of motion. Some fluctuations are so distinct that the walking agent does not stay on one side with respect to the standing pedestrian, see e.g. the bright-blue trajectory. In contrast, there are also two segments of the trajectories
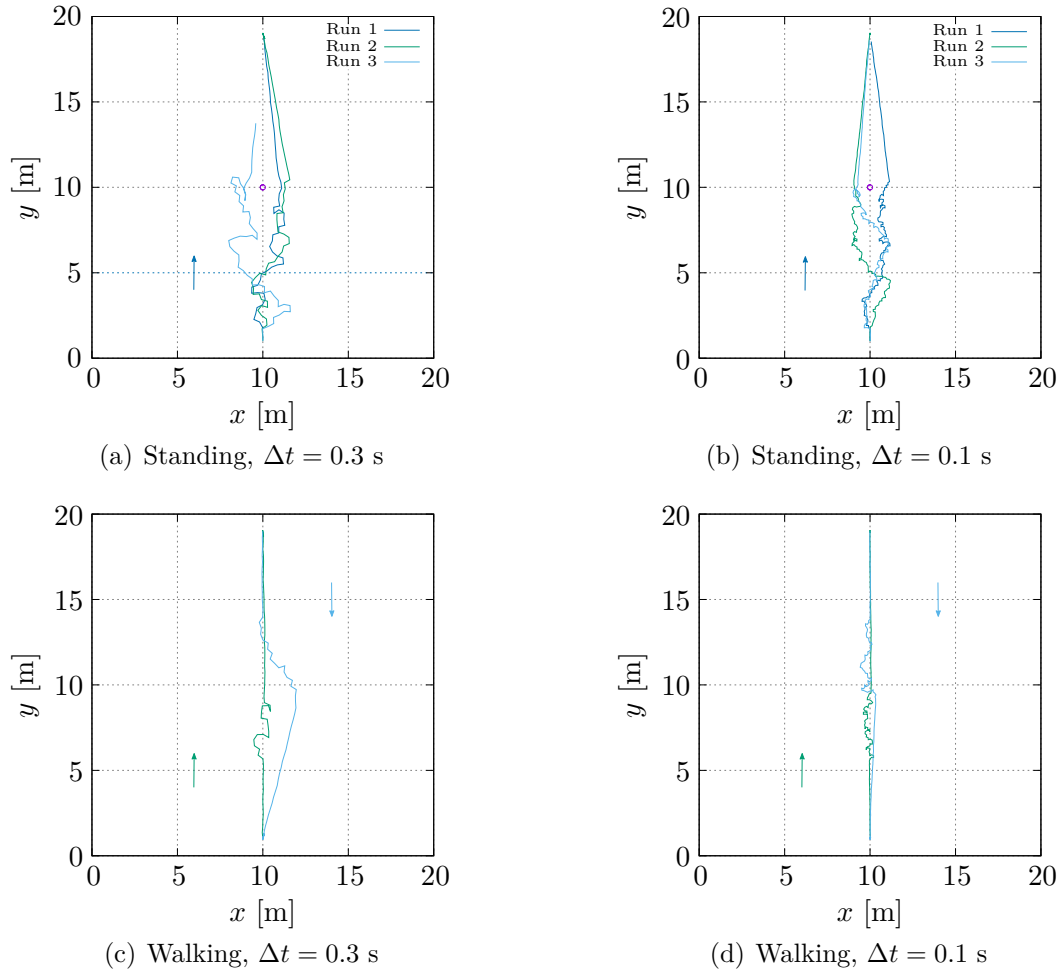
Figure 4.1: Trajectories of the collision avoidance behaviour for different scenarios (the general direction of motion is indicated by the arrows). Due to the underlying stochasticity, fluctuations occur during the interaction that are reduced using a smaller time step. Nevertheless, for the 'Walking' scenario, a larger time step leads to more realistic results.

that seem to be smoother: the very short segment at the beginning of the motion represents the time steps in which the standing opponent has not been detected yet, the segments starting at the level of the standing pedestrian display the phase in which the standing agent has already been passed and does no longer lie within the

visual field. In both stages, the walking agent is able to focus on reaching its target. Stochastic fluctuations due to the Gaussian distribution are not as significant as in the interaction regime due to the comparatively small variance $\sigma = 0.05\,\mathrm{m}$. Taken together, it is shown that the walking agent, as soon as it has registered the presence of another pedestrian, starts to react and change its direction of motion. In doing so, it passes the pedestrian at a lateral distance of approximately 1-2 m and focuses then again on its target.

As for the modelling of more complex situations in the further course a smaller time step $\Delta t = 0.1\,\mathrm{s}$ is used, the two-person interaction as described above is also regarded in this case. The result for 'Standing' is shown in Fig. 4.1(b). In comparison to the result for $\Delta t = 0.3\,\mathrm{s}$, it can be seen that the fluctuations of the trajectories are smaller, simply because the agent does not have enough time to walk a larger distance before the next change of the direction of motion occurs. However, the overall progress of the curves does not differ significantly in both cases. This is different when considering two walking pedestrians that approach one another. In Fig. 4.1(c) the green trajectory represents an agent walking from the bottom up, whereas the blue trajectory displays the path of the other pedestrian walking from the top down. The starting points and the targets of both agents lie at one level. Here, the time step is $0.3\,\mathrm{s}$. It can be seen that the pedestrian coming from the top (blue) changes its direction of motion significantly in order to elude the opponent agent. In contrast, this pedestrian merely deviates from the ideal route. After a short phase of orientation, represented by the segment with larger fluctuations, the agent coming from the bottom (green) is able to walk with little interference since the other pedestrian has already made way. However, the collision avoidance is different when reducing the time step Δt (see Fig. 4.1(d)). Because the pedestrians change their direction of motion more often during the interaction, they are not able to create sufficient space between each other and almost collide. During one time step, the distance covered by an agent is not that large that the current situation changes significantly. Therefore, the stochastic process of the interaction leads to a trajectory fluctuating around the direct route towards the target, but not to a

realistic avoidance behaviour. In contrast to the case of one of the agents standing still, both agents have to react on the current dynamics of the opponent. As the current position and direction of motion permanently change, the pedestrians are not able to recognise a clear preference of the opposite agent and therefore cannot decide which side to choose for collision avoidance. For the larger time step, the pedestrians travel a sufficiently large distance in one step to react appropriately. It can be followed that dynamics using $\Delta t = 0.3\,\text{s}$ produces more realistic results.

Nevertheless, even the simulations with $\Delta t = 0.3\,\text{s}$ may obtain unrealistic results due to the underlying stochastic process, see e.g. Fig. 4.2(a). Here, the agents start to evade, but the pedestrian coming from the top (blue) takes a 'wrong' decision and starts to walk again towards the middle of the room. This changes the situation for both agents since they now have to solve the conflict over a shorter distance. As the pedestrians try to avoid the collision, they misjudge the motion of the opposite agent, cannot react appropriately and almost collide. This behaviour is again caused by the stochastic interaction mechanism where unlikely and disadvantageous choices of the direction of motion are not excluded. Nonetheless, near collisions when two pedestrians have to avoid each other in limited space thoroughly occur also in the real world. Therefore, occasional, non-perfect collision avoidance is not fully unrealistic.

For two pedestrians crossing the room diagonally, the modelling results show mostly realistic collision avoidance behaviour, but also occasional unrealistic trajectories. In Fig. 4.2(b), the agent coming from the bottom left and walking towards the upper right corner of the room (green trajectory), eludes its opponent which is able to walk in an almost undisturbed way. This behaviour is consistent with the expectations. In contrast, the trajectories shown in Fig. 4.2(c)) display a detour of one of the agents which clearly is not an appropriate representation of a pedestrian's walking behaviour. It is probably a consequence of a series of 'wrong' decisions on the interaction angle that leads to the reacting pedestrian having the opponent on its right side instead of its left side as before. In seeking to avoid a collision with its opponent, the pedestrian is in a self-enhancing situation: the more to the right

(a) Walking, $\Delta t = 0.3$ s, near collision

(b) Diagonal, $\Delta t = 0.3$ s

(c) Diagonal, $\Delta t = 0.3$ s, with detour
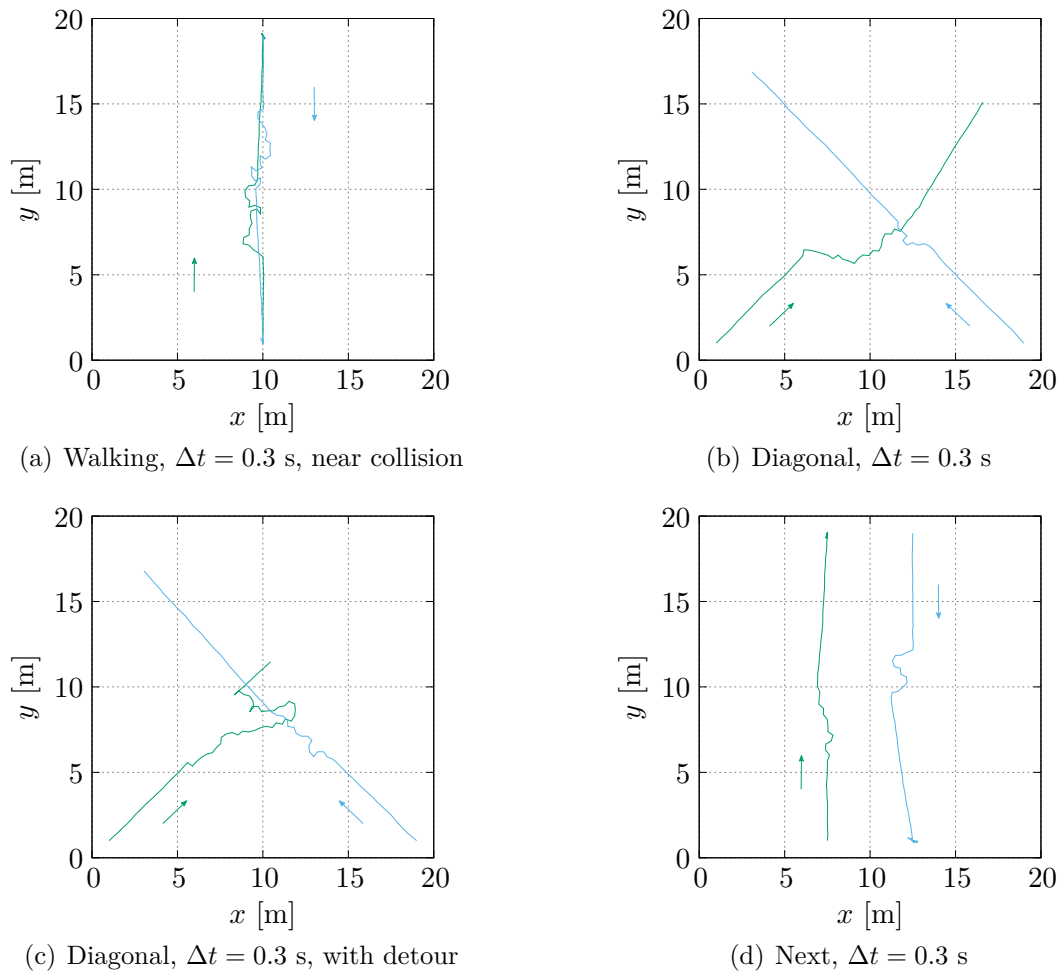

(d) Next, $\Delta t = 0.3$ s

Figure 4.2: The collision avoidance mechanism is able to reproduce realistic behaviour also for a diagonal crossing of two agents (see (b)). However, the underlying stochasticity also causes near collisions (as in (a)) or unrealistic avoidance manoeuvres as in (c). In (d), the agents react on each other's presence without need.

the other agent is perceived the more likely it is for the agent to turn to the left. Not until the other pedestrian is out of sight the agent is able to focus again on its goal and to move in target direction. In this case, the stochasticity leads to an unrealistic choice of the direction of motion.

In the fourth scenario two pedestrians walk in opposite directions but their starting points and targets have a distance of five metres. Therefore, the agents can directly reach their targets and a collision is not expected to happen. As a consequence, both pedestrians should walk in an undisturbed way. However, as it can be seen in Fig. 4.2(d), the trajectories show fluctuations in certain segments indicating that the agents have chosen the interaction angle instead of the target angle as direction of motion. Both pedestrians reacted to the presence of the other agent without any need since their motion towards their target would not have been affected. Of course, this behaviour is totally unrealistic. It is caused by a misjudgement during the model development process. As explained in Sec. 3.4.3, as final direction of motion the angle for which the respective distance-to-collision is larger is chosen. To be more precise, Eq. (3.17) states that $\alpha_i\left(t + \Delta t\right) = \alpha_{\mathrm{t}}^{\mathrm{fin}}$, if $d\left(\alpha_{\mathrm{t}}^{\mathrm{fin}}\right) > d\left(\alpha_{\mathrm{ia}}\right)$, that means that the agent chooses to walk into the target direction only if the distance-to-collision for the interaction angle is smaller. In case of both distances to be equal, the interaction angle is taken as direction of motion. This emphasises the interaction and collision avoidance behaviour which seemed to be reasonable during the model development when thinking of dense crowds and an urgent need to avoid collisions. However, in the scenario described above, the distances-to-collision in interaction and target direction are also equal: since the room is sufficiently large, the distances-to-collision considering walls is equal to the maximum visual range for both angles. There is only one other agent in the room, so it is highly likely to choose an interaction angle that leads towards free space. In this case, the distances-to-collision considering pedestrians is also equal to the maximum visual range. As a consequence, the distances for both interaction and target angle are equal and the agent chooses to use the interaction angle. This problem is solved if Eq. (3.17) is slightly rewritten, replacing 'greater' by 'greater or equal to',

$$\alpha_i\left(t + \Delta t\right) = \begin{cases} \alpha_{\mathrm{t}}^{\mathrm{fin}} & : d\left(\alpha_{\mathrm{t}}^{\mathrm{fin}}\right) \geq d\left(\alpha_{\mathrm{ia}}\right), \\ \alpha_{\mathrm{ia}} & : \text{else.} \end{cases} \tag{4.1}$$

53

An agent now chooses to go also in target direction if the distance-to-collision for the target and interaction angle is equal. This sets priorities for reaching the goal instead of interacting and avoiding collisions.

Fig. 4.3 shows the simulation results for the one-on-one scenarios using Eq. (4.5). It can be directly seen from Fig. 4.3(d), that in the 'Next' scenario, both trajectories do not show any fluctuations indicating an evasion manoeuvre, that means that the pedestrians stay focussed on their respective target. This change in the dynamics also has an impact on the results in the other three scenarios. In all simulations, $\Delta t = 0.3\,\mathrm{s}$ was used. In comparison to the previous results a focus on the agent's target reduces the fluctuations of the trajectories. The agent chooses less often to interact rather than to go towards the target. However, therefore the collision avoidance can be seen less distinctly in the trajectories than in the previous case because the agents pass each other with a smaller distance. For the diagonal crossing, the agents react late and occasionally almost collide (see Fig. 4.3(c)). Of course, reduced avoidance behaviour also leads to less unwanted, large changes of the direction of motion as they were observed previously (see e.g. Fig. 4.1(a) or 4.2(c)). In total, shifting the focus towards the target direction has a similar impact to introducing some kind of inertia in these special situations. The agents reach their targets with minimal effort for interacting and collision avoidance and the deviations from the ideal route are smaller compared to the case described above. Once the pedestrians find themselves in a configuration in which every participant is able to reach its personal target without further changes, they neglect the presence of the other agent.

Taking all four scenarios together, introducing the reworking in Eq. (4.5) leads to more realistic results in terms of large fluctuations, turnarounds or unnecessary interactions. Minor fluctuations can be observed nonetheless. It should be noted, however, that the trajectories represent concrete realisations of a stochastic process and therefore also show deviations from the optimal route that are inherent to this mechanism. Usually, averaging is an appropriate and effective way to handle fluctuating values. However, an 'averaged trajectory' would only state a path somewhere

(a) Standing, $\Delta t = 0.3$ s

(b) Walking, $\Delta t = 0.3$ s

(c) Diagonal, $\Delta t = 0.3$ s
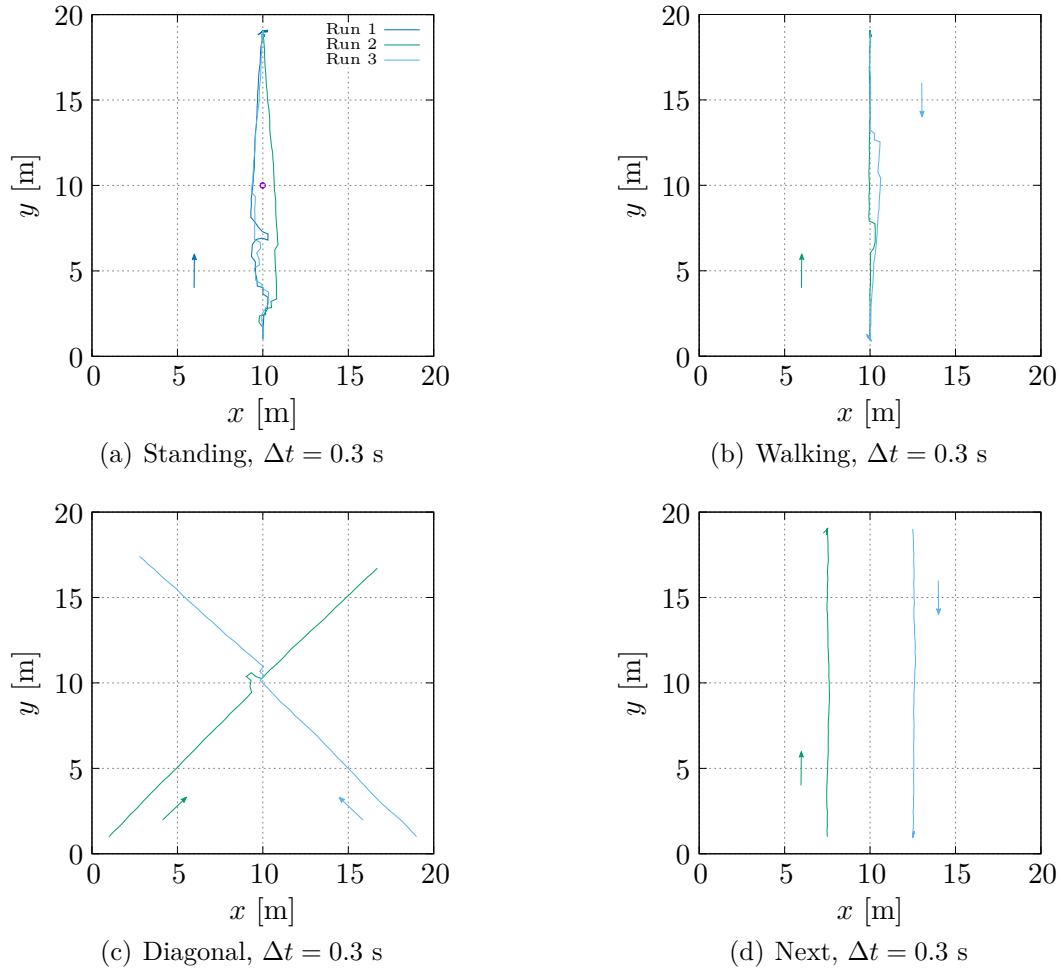
(d) Next, $\Delta t = 0.3$ s

Figure 4.3: Focussing on the target direction reduces unnecessary changes of the direction of motion and fluctuations. As soon as the agents have found a configuration in which both can reach their goal in an undisturbed way, they neglect the presence of the other.

in between the simulated trajectories that does not have any 'real' equivalent. This would not be sufficient to assess the concrete interaction procedure and exclude unrealistic movements or collisions so that the trajectories shown here answer the purpose intended.

Despite the fluctuations there is another aspect shown in the trajectories that may

not meet the expectations from the real scenario. Considering especially the 'Standing' situations, one can see that the agent's interaction mechanism is restricted to the visual field. As can be seen from Fig. 4.1(a), 4.1(b) and 4.3(a), the walking agent first moves shortly towards its target before the other pedestrian is recognized and the evasion starts, caused by the limited range of the visual field. This does not need to be consistent with reality: on the one hand, in an empty room like this, another pedestrian is probably perceived at a larger distance than 8 m. On the other hand, it is not known whether the distance real pedestrians start to interact is equal to the sight distance. If scenarios in free space like these are simulated with this model, the coherence between visual perception and interaction should be kept in mind.

All things considered, this model is able to produce a collision avoidance behaviour that approximates the behaviour of real pedestrians appropriately.

4.2 Single-File Motion

As mentioned before, the SHDV model [102, 119, 120] was developed in order to reproduce the characteristic pedestrian dynamics of one-dimensional single-file motion. Since the model acts as a basis for the approach presented in this work, the new model should also be able to reproduce pedestrian single-file motion despite its two-dimensional nature. Investigating this scenario allows for the measurement of two basic quantities: the fundamental diagram which shows if the model dynamics leads to a reasonable relation of velocity or flow and density, and the phase separation of the system into slowly walking and standing agents which is distinctive for single-file motion of pedestrians.

The simulations are performed similarly to the investigations done with the original SHDV model. The system involves a corridor of length $L = 26.0$ m and width $B = 0.8$ m. Using periodic boundary conditions, the pedestrians are assumed to walk on a closed course and the number of agents in the system is conserved. The general direction of motion is determined by the agents' target coordinates which

are given by $x_{t,i}(t+\Delta t) = x_i(t) + 5.0\,\text{m}$ and $y_{t,i}(t+\Delta t) = \frac{1}{2}B$. The pedestrians walk in positive x-direction while trying to stay in the middle of the corridor. In contrast to the SHDV model which uses genuine one-dimensional motion, the corridor has a finite width and allows two-dimensional movement. It is assumed, however, that the main direction of motion of the agents is along the corridor.

The modelling results are compared to experimental single-file motion data from laboratory experiments performed in 2005 and 2006 [160, 161]. Both sets contain data from single-file motion in a circular set-up. In both cases, the number of pedestrians was varied in order to investigate the influence of density on the dynamics. The experiments as well as their analysis are described in greater detail in [45, 46, 95].

The experimental runs were started distributing the participants almost uniformly in the experimental set-up [46]. In order to approximate the experiment, so-called almost homogeneous initial conditions as described in [102, 120] were used. The pedestrians are distributed homogeneously in the corridor. Then, every agent is slightly shifted since a perfectly uniform distribution of the pedestrians is unrealistic and can lead to unwanted absorbing states during the simulation [120]. The size of the shift is determined by a Gaussian distribution which is cut off for higher values in order to prevent overlapping of the agents.
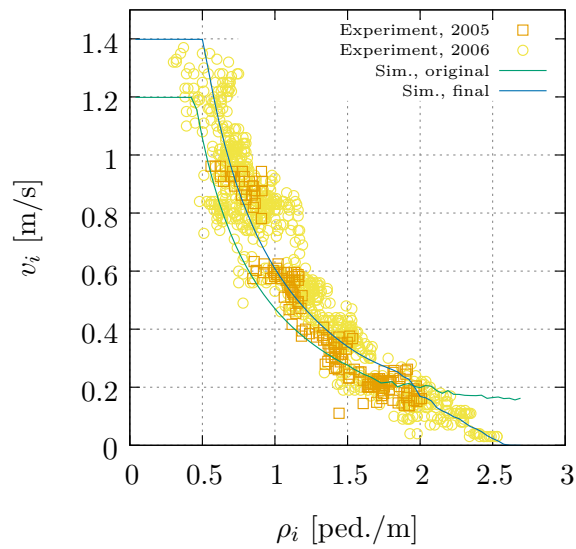
4.2.1 Fundamental Diagram

The fundamental diagram is one of the most important quantities of pedestrian dynamics and can be used to describe the general walking behaviour of agents in the respective situation. Therefore at this point it is used to calibrate the model parameters for single-file motion. Here, the fundamental diagram is understood as the relation of velocity and density in the stationary state of the system. Due to the different concepts of determining these quantities for pedestrian motion, the appearance of the fundamental diagram also depends on the choice of the measurement methods for both velocity and density. In this chapter, it is resorted to two different concepts. For the *global* fundamental diagram density and velocity are

averaged over time and the number of pedestrians whereas individual densities and velocities are included in the *local* diagram. While the global fundamental diagram shows the general behaviour of the entire system, the relation of the local quantities allows insight into the individual behaviour. Phase separation and the formation of jams is represented by two branches of the velocity at high densities in the local fundamental diagram. While one part of the pedestrians stands still ($v_i = 0\,\mathrm{m/s}$), the other pedestrians have a finite, small velocity. This effect cannot be observed in the global diagram due to averaging. An elaboration of the determination of velocity and density using the different concepts is given in the Appendix, Ch. C. It should be noted that in the analysis of the simulated as well as the experimental data density and velocity are calculated for one dimension, i.e. always along the corridor (in x-direction), despite the two-dimensional nature of the model. It is assumed that the main direction of motion in single-file motion is along the corridor and that perpendicular movements can be neglected.

All simulations were performed for a total simulation time $T_{\mathrm{sim}} = 1100\,\mathrm{s}$. In order to ensure the system to be in a stationary state, fundamental diagrams were measured for the last $100\,\mathrm{s}$, this follows the analysis in [102, 120], where this value was chosen comparable to the measurement times in the experimental data basis. The maximum number of agents used in the simulations was $N = 70$; global measurements were done with 10 simulation runs for each density.

Fig. 4.4 shows the modelling results for the global and the local fundamental diagram as well as the corresponding experimental data. The green curve in Fig. 4.4(a) shows the global fundamental diagram obtained by using the original parameter set as in the basic SHDV model or the two-person-interaction scenario described in Sec. 4.1 ($\Delta t = 0.3\,\mathrm{s}$, $v_{\mathrm{min}} = 0.1\,\mathrm{m/s}$, $v_{\mathrm{max}} = 1.2\,\mathrm{m/s}$, $\alpha_{\mathrm{S}} = 0.5\,\mathrm{1/s}$, $d_{\mathrm{S}} = 0.1\,\mathrm{m}$ and $p_0 = 0.5$). In contrast, the blue curve in Fig. 4.4(a) and the blue points in 4.4(b) show the simulation results for which some of the parameters and the modelled decision processes were optimised in comparison to the experimental data considering both the global and the local fundamental diagram. In doing so, the maximum speed was increased to $v_{\mathrm{max}} = 1.4\,\mathrm{m/s}$, the slope of the velocity-headway relation

(a) Global fundamental diagram
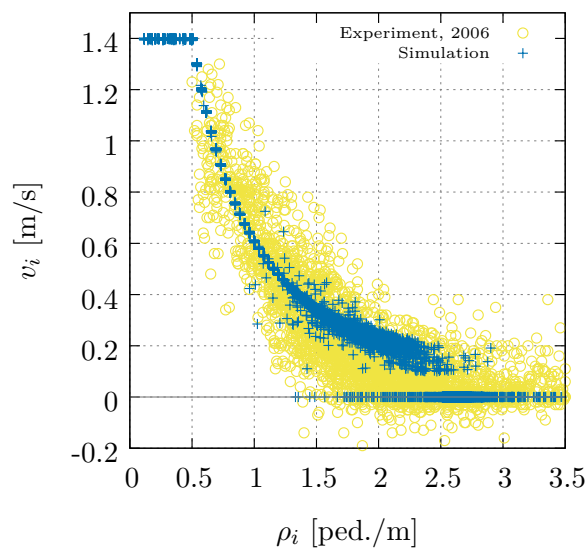
(b) Local fundamental diagram

Figure 4.4: Global and local fundamental diagram for single-file motion comparing simulated and experimental data. The green global curve represents the result for the original parameter set, the blue one shows the results for the optimised set which fits the experimental data better. The optimised local diagram also shows good agreement with the experiments.

was set to $\alpha_{\mathrm{S}} = 0.65\,1/\mathrm{s}$ and the stopping probability was also increased to $p_0 = 0.6$. In addition, the criterion for the third step in the decision-making phase, when the agent has to choose between target and interaction angle, was adjusted. Additional to using the direction providing the larger distance-to-collision, a pedestrian now decides to walk also towards its target if the interaction angle would lead to a deviation from the desired direction of motion greater than approximately 37°. Whereas the curve of the simulations with the original parameters shows large deviations from the experimental result, the modelling results using the optimised parameter set fit well to the experimental data and display the expected progress which strongly resembles the behaviour of the SHDV model [102, 120]. For low densities up to $\rho_i = 0.5\,1/\mathrm{m}$ the velocity is constant and corresponds approximately to the maximum velocity. In this density regime, the pedestrians' motion is not affected by the presence of other agents, and they can walk with their desired free-flow speed. Considering intermediate densities, $0.5\,1/\mathrm{m} \leq \rho_i \leq 1.8\,1/\mathrm{m}$, the walking speed of the agents is influenced by the others. The pedestrians distribute uniformly over the system, and the headway h_i between the agents depends on the global density ρ_i: $h_i = 1/\rho_i$ which gives the mean free space available for a pedestrian. In this regime, the speed depends linearly on the headway and therefore on the reciprocal global density:

$$v_i(h_i) = \alpha_{\mathrm{S}}\,(h_i - d_{\mathrm{S}}) + v_{\min} = \alpha_{\mathrm{S}} h_i + \text{ const.} = \alpha_{\mathrm{S}} \frac{1}{\rho_i} + \text{ const.} \qquad (4.2)$$

Therefore, the velocity-density curve shows a reciprocal relation in this intermediate regime. At first, the headways are large enough to prevent the agents from stopping, so the behaviour of the system is fully deterministic in terms of the determination of the speed (i.e. neglecting stochastic elements newly added in this model like the Gaussian distribution for the target angle). The global fundamental diagram shows a very smooth progress, and even for the local diagram, there are only few fluctuations in the individual velocity up to a density of $1.4\,1/\mathrm{m}$. For $1.4\,1/\mathrm{m} \leq \rho_i \leq 1.8\,1/\mathrm{m}$, there are first indications for jamming and a phase transition of the system visible in the local fundamental diagram. Few of the pedestrian have

already stopped ($v_i = 0 \, \text{m/s}$), while the others are able to walk with a higher velocity $v_i = 0.2 - 0.4 \, \text{m/s}$. The fluctuations in the velocity become larger due to the initiating influence of the slow-to-start-rule with the stopping probability p_0. Because of this stochastic influence by standing pedestrians, the headways are not as uniform as before, and the agents have to adjust their speeds. However, the effect is still not large enough to be significant even in the averaged global fundamental digram. For densities larger than $\rho_i = 1.8 \, 1/\text{m}$, the system is in a 'congested state' [120] where the motion of the agents is strongly influenced by the other pedestrians. The stochastic process is dominant which leads to a point cloud in the local fundamental diagram and a change in progress of the global curve. Since the number of pedestrians with a velocity zero increases strongly, the averaged velocity decreases now linearly with increasing density until it reaches $v_i = 0 \, \text{m/s}$ at $\rho_i \approx 2.6 \, 1/\text{m}$.

In order to reach this agreement with the experimental data, adjustments of the parameters $v_{\max}$, α_{S} and p_0 as well as of the third decision were necessary. In the following, each of these adjustments will be considered in greater detail and assessed whether this can give insight into the walking behaviour and the way of decision-making of pedestrians.

At high densities, the global fundamental diagram measured with the 'original' parameters deviates strongly from the experimental data. Instead of following the general behaviour and reaching $v_i = 0 \, \text{m/s}$ at some point, the curve strongly flattens and becomes almost constant for $\rho_i \approx 2.5 \, 1/\text{m}$ despite minor fluctuations. This behaviour is not realistic for single-file motion and also does not occur in the results of the SHDV model. In fact, it is a consequence of the two-dimensional nature of this new approach. For lower densities, an agent's final direction of motion is mostly given by the direction towards the target because the distance-to-collision is significantly larger than the distance-to-collision of the interaction angle. In terms of collision avoidance, a pedestrian tries to evade its predecessors, but due to the narrow corridor the direction for avoidance always points directly towards a wall. As a consequence, the distances-to-collision for interacting are always smaller than the

distances towards the target. However, with an increasing number of pedestrians in the system, the distance-to-collision in target direction becomes smaller. At higher densities the system reaches a point where this distance becomes even smaller than the distance-to-collision of the interaction direction. Since a pedestrian chooses the direction which provides the larger distance-to-collision, the agents start to elude. This leads to a kind of zipper effect: the pedestrians start to shift their position in y-direction perpendicular to the general direction of motion in order to use the accessible space as optimally as possible. For the corridor width of $B = 0.8\,\text{m}$ and the diameter of a pedestrian of $2r = 0.30\,\text{m}$ it is even possible for the agents to stand next to each other. In this case, the distance-to-collision into the target direction increases again since the agent aims at the 'free' space next to its predecessor. Especially considering the included anticipation, a balanced configuration can appear which leads to low, but constant and finite velocities for all pedestrians. Thereby, the decrease in velocity that would be expected is shifted to even higher densities that do not allow for a more efficient use of the available space. Such a zipper effect has been observed for example in bottlenecks whose capacity increases linearly with the bottleneck width due to this effect [23, 27]. However, it is excluded in single-file motion by definition. In the experiments, the participants were told not to pass [46]. Therefore, they obviously decided not to use the space optimally, but to follow the instructions and keep the single-file configuration. Such a global knowledge of the intention of the scenario or concious decision not to optimise the personal motion is not included in the model so far. Therefore, another criterion was added to the decision on the final direction of motion: the agent decides to choose the target direction if the distance-to-collision into this direction is greater or equal to the distance-to-collision for interaction or if the interaction direction would lead to a deviation from the optimal desired direction larger than $37°$. In this case, the optimal target direction is $\alpha_t^{\text{ideal}} = 0°$, and the additional restriction can be rewritten as $|\alpha_{\text{ia}} - \alpha_t^{\text{ideal}}| > 37°$ or $\cos(\alpha_{\text{ia}}) < 0.8$[1].

---

[1]In Fig. 4.5(a) this is stated the other way round for reasons of clarity, e.g. the bright-blue curve represents a simulation for which the choice of the interaction angle was restricted to $\cos(\alpha_{\text{ia}}) \geq 0.8$.

Therefore, it follows for the third decision that

$$\alpha_i\left(t + \Delta t\right) = \begin{cases} \alpha_{\mathrm{t}}^{\mathrm{fin}} & : \left[d\left(\alpha_{\mathrm{t}}^{\mathrm{fin}}\right) \geq d\left(\alpha_{\mathrm{ia}}\right)\right] \quad \vee \quad \left[\cos\left(\alpha_{\mathrm{ia}}\right) < 0.8\right], \\ \alpha_{\mathrm{ia}} & : \text{else.} \end{cases} \tag{4.3}$$

Fig. 4.5(a) shows the influence of different thresholds on the progress of the fundamental diagram. The measurement with no restriction strongly deviates from the expectations and the experimental data. Even if the interaction angles are restricted to $\cos\left(\alpha_{\mathrm{ia}}\right) \geq 0.5$, the zipper effect has a significant impact. For $\cos\left(\alpha_{\mathrm{ia}}\right) \geq 0.8$, which was used for the final simulations, the fundamental diagram fits well to the experimental data. Further restrictions do not lead to corresponding improvements as can be seen from the lilac-coloured curve for $\cos\left(\alpha_{\mathrm{ia}}\right) \geq 0.9$. In order to maintain as much freedom of choice as possible and to not infer with the model dynamics too much, the threshold was set to 0.8 as described above. It represents global, abstract knowledge of the pedestrians that overtaking and standing next to each other should be omitted. The prioritisation of the agents shows that they accept lower velocities and stand still in order to keep the requested single-file configuration. It also indicates that the application of two-dimensional dynamics on one-dimensional scenarios is a non-trivial problem and may require further restrictions. This should be particularly considered for validation purposes.

The high-density regime of the fundamental diagrams is also influenced by the value of the stopping probability p_0 that is used for the slow-to-start rule in the decision on the speed. This parameter determines the value of the densities at which some pedestrians stand still and the congested phase starts. Its impact on the global fundamental diagram is not as significant as in the local diagram due to the averaging. In Fig. 4.5(b) it can be seen that an increasing stopping probability shifts the change in the slope of the curve towards smaller densities and that the velocity for a fixed density also decreases with an increasing p_0. Whereas the curve for the original parameter $p_0 = 0.5$ lies at the upper edge of the experimental data, the fit becomes better with larger p_0 in terms of the relative position of the simulated

(a) Influence of the decision process

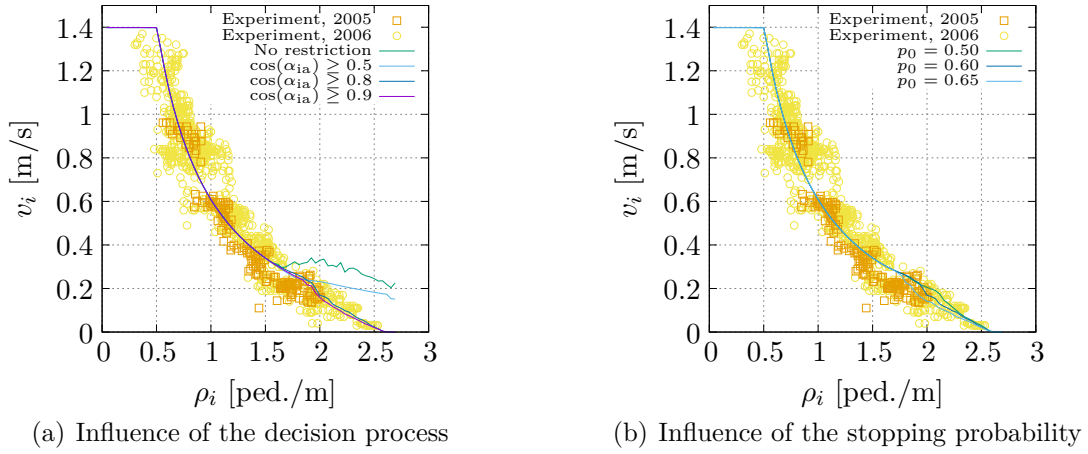(b) Influence of the stopping probability

Figure 4.5: Influence of the decision process and the stopping probability on the global fundamental diagram at higher densities. The restriction of the interaction angles prevents the occurrence of zipper effects and maintains the single-file configuration; with an increasing p_0 jamming starts at lower densities and the average velocity is decreased for a specific density.

curve and the empirical data. Considering only the global fundamental diagram, $p_0 = 0.65$ provides the best results of all three curves that are shown. However, when considering the local fundamental diagrams for $p_0 = 0.5$ and $p_0 = 0.65$ in Fig. 4.6(a) and 4.6(b), respectively, it is shown that both results do not represent these experimental data as well as the curve for $p_0 = 0.6$ (see Fig. 4.4(b)). The branch at $v_i = 0\,\mathrm{m/s}$ which represents the standing pedestrians in the jam, respectively the phase transition into standing and walking agents of the system, starts at too high densities for $p_0 = 0.5$ and at too low values of ρ_i for $p_0 = 0.65$. In contrast, for $p_0 = 0.6$ the jamming phase seems to start similarly in the simulations compared to the experiments. Therefore, the value for the stopping probability seems to be the best compromise in order to describe the global as well as the local fundamental diagram. An increasing p_0 also has an impact on when statistical fluctuations in the velocity start to appear. However, even if the local fundamental diagram for $p_0 = 0.65$ shows significantly more outliers in the speed, all data points overlap
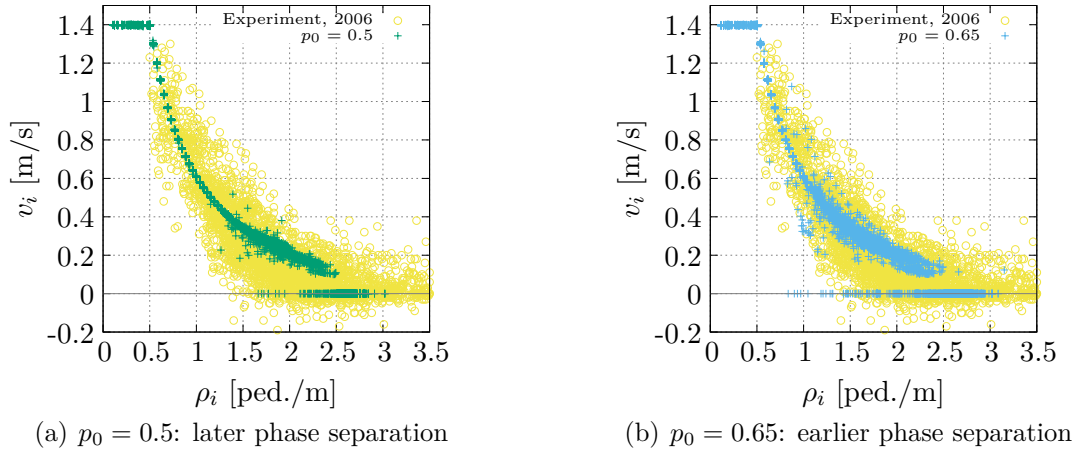
(a) $p_0 = 0.5$: later phase separation

(b) $p_0 = 0.65$: earlier phase separation

Figure 4.6: Local fundamental diagrams for $p_0 = 0.5$ and $p_0 = 0.65$. The value of the stopping probability influences the start of the congested state and the phase transition. For $p_0 = 0.5$, it starts at too high, for $p_0 = 0.65$ at too low densities.

with the point cloud representing the experimental data. One can therefore not draw any conclusions in terms of parameter optimisation based on this criterion and has to stick to the phase separation and jamming phenomenon.

The second parameter that was adjusted during the calibration process is the slope of the velocity-headway relation in the determination of speed, α_S. For intermediate densities, the velocity is mainly determined by the relation Eq. (4.3) that was already discussed above. Here, α_S acts as proportionality constant between the velocity v_i and the reciprocal density $1/\rho_i$. It therefore influences the slope of the curve and represents the pedestrians' urge to follow their predecessors and how strongly they adjust their speed according to the distance to the agents walking in front. The higher α_S is, the faster an agent follows and reacts to velocity changes of the others.

The impact of α_S on the global fundamental diagram is shown in Fig. 4.7(a). Whereas the curve for the original value $\alpha_S = 0.5 \, 1/s$ lies on the lower edges of

(a) Influence of slope α_S
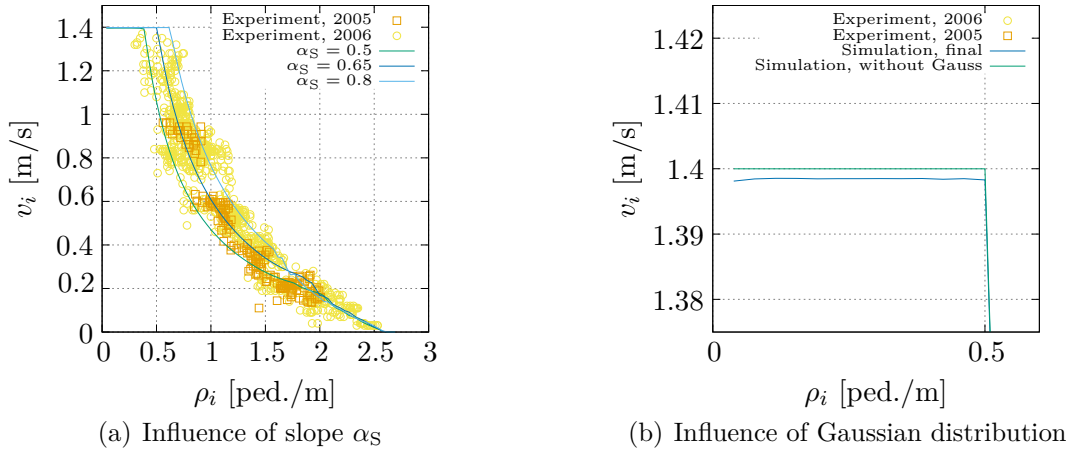

(b) Influence of Gaussian distribution

Figure 4.7: (a) An increasing slope α_S leads to a shift of the intermediate part of the fundamental diagram towards higher densities / velocities and represents the strength of the adaptation of the agents. (b) The Gaussian distribution used in the decision on the target angle leads to a small deviation in the free-flow speed since the motion is influenced by the confined space in the corridor.

the experimental data, it is shifted towards higher densities and velocities for an increasing α_S. Additionally, the point at which the system is dominated by the stopping and jamming behaviour is shifted to lower densities for increasing slopes. This seems to be reasonable since a larger α_S leads to higher velocities for the same density, and therefore headway. That means that the agents can pass more space during one time step and come closer towards their predecessor than for lower values of α_S. When they come closer for a smaller density they have to stop earlier ($v_i = 0\,\text{m/s}$) compared to larger density values. Therefore, the influence of the slow-to-start rule can start at lower densities.

Considering all three curves for $\alpha_S = 0.5\,1/\text{s}$, $0.65\,1/\text{s}$ and $0.8\,1/\text{s}$, the simulation results fit to the experimental data best for $\alpha_S = 0.65\,1/\text{s}$. This means that the dynamics displays a larger urge to follow the other and a more imminent reaction to changes of the headway. In the SHDV model, the relation between velocity and headway was based on the dynamics of the optimal velocity model [121, 122]

which was developed for vehicular traffic. This model describes the relation between velocity and headway using a tanh-function which is approximated linearly with $\alpha_S = 0.5/\text{m}$ as used by Eilhardt [120]. If one reset the purely mathematical aspect and focused on the physical meaning, an increased α_S for pedestrian dynamics would indicate that pedestrians can react faster on changes of the headway and therefore reach higher relative velocities than cars in the vehicular traffic. This seems to be a reasonable assumption since pedestrians, for example, show less inertia than vehicles and can de- and accelerate almost instantaneously. In [49], Jelić et al. analysed single-file motion experiments with pedestrians and assumed a similar concept for the meaning of α_S. For the headway-velocity relation (reciprocal to the velocity-headway relation used in the SHDV model) the authors determined a proportionality constant (now in dimensions of time), as 'adaptation time' that elapses until an agent reacts to changes in the headway in front. It can be understood as the 'sensitivity' of the pedestrians to the distance towards their respective predecessor. Based on this, a larger α_S as used in the optimised global fundamental diagram would imply that pedestrians have a smaller adaptation time than cars. This would be consistent with the considerations made above.

For very low densities, the experiments do not provide many reliable data points. In this regime, the simulation results are mainly influenced by the maximum free-flow velocity $v_{\max}$. Since the global fundamental diagram using the original free-flow velocity $v_{\max} = 1.2\,\text{m/s}$ misses some experimental data points at higher velocities, $v_{\max}$ was increased for this model approach to $v_{\max} = 1.4\,\text{m/s}$. This choice seems also reasonable as even higher free-flow velocities were measured in different experiments [41].

However, if the fundamental diagram for the optimal parameter set is considered in detail for low densities, a small difference can be observed between the measured speed v_i and the free-flow velocity $v_{\max}$, see Fig. 4.7(b). This gap stems from the stochasticity included in the model during the decision process. As described in Sec. 3.4.1, the final target angle is drawn from a Gaussian distribution around the optimal target direction in order to cover small uncertainties and fluctuations in

the walking behaviour. In a narrow corridor as it is used for the single-file motion scenario, even slight deviations from the optimal direction lead to a target direction pointing towards a wall. Therefore, the distance-to-collision becomes significantly smaller; at least for some cases where the velocity of an agent is then slightly decreased. When averaging over time and all agents, this results into a small deviation. However, it seems likely that a confined space like a corridor with a width of $B = 0.8\,\mathrm{m}$ influences the walking behaviour of pedestrians even at low densities. Since the effect is weak for the entire fundamental diagram, there were no additional adjustments done during the calibration and optimisation process to prevent this deviation.

4.2.2 Phase Separation

A characteristic of pedestrian single-file motion is the separation of the system in a standing and a slowly moving phase at high densities. In contrast to vehicular traffic the walking pedestrians do not move with free-flow velocity (see Sec. 2.1). This collective phenomenon is therefore an important test for a model's validation. The SHDV model is one of the few models for pedestrian dynamics that is able to reproduce this behaviour. Therefore, it should also be observed in the new model. In Fig. 4.4(b) the local fundamental diagram is shown which is a first way to assess whether the system shows phase separation. At densities around $\rho_i = 1.4\,1/\mathrm{m}$, a second branch develops for $v_i = 0\,\mathrm{m/s}$ which indicates that first pedestrians are standing while other agents are still moving. The number of agents with zero velocity rises with increasing density, while the proportion of walking pedestrians is reduced.

In [45, 95, 120] two other measurements of the phase separation were introduced which are applied now. First, the velocity distribution for different local density regimes is shown in Fig. 4.8 for both experimental and simulated data. The locally measured velocities are distributed in bins of size $0.1\,\mathrm{m/s}$. The experimental data (from 2006 [161], shown in Fig. 4.8(a)) shows the different behaviours of the system for the different density regimes: at intermediate densities,

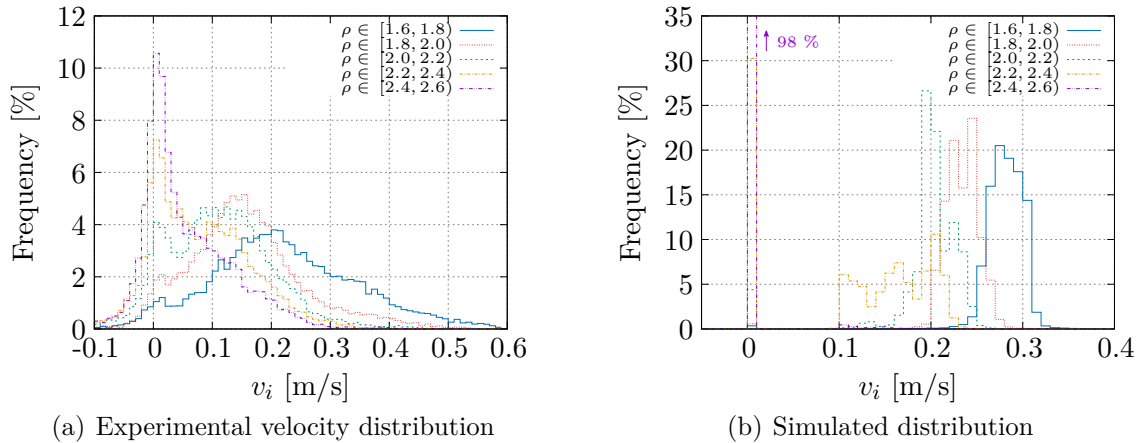(a) Experimental velocity distribution (b) Simulated distribution

Figure 4.8: Phase separation in single-file motion is represented by a double-peak structure in the velocity distribution (green, orange curves). Compared to the experiments (2006) [161], the simulated distributions are sharper, and the second peak is slightly shifted towards higher densities.

$1.6\,1/\mathrm{m} \leq \rho_i < 1.8\,1/\mathrm{m}$, the velocity distribution is rather broad with a small peak at approximately $v_i = 0.2\,\mathrm{m/s}$ and another, much smaller peak at $v_i = 0\,\mathrm{m/s}$. With increasing density, the distribution becomes narrower. The peak at higher velocities becomes more apparent and is shifted towards smaller velocities. For densities $2.0\,1/\mathrm{m} \leq \rho_i < 2.2\,1/\mathrm{m}$ and $2.2\,1/\mathrm{m} \leq \rho_i < 2.4\,1/\mathrm{m}$ a significant double peak structure appears: one of the peaks is at finite velocities around $v_i = 0.1\,\mathrm{m/s}$ while the second peak is shown at $v_i = 0\,\mathrm{m/s}$. This structure shows the phase separation into standing and slowly walking pedestrians. If the density is increased further, the peak at higher velocities disappears and the peak at $v_i = 0\,\mathrm{m/s}$ becomes very distinct. At this point the system enters the fully congested state. The velocity distributions for all densities are very broad. This is, at least partially, due to the measurement method. For the experiments, the participants' motion was measured by tracking their heads [45, 95, 120]. Movements of the heads that are not related to the general motion of the centre of mass, for example due to body swaying, can cause even negative velocities as shown here.

In contrast, the velocity distributions of the simulated data are very sharp. Es-

pecially the influence of the minimum velocity $v_{\min} = 0.1$ is significant. Instead, the single distributions show larger frequencies, probably because the speeds for the same number of pedestrians are distributed over a smaller velocity regime. In comparison to the experimental data, the peaks at finite velocities are slightly shifted towards higher velocities but lie within the velocity regime that is observed in the experimental data (for the same density). The double peak structure can be clearly seen, especially for $2.0\,1/\text{m} \leq \rho_i < 2.2\,1/\text{m}$ and $2.2\,1/\text{m} \leq \rho_i < 2.4\,1/\text{m}$, here there are distinct contributions at $v_i = 0\,\text{m/s}$ and $v_i = 0.1 - 0.23\,\text{m/s}$ and $v_i = 0.1 - 0.27\,\text{m/s}$, respectively. The density regimes of this phase separation correspond to those found in the experiments, albeit the second peak at finite velocities is shifted towards higher values. Nevertheless, the measurements of the velocity distribution show that the model is also able to reproduce phase separation in a reasonably quantitative way.

Another way to gain insight into the modelled behaviour is the analysis of the pedestrians' trajectories as shown in Fig. 4.9. For that, the x-coordinate of a pedestrian is plotted against time. This also helps at identifying congested states or how long a pedestrian is in the jam.

In the experimental data (2006 [161], Fig. 4.9(a)) the agents walk into the negative x-direction, whereas the general direction of motion in the simulated system was in positive x-direction. The plots show a segment of the corridor which in both cases corresponds to the length of the measurement area of the experiments. Both experimental and simulated trajectories show segments that are almost parallel to the t-axis whereas other parts are clearly diagonal. This is the graphical representation of the phase separation: in the congested phase, the pedestrian that has zero speed spends more time at the same place, this is represented by the vertical parts of the trajectories. When the pedestrian is walking, the trajectories show a diagonal progress. This effect is visible in both experiment and simulation although the experimental data shows more fluctuations. Additionally, it can be seen that the jam (the congested phase) moves in the opposite direction to the agents' direction of motion through the system, which is typical for a phase separated system.

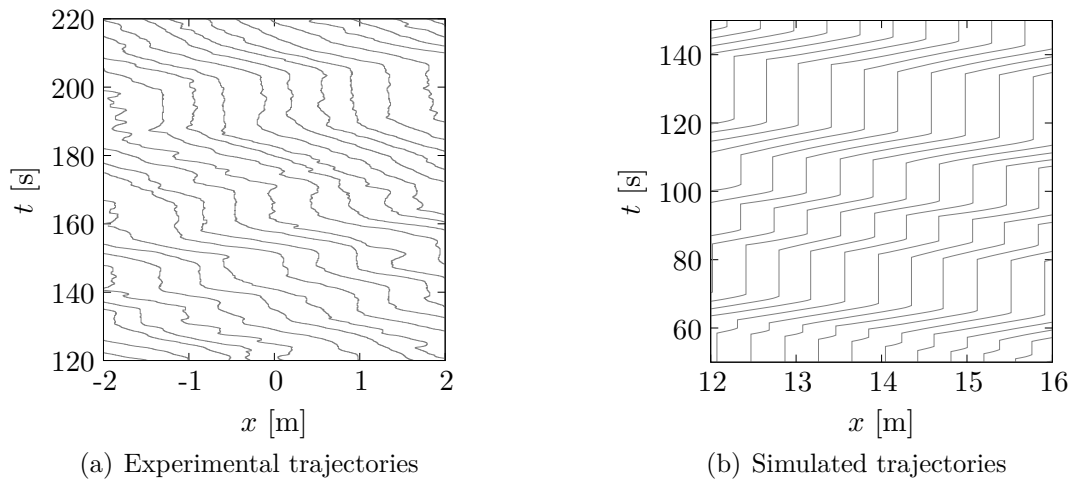(a) Experimental trajectories

(b) Simulated trajectories

Figure 4.9: Both experimental (2006) [161] and simulated trajectories show the phase separation in a jam (vertical segments) and a moving phase (diagonal segments). The experimental data shows more fluctuations due to the measurement method.

Taken together, the new model approach is, with the aid of some parameter optimisations and adjustments in the decision process on the final direction of motion, able to reproduce single-file motion of pedestrians qualitatively as well as quantitatively. The shape of both local and global fundamental diagrams fits well to the experimental basis and phase transition can be detected. How the parameters are changed can help to understand more about the prioritisation of pedestrians as well as their general walking behaviour.

4.3 Evacuation

An evacuation scenario might be the basic pedestrian situation one intuitively thinks of when considering the need for investigating and steering pedestrian walking behaviour, since the public awareness of safety and the threat of crowd disasters has risen in recent years. Therefore, it seems natural to test and optimise the dynamics of the new model by simulating evacuations.

The empirical basis in this section is given by data from two evacuation experiments performed in schools in Wuppertal, Germany. One of this data sets, called 'GymBay'[2] [31] is used for calibrating the model parameters and dynamics, the data of the other school, 'WDG'[2] [162] is then compared to the simulation results in order to assess the model predictions. In both cases, the experimental set-up was the same: the participants, students (aged 16 to 18 years) are placed in the middle of a square room of $5\,\mathrm{m} \times 5\,\mathrm{m}$ (Fig. 4.10). After a starting signal, they were asked to leave the room using an exit that leads to a small corridor of $0.6\,\mathrm{m}$ length. The width of the door and the corridor was $1.2\,\mathrm{m}$. The pedestrians were told to walk briskly but naturally without scrambling or pushing. The evacuations considered here were part of a larger study and one of several runs, respectively. They are representative for non-competitive, ordered evacuations under laboratory conditions without any limitations considering sight, orientation or the composition of the crowd.

In the simulation, the set-up of the experiments is reproduced, see Fig. 4.10. The number of participants as well as their initial positions in the room are taken from the experimental data. Since the geometry of this scenario is more complex, wayfinding and route choice play an essential role for the results. The target co-ordinates of an agent depend on the pedestrian's position. The general target (dark blue cross) is a single point far behind the end of the exit corridor. Whenever a pedestrian is on the same level as the exit corridor (bright blue shaded area), the target coordinates are adjusted so that the agent keeps its level and walks directly towards the exit. Due to the corners build by the exit corridor and the other parts of the room, the target might be screened by walls for some positions in the room. Therefore, the use of intermediate targets is necessary to navigate the agents out of the room. For these simulations, four intermediate targets (black crosses) were placed on a straight line in the middle of the corridor around the actual exit. As a first measure, their positions were chosen naively in order to find a good qualitative

---

[2]The labels are abbreviations for the schools' names: 'GymBay'= Gymnasium Bayreuther Straße, 'WDG' = Wilhelm-Dörpfeld-Gymnasium.
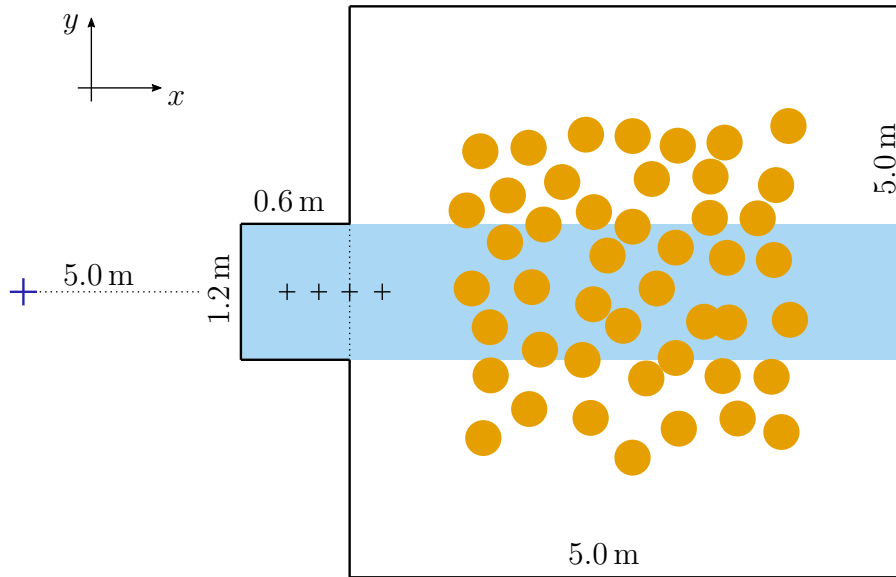
Figure 4.10: Experimental and simulated set-up for evacuation scenarios. The pedestrians (orange circles) leave the square room through an exit leading into a small corridor. The general target (dark blue cross) is set behind the exit, if an agent is on one level with the exit or within the corridor (bright blue area), it keeps its y-coordinate and goes straight forward. Four intermediate targets (black crosses) are set in the middle of the corridor for route choice.

progress of the evacuations and do not rely on any elaborate route choice model.

One of the most important quantities investigating evacuation scenarios is the exit or evacuation time. Here, T_{evac} is given as the time needed to leave the room, plotted against the respective number of evacuated persons. Since the number of pedestrians is relatively low and the total simulation time small, the simulated evacuation times are averaged over 100 runs in order to reduce stochastic fluctuations. Fig. 4.11 shows the simulation results for the evacuations with the original parameter set of the two-person interaction ($\Delta t = 0.3\,\mathrm{s}$, $v_{\mathrm{min}} = 0.1\,\mathrm{m/s}$, $v_{\mathrm{max}} = 1.2\,\mathrm{m/s}$, $\alpha_{\mathrm{S}} = 0.5\,1/\mathrm{s}$, $d_{\mathrm{S}} = 0.1\,\mathrm{m}$ and $p_0 = 0.5$) and the optimised parameter set, respectively, compared to the experimentally measured evacuation times. All three curves show a linear progress. Whereas the experimental data show some fluctuations in

the form of small plateaus and sharper inclines, the progress of the simulated curves does not fluctuate due to the averaging process. In the experiments, the students reacted to an acoustic signal and started with the evacuation whereas the simulated group of agents is able to start instantaneously. This leads to a constant offset of the evacuation time which could be compensated introducing a pre-movement time. In general, the pre-movement time describes the time lapse between the alarm or starting signal for an evacuation and the actual start of the evacuation movement. It includes the time needed to detect and recognise the signal, decide and react to it [22]. Pre-movement times have a significant influence on the evacuation behaviour [163–165]. Therefore, it was introduced in the simulations as an additional time lapse that had to be passed until the agents start moving. For the 'GymBay' data set, the pre-movement time is $t_{\mathrm{pre}} = 1.0\,\mathrm{s}$.

It can be seen in Fig. 4.12 that single runs of the simulation result in a similar progress than the experiment. A plateau in the evacuation time curve shows that multiple pedestrians left the room at the same time, whereas steeper increases represent phases in which the time between two exiting agents was larger. The standard deviation of the averaged simulation results (Fig. 4.11) increases with an increasing number of pedestrians for both parameter sets. Conflicts and clogging at the exit can cause short delays in the evacuation process which are random and not equal for each run, especially because the model approach is not deterministic in the collision avoidance procedure. Since conflicts require a certain number of pedestrians that are in front of the exit at the same time, their impact becomes significant only with an increasing number of agents. The longer the evacuation has progressed, the higher the probability for conflicts is.

Out of these reasons the standard deviation of the averaged curves in Fig. 4.11 increases in the course of the process. Both simulated curves show a change in their slope at the end of the evacuation that is more distinct for the simulation with the original parameter set. In this regime, the evacuation time increases overproportionally indicating the impact of additional conflicts that slow down the evacuation. While the evacuation times measured by using the original parameter set show sig-
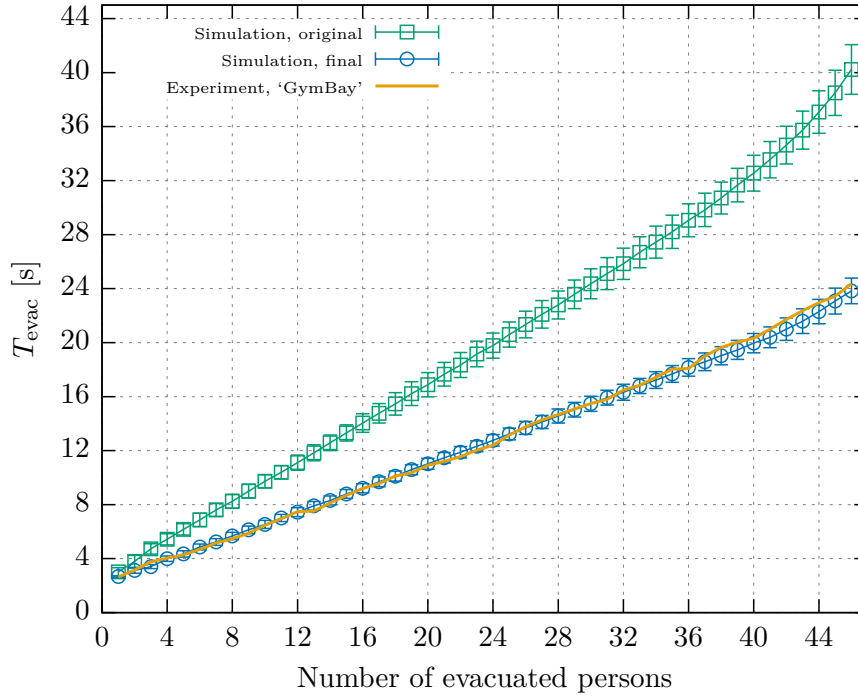
Figure 4.11: Evacuation times with final and original parameters: the slope of the evacuation time curve with the original parameter set is too high compared to the experimental results. In contrast, the simulations with the final parameters is able to reproduce the experiments well.

nificant deviations from the experimental curve, the optimised results fit well to the empirical data. Solely at the end of the evacuation the simulated curves do not follow the experimental one as well as before, however, the experimental results still lie within the standard deviation of the simulation results. In contrast, the slope of the original parameter curve is much too high to reproduce the experiment. Additionally, the standard deviation of the original curve is slightly larger compared to the optimised result.

To achieve a good agreement of the model and the experimental results, the adjustment of several parameters and of one part in the decision process was necessary. Overall, the slope of the SHDV model is increased to $\alpha_S = 1.3 \, 1/s$, and the size
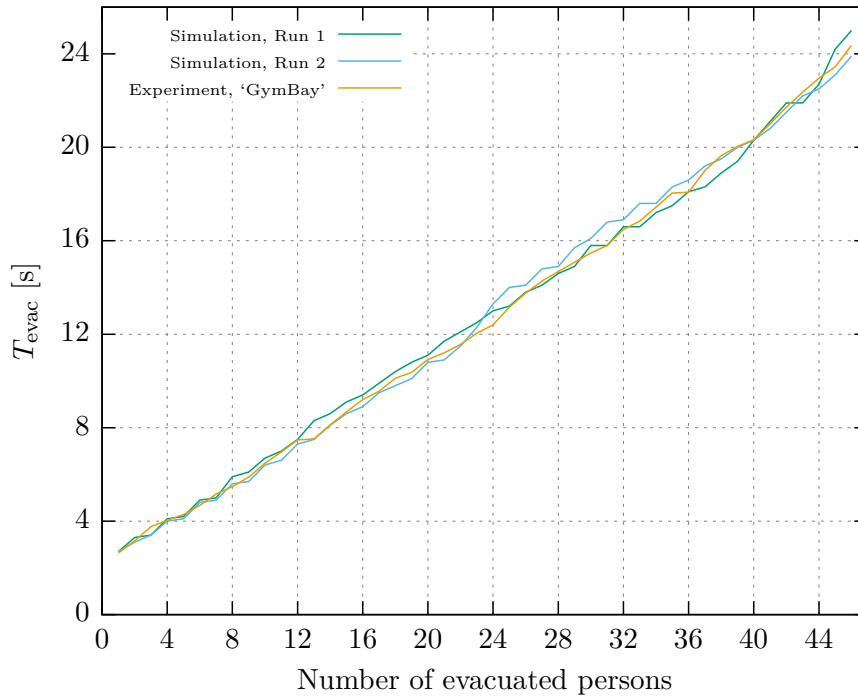
Figure 4.12: Single evacuation runs simulated with the final parameter set. Beneath the general progress, the modelled curves as well as the experimental one show small plateaus and fluctuations indicating several pedestrians exiting at the same time or larger gaps between agents leaving the room.

of the time step and the lower threshold of the SHDV model are decreased to $\Delta t = 0.1\,\mathrm{s}$ and $d_\mathrm{S} = 0.03\,\mathrm{m}$, respectively. Additionally, large deviations of the final direction of motion from the desired direction are suppressed and a concept of body rotation is introduced.

The most distinct difference between the results of the two parameter sets was the difference in the slope of the evacuation time curve. Fitting the model results to the experimental data required a strong increase of the slope of the velocity-headway relation, α_S. Fig. 4.13 shows the evacuation times for different values of α_S. It can clearly be seen that the slope of the curve decreases with increasing
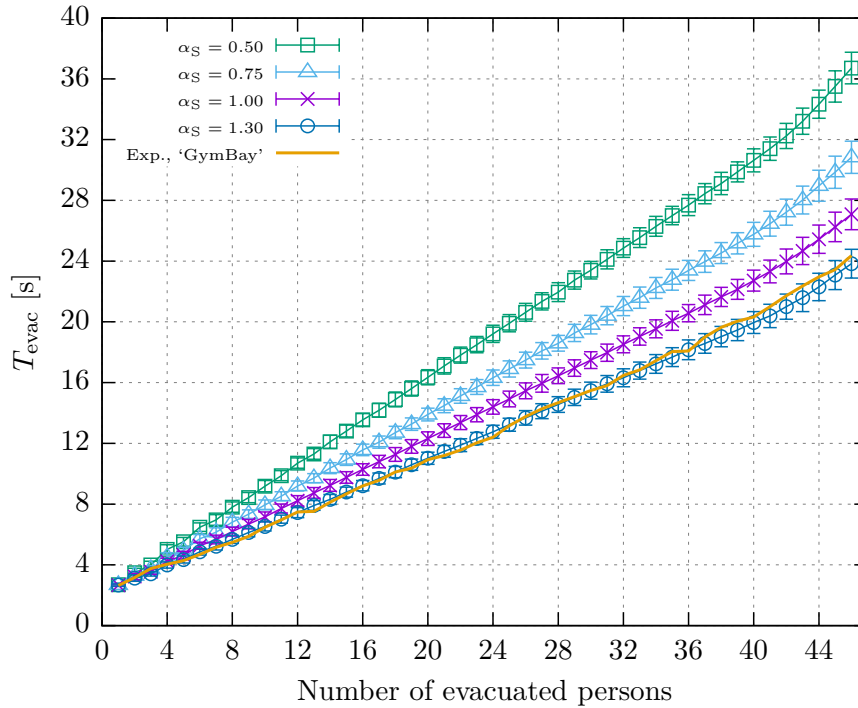
Figure 4.13: Increasing α_S results in shorter evacuation times since the agents close the lines in front of the exit and leave more efficiently.

α_S. The best results are obtained for $\alpha_S = 1.3\,1/\text{s}$. Therewith, this parameter was adjusted towards larger values as in the single-file motion scenario. However, the final value is far higher. That means that if the same distance-to-collision is ahead, the speed of an agent in the evacuation is higher. The pedestrian covers a greater distance and comes closer to other agents during one time step. Relating to the interpretation given in Sec. 4.2.1, this indicates that the urge of an agent to follow pedestrians walking in front is much more pronounced than in the single-file scenario. Also, it leads to the conclusion that a pedestrian's adaptation time is significantly shorter, that means that it reacts faster to the perceived situation and changes in the distance-to-collision. With regard to the scenario, this seems to be reasonable: in evacuations the general aim is to leave the room as fast as possible. Therefore, allowing large distances is disadvantageous because a single pedestrian

has to wait longer before there is enough space to exit the room. An increased α_S causes the agents to close the lines, making the group of pedestrian more compact and the use of space more efficient. Overall, this results in a shorter evacuation time, especially for those agents who would have to wait very long because many other agents exit before them. Therefore, the impact becomes even more significant with an increasing number of pedestrians and mainly influences the slope of the evacuation time curve. Of course, the personal space of an agent is much smaller than e.g. in one-on-one situations. However, it might be assumed that a pedestrian neglects its need for comfort and personal space over the urge to leave the room, especially since it is known that it is only a temporary situation. That means that changing the scenario can also shift the priorities of the agents.

Fig. 4.14 shows the impact of the size of the time step Δt on the evacuation times. The simulation results for a larger time step of $\Delta t = 0.3\,\mathrm{s}$, as used in the single-file scenario, show larger evacuation times whose standard deviations are also larger compared to the curve for $\Delta t = 0.1\,\mathrm{s}$. This behaviour could be explained by the following reason: a larger time step means that an agent decides less often on its next velocity and each decision is valid for a longer time. Therefore, directions that would lead to a collision in $0.3\,\mathrm{s}$, but provide enough space for walking for $0.1\,\mathrm{s}$, lead to a standstill in the first case, in the latter case they can help to close the lines in front of the exit door. The agent is not flexible enough to react to free space in front since it has to plan for a time that is too long. Using an anticipation time which corresponds to one time step, the agent also does not consider that the other pedestrians might adjust to the current situation, but assumes their motion to be constant. Overall, decreasing the time step brings more flexibility that is obviously needed to reproduce the evacuation behaviour appropriately. This indicates that not only the adoption time a pedestrian needs to adjust its velocity, but also the anticipation time that the agent takes for a single decision is shorter. In conclusion, in evacuations a pedestrian reacts faster but projects shorter.

In contrast to the time step Δt and the slope of the velocity-headway relation, α_S, the lower threshold d_S used in this relation has only a minor influence on the evac-
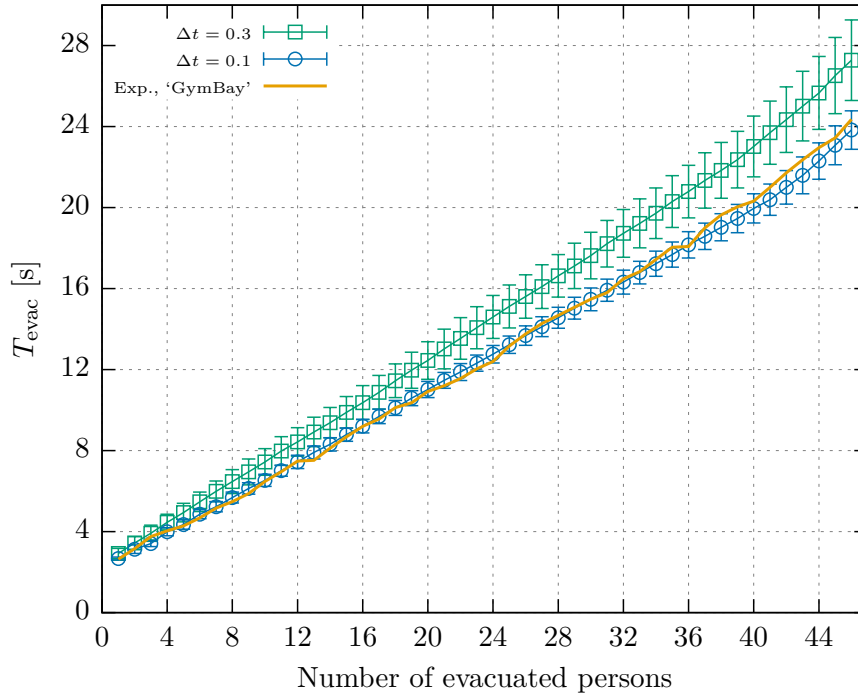
Figure 4.14: A change of the time step Δt influences the evacuation times which become shorter with a decreasing time step. This is probably due to a higher flexibility since the decisions on the velocity are made more often and do not hold for a longer time span.

uation time (see Fig. D.1 in the Appendix). The exit times for a larger number of pedestrians are only slightly higher for the original parameter $d_S = 0.1\,\text{m}$ than for the reduced value $d_S = 0.03\,\text{m}$. Instead, the influence can be visualised using Voronoi diagrams[3] within the set-up. In heat maps the Voronoi cells can be coloured according to their (reciprocal) size, representing smaller or larger cells (densities), respectively. In the figures shown below, large cells / small local densities are coloured in dark blue and become brighter with decreasing size / increasing density. Small cells are coloured in yellow indicating a high local density.

In Fig. 4.15 the Voronoi diagrams at $t = 12.0\,\text{s}$ are compared for a simulation with

---

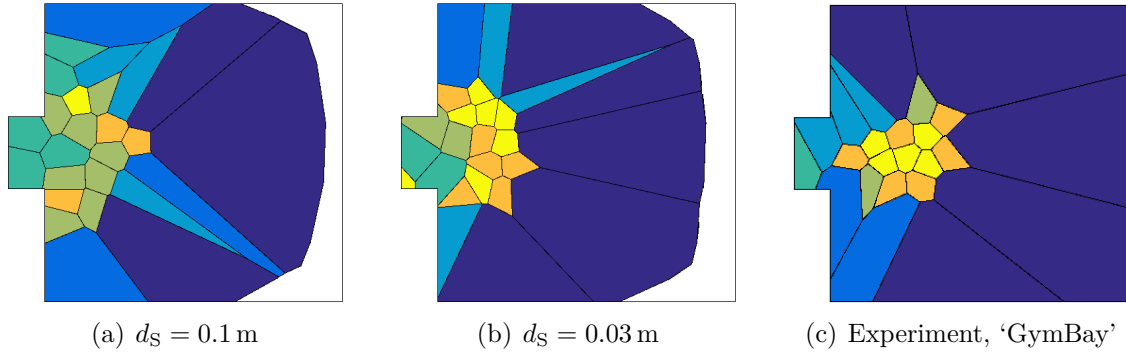[3]For more information on Voronoi diagrams and their use for the determination of local densities, see Sec. C.2

(a) $d_\mathrm{S} = 0.1\,\mathrm{m}$ (b) $d_\mathrm{S} = 0.03\,\mathrm{m}$ (c) Experiment, 'GymBay'

Figure 4.15: Comparison of different values of d_S using Voronoi diagrams at $t = 12.0\,\mathrm{s}$. A smaller threshold d_S results in a more dense configuration in the simulations like it is observed in the experiments.

the original (Fig. 4.15(a)) and the final optimised parameter (Fig. 4.15(b)) and the experimental run (Fig. 4.15(c)). It can be clearly seen that a smaller threshold d_S leads to higher local densities. Thereby, the pedestrians also spread over a smaller area around the exit. The configuration of the participants in the experiment is, in contrast, much more compact. Reducing the lower threshold allows the pedestrians to move closer together because the speed that is determined in the last decision is still finite even for smaller distances-to-collisions. As the difference between the original result and the experimental one is such distinct, the threshold was set to a minimal value of $d_\mathrm{S} = 0.03\,\mathrm{m}$ to enable a dense packing of the agents while preventing unwanted overlaps. It results in a more dense, semicircular configuration of the pedestrians in front of the exit. In contrast to the parameters described above, the threshold d_S also causes smaller distances between agents, but has almost no influence on the evacuation time. Whereas α_S makes the agents walk faster for the same headway and reproduces a brisk walking behaviour, the lower threshold causes that a pedestrian can walk at very small distances. In doing so, the agents are able to fill smaller gaps between agents with still very low speed, but not cover large distances towards other agents in order to make the evacuation more efficient. Summed up, α_S ensures that people can come close enough to the others, while d_S

is needed so that they do not have to stop and wait in the next time step until the headway is again large enough. A similar argumentation holds for the comparison to Δt, which influences the evacuation behaviour by making the agents more flexible and therefore more efficient, while d_S acts on a smaller length scale.

Similar to the single-file motion the third decision on the final direction of motion has to be adjusted in order to get realistic results. As it can be seen from the Voronoi diagram in Fig. 4.16(a), no restriction considering the choice of the direction of motion results in a very broad configuration of the pedestrians. All agents distribute almost uniformly causing low local densities. Compared to the general expectations and the experimental run in Fig. 4.16(c) this behaviour is highly unrealistic. When the first pedestrians start to jam in front of the door, the distance-to-collision into the target direction becomes small for the agents behind. They therefore choose the interaction angle as direction of motion. In terms of collision avoidance it is reasonable to keep as much space as possible to other agents, so that the interaction results in an unrealistically broad crowd. Therefore, the decision on the direction of motion was adjusted to

$$
\alpha_i \left(t + \Delta t \right) = \begin{cases} \alpha_t^{\mathrm{fin}} & : \left[d \left(\alpha_t^{\mathrm{fin}} \right) \geq d \left(\alpha_{\mathrm{ia}} \right) \right] \quad \vee \quad \left[|\alpha_{\mathrm{ia}} - \alpha_t| > 57° \right], \\ \alpha_{\mathrm{ia}} & : \text{else.} \end{cases} \tag{4.4}
$$

Here, the target angle α_t is chosen as final direction of motion if the headway towards the interaction direction $\alpha_{\mathrm{ia}}^{\mathrm{fin}}$ is smaller or if the deviation between interaction and target angle becomes larger than $57°$ ($1.0\,\mathrm{rad}$). It restricts the interaction to narrower angles and shifts the focus towards reaching the goal instead of avoiding close proximity to others. Whereas the exact threshold for this restriction has no significant impact on the evacuation times (see Fig. D.2 in the Appendix), the Voronoi diagram of the simulated evacuation with $|\alpha_{\mathrm{ia}} - \alpha_t| \leq 57°$ still shows some deviations from the experimental run. However, taking $57°$ as the threshold already is a large intervention into the model and leads to a semicircular configuration of the group and arching processes in front of the exit as they are known from evacuation
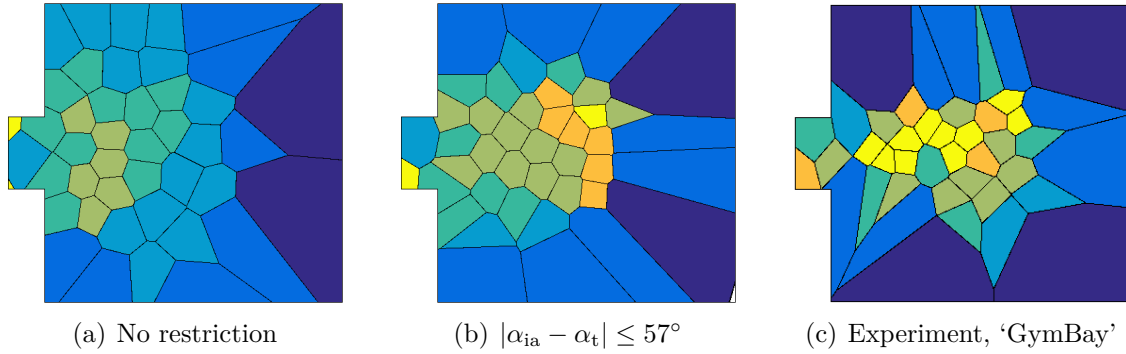
(a) No restriction   (b) $|\alpha_{ia} - \alpha_t| \leq 57°$ (c) Experiment, 'GymBay'

Figure 4.16: Voronoi diagrams for $t = 4.0\,$s show that the restriction of the final direction of motion increases the local density. However, the experimental run displays an even narrower and denser configuration.

and bottleneck scenarios (see e.g. [24] and references therein). It is still larger than the value that was used in the single-file motion ($37°$). One has to keep in mind that the general direction of motion in evacuations is not as predetermined as it is in single-file situations. Overall, it seems to be reasonable to take this threshold as a compromise between a pedestrian's freedom of choice and the comparison to the experimental result.

In terms of pedestrian walking behaviour, this restriction represents a change in the priorities of the agents as it has been indicated already when investigating the influence of the slope α_S. Instead of avoiding others and eluding, the agents accept smaller distances and the invasion of other pedestrians into the own personal space in order to reach their goal. They also do not optimise their velocity to a higher one choosing the direction of the larger distance-to-collision. Instead, the agents wait in front of the exit and therefore optimise their evacuation time.

The last measure to fit the simulation results to the expectations and experimental results is the introduction of body rotations. In general, a pedestrian's extent perpendicular to its walking direction is given by the width of its shoulders in addition to some 'safety distance'. In dense or narrow situations, a pedestrian is able to

reduce this extent temporarily by rotating the upper body, bringing one of the shoulders to the front. This behaviour was explicitly observed in experiments on lane formation in corridors [39, 166] and should be represented also in the model. If a pedestrian's speed has been zero in the previous time step, it assumes its own radius r to be reduced to $r/3$ for the decision in the next time step when the agent has to determine the distance-to-collision for target and interaction angle. Therefore, the space that is required to pass another agent or a wall is also reduced for a short period of time. The introduction of body rotation has almost no impact on the evacuation times (see Fig. D.3 in the Appendix, Ch. D), it minimally reduces the evacuation times for larger numbers of pedestrians. In fact, the simulation without body rotation seems to fit better to the data at the end of the evacuation than the optimised run.

The benefit of body rotations cannot been proven quantitatively. They were introduced to solve unrealistic conflicts in the region in front of the door.

Clogging and arching processes are well-known characteristics of pedestrian behaviour, however, they mostly include pedestrians directly in front of the door and are solvable in a short time frame. In contrast, in the simulated evacuation runs, conflicts occurred that could last for 9 or 15 time steps like in the two situations shown in Fig. 4.17(a) and 4.17(b), respectively. In both scenarios, the distance-to-collision in front of the two agents shaded in red is large enough to move, but the pedestrians block each other and cannot solve the situation. The number of these blockages is reduced when introducing body rotation. It increases the range of possible directions that do not lead to a collision with other agents and therefore improves the evacuation behaviour. Despite body rotation, arching still occurs in the simulated evacuations as exemplarily shown in Fig. 4.17(c), where the agents in red form an arch that encompasses the entire exit. Therefore, it is reasonable to include body rotations even if the evacuation times at the end of the evacuations can be better reproduced without them. It might be conceivable to assume that the last participants who left the room in the experiment lacked motivation or did not have the urge to follow their predecessors as fast as possible.
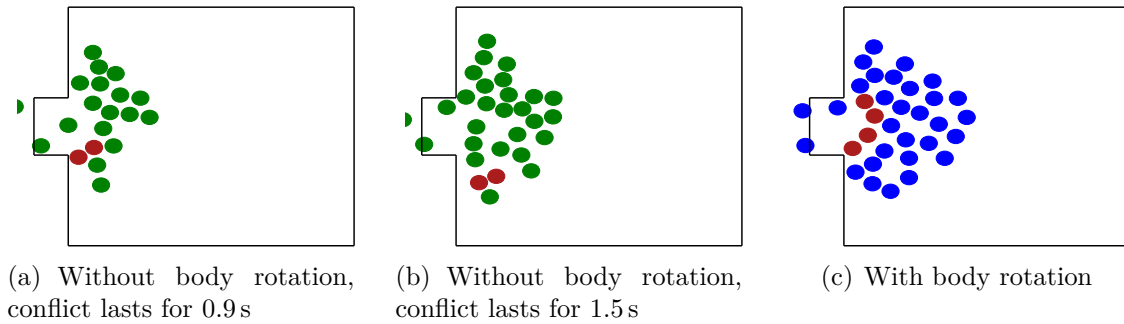
(a) Without body rotation, conflict lasts for 0.9 s

(b) Without body rotation, conflict lasts for 1.5 s

(c) With body rotation

Figure 4.17: (a), (b) Without body rotation more unrealistic conflicts occur that are solved more easily when introducing the reduction of an agent's radius. (c) Even with body rotation, arches are found in the simulations.

The model performance with the optimised parameter ('GymBay') set was tested on a second data set of another school ('WDG') [162]. Here, the pre-movement time was set to $t_{\text{pre}} = 3.7$ s.

As it is shown in Fig. 4.18, the simulations using the 'GymBay' parameter set are not able to reproduce the evacuation times of the 'WDG' experiment which significantly differs from the 'GymBay' curve. To achieve a better agreement between simulation and experimental results the slope has to be further increased to $\alpha_{\text{S}} = 3.3\,1/$s which is 2.5 times the slope of the calibration experiment and 6.6 times the original value of the SHDV model. This means that in this run, the participants had an even higher urge to follow others, used the available space more efficiently and, as a result, showed a significantly shorter evacuation time.

In terms of model development this results may be disappointing since it is usually aimed at finding a general parameter set that can be used to simulate several situations. Here, the set is not able to reproduce another experiment of the same situation. However, it shows that the model is highly flexible and can be adjusted easily for an arbitrary data set. Moreover, it is not clear whether there is one unique, optimal parameter set for any model and if so, it may include other quantities than considered here.
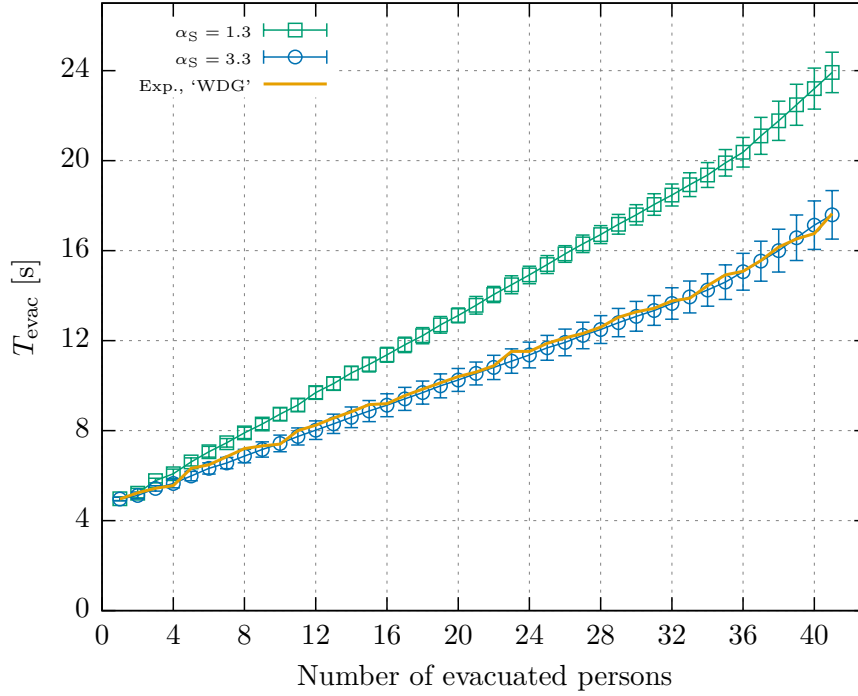
Figure 4.18: The evacuation times of the second experiment, 'WDG' cannot be reproduced with the optimised parameter set and $\alpha_S = 1.3 \, 1/s$. Instead, the slope α_S has to be further increased, indicating a higher urge to follow the predecessors.

4.4 Bidirectional Flow

For the investigation of pedestrian dynamics, bidirectional flow is a key scenario since it is insightful as well as challenging to reproduce. Lane formation in bidirectional motion is a paramount example for self-organisation in pedestrian dynamics and can therefore provide useful information on the quality of a model.

In this scenario $N = 50$ agents are set in a corridor (parallel to the x-direction) with length $L = 12.5 \, \text{m}$ and width $B = 3.0 \, \text{m}$ with periodic boundary conditions (this leads to a global density of $\rho = \frac{N}{LB} = 1.33 \, 1/\text{m}^2$). The pedestrians are equally distributed into two groups, one group walks from the left to the right, the other one vice versa. The desired direction of motion is determined by the target co-

ordinates which, similar to the single-file motion scenario, depend on the current position: $x_{\mathrm{t},i}(t + \Delta t) = x_i(t) \pm 5.0\,\mathrm{m}$ and $y_{\mathrm{t},i} = y_i(t)$, which means that the agents aim at keeping their current height within the corridor and walk along the corridor to the right $(+5.0\,\mathrm{m})$ or to the left $(-5.0\,\mathrm{m})$, respectively. At the beginning of the scenario, the pedestrians are placed randomly within the system with prevented overlaps with the walls, but not with other agents. The simulations ran in total for $T_{\mathrm{sim}} = 180\,\mathrm{s}$.

Out of all scenarios described so far, the bidirectional motion needed the most adjustments of the modelled mechanisms in order to obtain even qualitatively good results. In particular, three aspects inhibited realistic motion in the simulations. First, the occurrence of gridlocks is a common problem in simulating counterflow in a corridor [9, 11, 29, 112–118] and is also observed for this model. At a certain point of the simulation, the pedestrians are not able to elude others appropriately any longer. They start to block each other until the entire corridor is clogged by two groups facing each other. A gridlock is an absorbing state for simulated lane formation, the agents are totally disabled. It is not observed in empirical observations and an artefact of modelled systems (see also Sec. 2.1). Introducing mechanisms to prevent gridlocks leads to the second problem: in real pedestrian motion, lanes formed spontaneously can decay again, but they are stable enough to improve the agent's comfort while walking. Therefore, the model has to achieve a balance between inhibiting gridlocks and forming metastable, identifiable lanes. The third aspect is specific for this approach and caused by the stochasticity of the collision avoidance procedure. In counterflow, the pedestrians are constantly exposed to encounters, so they almost always choose to use the interaction direction. This, however, is drawn from a probability distribution for each time step and therefore changes significantly every time a new direction is calculated. Therewith, the motion of the agents shows large fluctuations (the pedestrians 'jitter' while walking) which makes the simulation look unnaturally and unrealistically.

To tackle these problems, several adjustments of the parameters were made and walking concepts introduced. In comparison to the original parameter set ($\Delta t =$

0.3 s, $v_{\min} = 0.1\,\mathrm{m/s}$, $v_{\max} = 1.2\,\mathrm{m/s}$, $\alpha_{\mathrm{S}} = 0.5\,1/\mathrm{s}$, $d_{\mathrm{S}} = 0.1\,\mathrm{m}$ and $p_0 = 0.5$, see Sec. 4.1) a few parameters were changed: similar to the single-file motion and the evacuation scenario, the proportionality constant of the velocity-headway relation is increased to $\alpha_{\mathrm{S}} = 1.5\,1/\mathrm{s}$, while the size of the time step is decreased to $\Delta t = 0.1\,\mathrm{s}$. Moreover, the body rotation concept that was already introduced in the evacuation scenario is included. Besides, two additional adjustments of the model were done. The first change considers the pedestrians' direction of view. Usually, the agents are assumed to look into their walking direction as the visual field is symmetrically set around it. Thereby, the line of view follows the direction of motion. For bidirectional motion, the pedestrian keeps looking at its desired direction. That means that the visual field spans around the final target direction $\alpha_{\mathrm{t}}^{\mathrm{fin}}$ independently of whether it is chosen as final direction of motion. Even if the agent avoids others and walks into the direction of the interaction angle α_{ia}, the direction of view is equal to the target direction. Of course, all relative angles during the perception phase are then determined with respect to the direction of view instead of the direction of motion. The second new concept considers the choice of the final direction of motion. While in single-file motion and evacuation a simple restriction of the interaction angle to directions near the desired direction was sufficient to obtain realistic results, the problem in bidirectional flow is more complex. On one hand, focussing on reaching the target like in the other scenarios facilitates the development of gridlocks because the pedestrians do not have enough freedom of choice to avoid approaching agents. On the other hand, the interaction mechanism leads to many fluctuations and changes in the direction of motion which inhibit the formation of stable lanes. Overall, the new concept tries to balance both aspects. Depending on different external and internal factors, the pedestrians have two strategies to decide on their direction of motion. The first strategy ('Interaction' / Strategy 0) uses the default choice of the direction of motion as used in the two-person interaction,

$$\alpha_i^0\left(t + \Delta t\right) = \begin{cases} \alpha_{\mathrm{t}}^{\mathrm{fin}} & : d\left(\alpha_{\mathrm{t}}^{\mathrm{fin}}\right) \geq d\left(\alpha_{\mathrm{ia}}\right), \\ \alpha_{\mathrm{ia}} & : \text{else}, \end{cases} \tag{4.5}$$

and therefore focuses on the interaction and collision avoidance. This strategy is used every time the measured distance-to-collision in either interaction or target direction is very small, $d\left(\alpha_{\text{t, ia}}\right) < 0.15\,\text{m}$, when the agent's speed has been low in the previous time step, $s_i(t) < 0.3\,\text{m/s}$, or the pedestrian stands near a wall, $d^{\text{W}} < 0.3\,\text{m}$. In addition, it is also randomly chosen with a probability $p_1 = 0.25$. In all other cases, the agent uses the other strategy ('Target' / Strategy 1) to decide on its direction. This strategy shifts the focus towards reaching the goal. The final target angle is chosen to be the direction of motion if the distance-to-collision in the interaction direction is small, $d\left(\alpha_{\text{ia}}\right) < 0.5\,d\left(\alpha_{\text{t}}\right)$, or stochastically with a probability that depends on the current speed, $p_2 = s_i(t)/1.5v_{\text{max}}$. Using this strategy means that going towards the target is preferred for higher velocities and when the interaction would lead to much lower distances-to-collision.

The interplay of the adjustments described above are used to reproduce realistic lane formation behaviour. Fig. 4.19 gives an overview of the simulation results of different parameter combinations. It is shown which fraction of simulation runs for different parameter configurations results in a gridlock ('Gridlock'), in a loose distribution of the pedestrians which still allows motion ('No Gridlock'), or in a configuration which indicates that a gridlock will develop shortly after the expiration of the simulation time ('Upcoming Gridlock'). In total, 50 simulation runs were done for each parameter configuration with a total simulation time $T_{\text{sim}} = 180\,\text{s}$ each. Beneath the optimised ('Final') interaction and the parameter set of the two-person interaction ('Original'), the simulation results for different values of the slope α_{S} and for a larger time step Δt are investigated. Moreover, simulations without the new concepts of body rotation, keeping the direction of view to the target direction and restricting the choice of the direction of motion are considered.

Comparing the final and the original simulation set-up, it strikes the eye that the simulation using the parameters of the two-person scenario is not able to reproduce realistic motion since all runs result in a gridlock. Adjusting the parameters and mechanisms decreases the number of gridlock runs by half. Considered qualitatively, the simulation using the original parameters shows that the agents collide
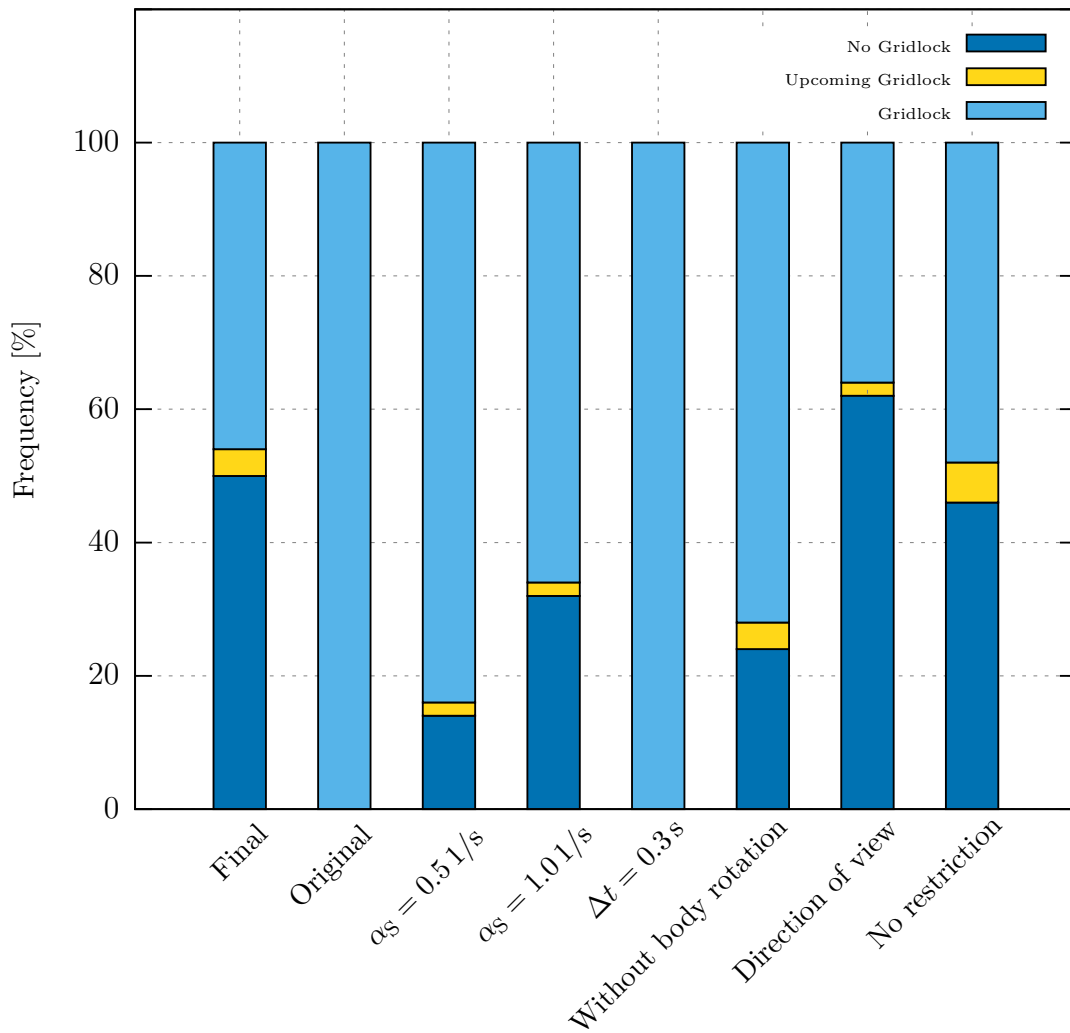
Figure 4.19: Frequency of simulation runs showing fully developed gridlocks, developing gridlocks and states where the agents are able to move for different simulation configurations. The original parameter set and a larger time step always result in gridlocks, whereas an increased α_S and three new concepts in the model can increase the number of successful simulations.

frequently and are not able to resolve conflicts of two agents facing each other, especially near the walls of the corridor. Thereby, the agents tend to gather at the corridor's edge and continuously block the space needed by others to pass. The reasons for this behaviour become more apparent when considering the single aspects that must be changed for lane formation.

If a simulation does not result in a gridlock, several patterns of lane formation are observed for the final simulation set up. Since the pedestrians are distributed randomly at the beginning of the simulation, the system needs a few seconds until the agents are distributed uniformly. When the system is in an ordered state, the ordering does not have to be permanent but can decay and redevelop during the simulation. The observed lanes are also not stable but decay due to local fluctuations of the chosen direction of motion. In addition, the system shows only a few states where all pedestrians walk in line; there often are several 'outliers'. In Fig. 4.20 several lane formation situations are shown. The blue circles represent pedestrians walking from the left to the right, red ones show agents walking from right to left. In Fig. 4.20(a), the agents walk in three lanes. The outer ones have the same walking direction, and the inner lane is used by pedestrians moving into the other direction. Here, the entire region in which the blue circles are located is interpreted as one single lane, although the agents are able to walk next to each other. In this context, a lane is defined as a cohesive area in which the agents have the same preferred walking direction. The system with two small and a third larger lane can be interrupted by another lane as shown in 4.20(b) where four lanes with alternating walking direction appear, even if the upper line with red circles is small compared to the other ones. A third configuration is shown in 4.20(c), where the system is split into two regions of opposite walking directions. In all these situations, the lanes are spread parallel to the walls and the preferred walking directions. Moreover, following pedestrians that have the same preferred direction were also observed in deviating directions, e.g. in Fig. 4.20(d). Here, two short diagonal lanes are highlighted for pedestrians walking to the left and the right. It can be assumed that, in terms of walking comfort and avoiding interaction, it also
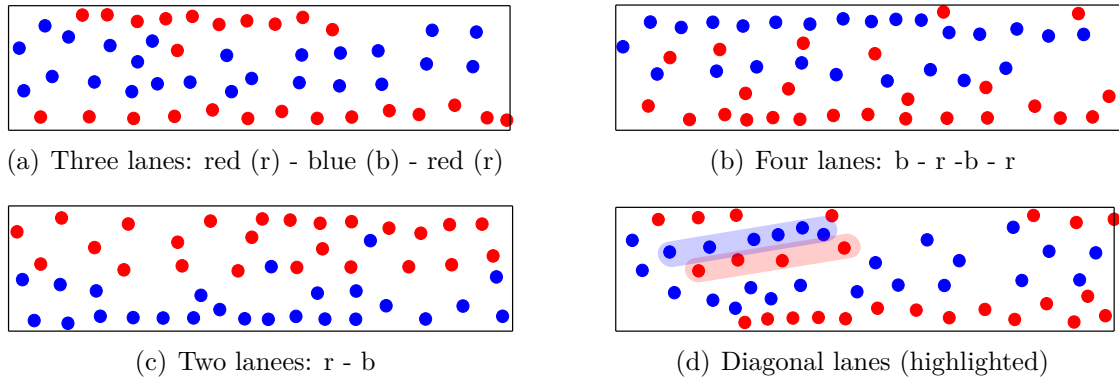
(a) Three lanes: red (r) - blue (b) - red (r)

(b) Four lanes: b - r -b - r

(c) Two lanees: r - b

(d) Diagonal lanes (highlighted)

Figure 4.20: Simulations with the 'Final' model configuration show different patterns of lane formation. The lanes are metastable, decay and change during the simulation.

is advantageous to deviate from the ideal walking angle and to follow others who head into the same direction. These kind of lanes are often short and decay faster or merge with other, larger lanes at the outer regions of the corridors.

For the optimised parameter set, the slope of the velocity-headway relation was increased to $\alpha_S = 1.5\,1/s$. The first, third and fourth bar in Fig. 4.19 show that a decreased slope increases the number of gridlocks in the simulations significantly. With $\alpha_S = 1.5\,1/s$, 46% of all runs showed a gridlock after $180\,s$, while this value increases to 66% and 84% for $\alpha_S = 1.0\,1/s$ and $\alpha_S = 0.5\,1/s$, respectively. As described in the sections before, the slope represents the urge of the pedestrians to accelerate towards free space, and an increased value of α_S means that the agents walk more briskly at the same headway. In the case of bidirectional motion, a larger value of α_S enables the agents to move faster towards free space and therefore helps at solving conflicts and small jams. Especially if the available space is additionally limited because the pedestrians walk near a wall, it is crucial for the agents to be able to use gaps in the pedestrian flow most efficiently. Decreasing α_S causes the agents to react slower to free space and miss the time at which it would have been possible to resolve the conflicting situation more often. They have to stand still while other pedestrians also arrive at the jam who cannot evade due to the

counterflow and also stop. If this process carries on, a gridlock develops, starting at the walls and growing into the middle of the corridor. Increasing α_S reduced the number of agents standing and waiting in the vicinity of the wall and therefore decreases the number of possible beginnings of a gridlock.

One main reason why the simulations using the original dynamics always result in gridlocks probably lies in the choice of the time step size. As it can be seen in Fig. 4.19, all runs using the larger time step $\Delta t = 0.3$ s are not able to reproduce realistic behaviour. The pedestrians often collide and are not able to resolve conflicts even at larger distances. This could be explained by the same mechanism as described for the evacuation scenario in Sec. 4.3. Decisions for a larger time step force the agents to plan for a larger time and suppress directions that would be advantageous only on a smaller time scale. The pedestrians stand still rather than move because the gaps within the crowd do not provide enough space for them to perform the entire motion. Using the smaller time step $\Delta t = 0.1$ s results in more decisions. The agents are again more flexible and can use the space around them more efficiently. For the lane formation, this effect is crucial since the agents start to block each other quickly within the confined space of the corridor. That shows that solving conflicts and interacting with lots of other pedestrians requires fast decisions and a distinct ability to close the lines and fill the gaps. The anticipation and planning time of pedestrians also seems to decrease in situations of higher density.

Bidirectional movement naturally involves a lot of interactions and encounters. The simulations show that especially one-on-one situations of two pedestrians walking in opposite directions often occur. In contrast to the two-person interactions described in Sec. 4.1, the available space for the two agents to solve the conflicts is severely limited due to walls or other pedestrians walking besides. In the original simulation set-up these conflicts are often the beginning of gridlocks when the agents are not able to solve the conflict rapidly. At this point, the concept of body rotation can

produce relief. The short-time reduction of the pedestrian's space facilitates the solution of conflicts as the agents need less space to pass each other. In fact, without body rotations 72% of the simulation runs end up in gridlocks, whereas including this concept reduces this value to 46%. The influence becomes even clearer if one considers the emergence of a gridlock which is exemplarily shown in Fig. 4.21 for a run without body rotation. As mentioned previously, a gridlock mostly starts to develop if two agents face each other in the vicinity of a wall (see Fig. 4.21(a) at the right-hand side near the lower wall). Here, the available space for the agents to pass each other is almost halved because the wall blocks one whole side of the agent. When other pedestrians pass the two agents standing at the wall, they do not have any space to evade and it becomes increasingly difficult for them to solve this conflict. Other pedestrians that want to pass mostly have to avoid collisions with approaching agents so that they either turn towards the wall or try to go around the two agents standing at the wall. In the first case, the agents start to form 'queues' along the wall which cause other pedestrians to start with their collision avoidance manoeuvre way before (Fig. 4.21(b)). In the second case, the pedestrians walk towards the middle of the corridor. Due to the constant flow of pedestrians they also might meet other opponent pedestrians besides the two agents at the wall. Now the situation is similar to the initial conflict: the available space is blocked by the standing agents at one side, and if the other side is also occupied by walking pedestrians, the agents cannot elude and stand still. This sets off a chain reaction: other pedestrians coming from behind the standing agents walk again into the middle of the corridor in order to pass the second standing pair of pedestrians. This results in a chain of standing pairs of pedestrians with different desired walking directions growing from the edge of the corridor towards the middle (see Fig. 4.21(c)). When on the other side of the corridor the remaining space is not large enough to allow pedestrians to pass the standing group, either because the chain has grown this far or because of similar procedures or other lanes on the other side, a gridlock is formed (Fig. 4.21(d)). As soon as the standing agents are distributed over the whole corridor width, the state cannot be changed

(a) $t = 22.0\,\mathrm{s}$

(b) $t = 30.0\,\mathrm{s}$

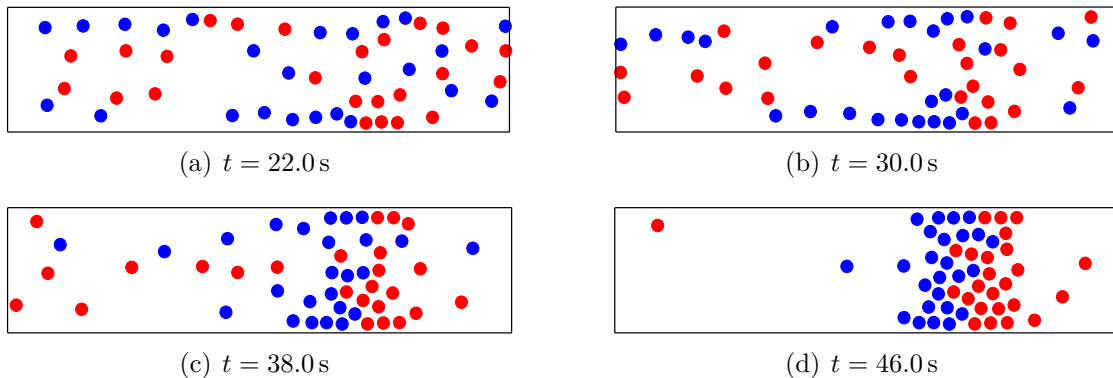(c) $t = 38.0\,\mathrm{s}$

(d) $t = 46.0\,\mathrm{s}$

Figure 4.21: Emergence of a gridlock: starting with two pedestrians with different walking directions facing each other (at the lower wall on the right), the agents start to queue behind them. Others stand besides and cannot pass due to the counterflow. Thereby, the gridlock grows from the wall towards the middle and eventually the other side of the corridor.

anymore. The more pedestrians arrive now, the worse the situation becomes until the entire system is in a stable, respectively absorbing state of a total standstill. As body rotation facilitates to solve these one-on-one conflicts, it reduces the number of gridlocks.

Following Fig. 4.19, the introduction of the fixed direction of view worsens the statistics for gridlocks in simulation scenarios. If the line of view is similar to the direction of motion, the fraction of gridlock runs is 36%, with the direction of view fixed to the target direction it is 10% higher. This seems reasonable: by forcing the agents to look towards their goal they have less freedom of choice for their directions, in particular for directions that deviate more from the target direction but could help to solve local conflicts. Also, the restriction of the direction of motion improves the dynamics only a little, by 2%. Why these adjustments to the model are reasonable nevertheless, can be seen when the ordering of the system is considered.

Nowak and Schadschneider [113] introduced a global order parameter Φ for pedestrian lane formation that indicates which fraction of the pedestrians in the system

is walking in a lane. For each pedestrian i the number of agents that walk in the same lane is counted for the same and the opposite walking direction, respectively. An agent n is assumed to walk in the same lane as a pedestrian i if their distance perpendicular to the desired walking direction is below a certain threshold γ, i.e.

$$|y_n(t) - y_i(t)| \leq \gamma. \tag{4.6}$$

Since Nowak et al. used a cellular automaton model which is discrete in space, they set a pedestrian's diameter as the threshold. However, they adopted this parameter from a concept for lane formation in colloidal suspensions [17]. In this work the authors set the threshold to 3/4 of a particle's diameter. Here, $\gamma = 3r/2$ with the pedestrian radius r is used as the threshold. With N_{L} the number of pedestrians that meet the criterion Eq. (4.6) and walk into the same direction as the pedestrian i, and N_{O} the number of agents moving into the opposite direction, the order parameter for a single pedestrian i is given by

$$\phi_i = \frac{(N_{\mathrm{L}} - N_{\mathrm{O}})^2}{(N_{\mathrm{L}} + N_{\mathrm{O}})^2}. \tag{4.7}$$

This parameter is zero for the same number of pedestrians walking in either directions and tends to one if there is almost only pedestrians with the same direction direction of motion in the lane. The global parameter is then given as the average over all N pedestrians,

$$\Phi = \frac{1}{N} \sum_{i=1}^{N} \phi_i. \tag{4.8}$$

Fig. 4.22 and 4.23 show the global parameter for single runs and the order parameter averaged over all runs that showed lane formation but no gridlocks, respectively. The final, optimised parameter set is compared to simulations without fixing the direction of view and without the additional strategy for the direction of motion. In both plots it is clearly shown that the optimised parameter set leads to a higher value of Φ than the other two configurations. Especially the results for simulations
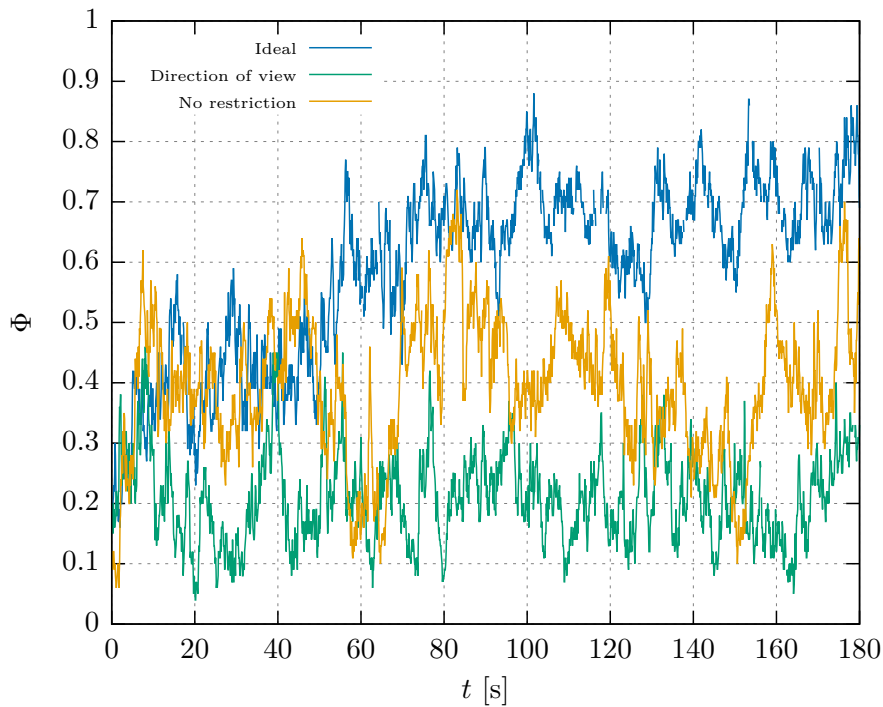
Figure 4.22: The order parameter for single simulation runs shows lane formation and self-organisation using the optimal parameter set, but reduced values if the choice of the direction of motion and the direction of view are not restricted.

without a fixed direction of view provide a much smaller order parameter. For the single 'ideal' run, the system organises itself within 80 s during which the order parameter increases in general. After this ordering phase, the order parameter fluctuates around $\Phi = 0.7$. The two other curves do not show this ordering phase at the beginning but level off at $\Phi \approx 0.4$ for the scenario without restriction on the direction of motion and $\Phi \approx 0.2$ for runs without the line-of-view concept. This indicates that the motion without the fixed direction of view can inhibit gridlocks well but does not provide distinct self-organisation in form of lane formation. Also, the introduction of the second strategy in the decision on the direction of motion enhances the ordering process.

Similar results are found for the averaged curves (Fig. 4.23). Here, the fluctuations are reduced and the general progress of the system becomes more apparent. For the 'ideal' simulations the organisation phase endures for $\sim 60\,\text{s}$, then the curve flattens at $\Phi \sim 0.6$. In contrast to the single runs, the averaged curves without a restriction on the direction of motion show a short organisation phase at the beginning of the simulation. After $\sim 40\,\text{s}$ the order parameter lies between 0.4 and 0.5. The small incline at the beginning of the direction-of-view curve is probably caused by the pedestrians that distribute uniformly from the randomly distributed initial positions. Afterwards, the order parameter is rather constant around $\Phi = 0.20 - 025$. The comparison of these three curves confirms what could be assumed considering the single runs. The formation of lanes can be described by the order parameter for the optimised simulation set-up. The distinction of this process is lowered when the direction of motion can be freely chosen. That means that the second strategy focussing on reaching the target enhances the formation of distinct lanes and stabilises them. Due to the velocity-dependent component it can also be understood as some kind of inertia which helps at reducing the fluctuations of the collision avoidance procedure. Despite the large number of imminent interactions, pedestrians in bidirectional flow still seem to concentrate on their personal goal. With a free direction of view the model is merely able to provide lanes and self-organisation that can be found if the pedestrians are forced to keep their gaze towards the goal. This indicates that the avoidance procedures in bidirectional flow have no impact on the general orientation of the pedestrians and supports the assumption that they keep focussing on the target while avoiding collisions with others. Another impact of this concept can be found in the simulations. Without restricting the pedestrians' orientation to the target direction they show unrealistic avoidance behaviours in one-on-one situations as shown in Fig. 4.24. The pedestrian highlighted in green walks from left to right and encounters another agent, coloured in orange, which is walking in the opposite direction. When they stand face to face (Fig. 4.24(a)), they, following the collision avoidance procedure, try to evade towards the upper wall, i.e. the green agent turns to the left, the orange one to
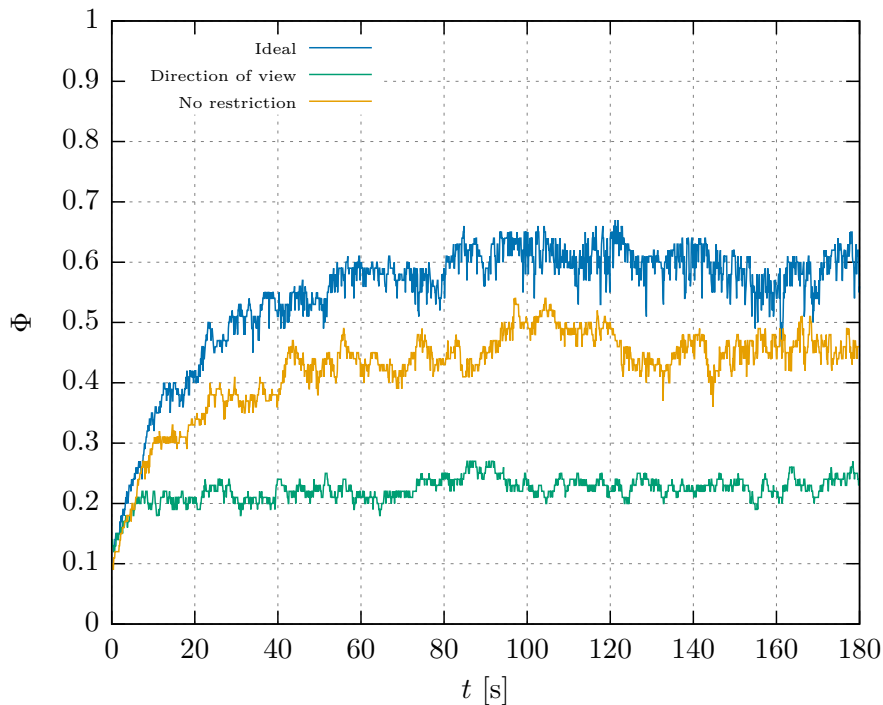
Figure 4.23: The averaged order parameters for runs without gridlocks show that the model is able to reproduced lane formation processes with the final configuration, but not without restricting the direction of view. It is slightly diminished if the agent does not focus on its goal.

the right. Instead of resolving this conflict in the next time step, the agents keep this configuration (Fig. 4.24(b)) and start to drift towards the edge of the corridor together until they have reached the wall (4.24(f)). Here, they are not able to solve the conflicts for several time steps (Fig. 4.24(g)) until one agent can free itself (Fig. 4.24(h)). This looks unrealistic and unusual, but is explainable when considering the relative positions of the two agents. After encountering each other, the agents decide to turn into the same direction. This is a consequence of the probability distribution which does not always provide the best solution, in fact, if the pedestrians stand directly in front of each other, evasions to either sides have similar probabilities. While making the step in order to avoid the collision, the

(a) $t = 18.2\,\text{s}$

(b) $t = 18.6\,\text{s}$

(c) $t = 19.0\,\text{s}$

(d) $t = 19.4\,\text{s}$

(e) $t = 19.8\,\text{s}$

(f) $t = 20.2\,\text{s}$

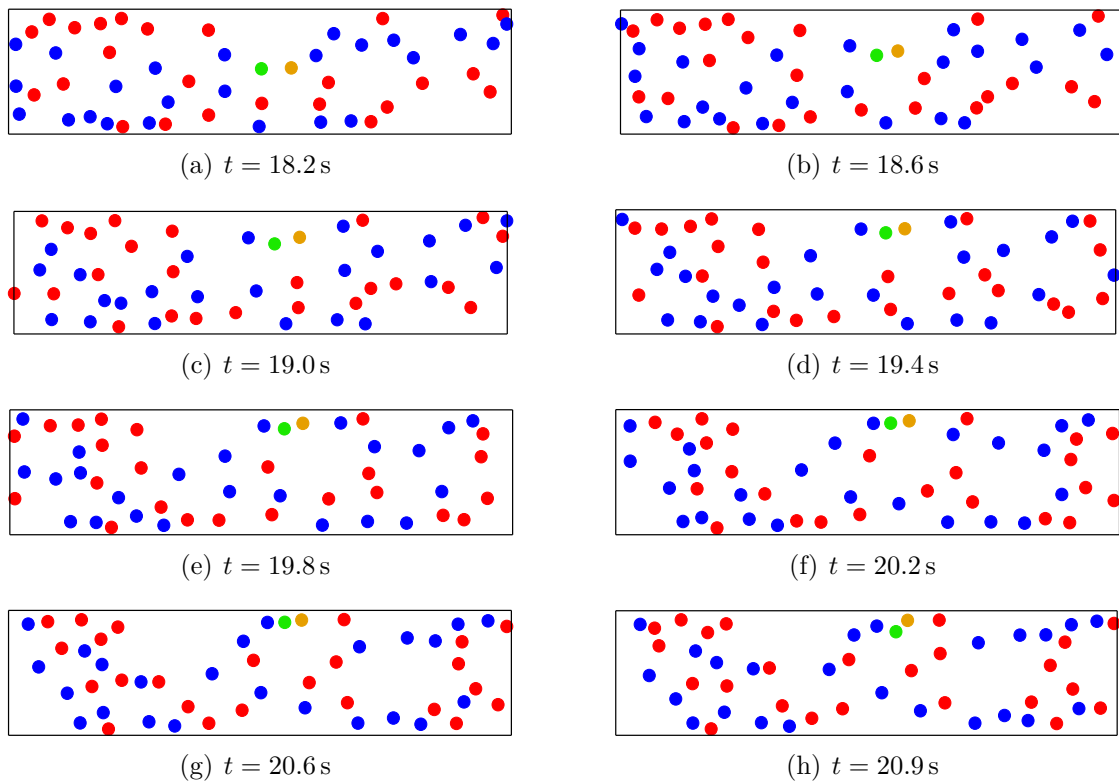(g) $t = 20.6\,\text{s}$

(h) $t = 20.9\,\text{s}$

Figure 4.24: Without keeping orientated towards the target, the agents show unrealistic interactions. They drift towards the wall because the relative positions screen each other's desired direction.

direction of view follows the direction of motion. Then, the relative situation has changed: while the green pedestrian stood directly in front of the orange one, it is now located on the left side, relatively. Vice versa, the orange agent moved to the right in the system of the green agent. Now, it is more likely for the green agent to walk straight forward or to the left instead of walking to the right which would lead to the target but also to a collision with the orange pedestrian. In each time step this configuration therefore stabilises itself, and the agents drift towards the wall staying in the same relative positions. The pedestrians are not able to solve the conflict until they have reached the wall where the possible directions are further

restricted. This effect is diminished when the direction of view is restricted to the target angle because the relative positions of the pedestrians change a little and the probability to choose a direction that enables an agent to pass the other one increases.

4.5 Summary

It has been shown that some of the model parameters have to be specifically adjusted for the two-person-interaction (TPI), single-file motion (SFM), evacuation (E) and bidirectional flow (BF). The parameter values and additional mechanisms that could represent realistic behaviour best are summarised in Tab. 4.1 and Tab. 4.2, respectively. For all situations, the minimal velocity $v_{\min} = 0.1\,\mathrm{m/s}$ was not changed.

	Δt [s]	$v_{\mathbf{max}}$ [m/s]	$\alpha_{\mathbf{S}}$ [1/s]	$d_{\mathbf{S}}$ [m]	p_0
TPI	0.3	1.2	0.5	0.1	0.5
SFM	0.3	1.4	0.65	0.1	0.6
E-GymBay E-WDG	0.1	1.2	1.3 3.3	0.03	0.5
BF	0.1	1.2	1.5	0.1	0.5

Table 4.1: Final model parameters for the specific scenarios

	$\alpha_{\mathbf{ia}}$	Additional mechanisms
TPI	-	-
SFM	$|\alpha_{\mathrm{ia}}| \leq 37°$	-
E-GymBay E-WDG	$|\alpha_{\mathrm{ia}} - \alpha_{\mathrm{t}}| \leq 57°$	Body rotation, pre-movement time
BF	Two strategies	Body rotation, view on target

Table 4.2: Additional mechanisms included for the specific scenarios

Conclusion and Outlook

In the course of increasing urbanisation and rising numbers and sizes of mass events, the understanding of pedestrian dynamics is not only important, but also necessary. However, empirical and experimental observations can be difficult, e.g. for practical or ethical reasons. In this instance, modelling and model development are crucial and have become a mainstay for research on pedestrian dynamics.

It has been the aim of this work to develop a new model for pedestrian dynamics that is based on continuous space and discrete time and therefore belongs to a model class whose potential is promising, but poorly investigated. The approach can reproduce pedestrian collective dynamics by modelling individual decision-making processes in an easily structured way and with high fidelity. It was intended to build the new approach on the SHDV model [102, 119, 120] which is set in discrete time and continuous space and that is able, as one of just a few models, to reproduce characteristic pedestrian movement in single-file motion (Sec. 2.3). The SHDV model was specifically developed for purely one-dimensional motion and therefore neglects the important aspects of real pedestrian motion. It is used as one component in the new model approach which aimed at representing the more general dynamics and interaction of pedestrians in two-dimensions, in particular, a decision-based collision avoidance procedure.

In many other models collision avoidance is based on the time-to-collision (TTC), e.g. [111, 126, 131, 141]. The TTC seems to be an intuitive way to model the perception and evaluation of imminent collisions by the agents. However, it has been shown early in the model development that including the TTC into the SHDV model is non-trivial. It cannot be used as an input parameter analogously to the distance headway because it explicitly considers the relative velocities of two interacting agents. Usually, a large TTC indicates that two pedestrians can walk freely with high velocities. However, in jammed states especially for one-dimensional single-file motion the TTC of two agents can also be large if both of them stand or walk slowly. Used as input parameter for the SHDV model, the TTC then leads to unrealistically high speeds in dense crowds. Instead, this model uses the distance-to-collision (DTC) which does not diverge in high densities and therefore provides more reliable information that can be easily used in the SHDV model. Especially when combined with anticipation it represents the relative motion of two agents in an intuitive way and helps at reducing the basis of decision-making in the model to one single quantity.

In the first stages of the model development, collision avoidance was considered to be solved by either the optimisation of a cost- or utility function or via stochastic methods. While many other models use optimisation problems (see Sec. 2.3), stochasticity is applied in this model that enables to explicitly capture the uncertainty of human behaviour and heterogeneities within the group of decision-makers. This is a key factor in order to describe pedestrian decisions while walking as realistically as possible.

Simulations of characteristic scenarios of pedestrian dynamics showed that the basic concept had to be adjusted. Thereby, insight into the relevant mechanisms in decision-based models and information on decision processes and behaviours of pedestrians was gained.

Besides route choice, more cognitive mechanisms and decisions had to be additionally implemented, e.g. the restriction of the direction of motion (Ch. 4). It was also not possible to find a single optimal parameter set that could be used to simulate

all scenarios realistically. Two conclusions on model development in general can be drawn from this. First, for cognitive agents an operational model only is not sufficient and requires supplements in the behaviour from the tactical level to reproduce realistic motion. Second, it is not known yet if there is one unique parameter set in any model that allows to reproduce most different situations on a quantitative level at all. This indicates that either the concept of such an 'optimal' parameter set must be reconsidered or that the parameters of operational models are not the relevant quantities to describe realistic behaviour of autonomous agents. Instead, still unknown (optimal) parameters of a tactical or even strategic model could be the key element for pedestrian models that determines which operational parameter set is suitable for a specific situation. Global knowledge on the scenarios, experiences and personal priorities seem to have a significant impact on pedestrian dynamics and could also be explicitly implemented in models.

The model reproduces realistic pedestrian motion by means of the adjustment of just a few parameters. Their physical interpretation enables to understand more about the motives and priorities of pedestrian decisions. Separating the decision process into several single decisions helps at considering the entire process more sophisticatedly. Since the adjustments for the simulations have been done mainly in the determination of the final direction of motion, this seems to be a point in a pedestrian's walking behaviour where psychology and sociology play an important role, rather than pure physics. On the contrary, it can be shown that it is sufficient to include psychological considerations occasionally and that physics-based approaches in general do not lose their validity, especially if stochastic elements are included. It is a particular advantage of this model that the decision process can be considered in detail which facilitates the identification of physical and psychological impacts on an agent's decision.

Dynamic lane formation can be simulated with this model. However, the emergence of gridlocks was also observed (Sec. 4.4). In contrast to single-file motion and evacuation, collision avoidance in lane formation was crucial not only for a correct adjustment of interpersonal distances, but also for the determination of

the walking direction. In this view, single-file motion, one-on-one scenarios and evacuations seem to be scenarios in which the agents are mainly goal-oriented, and counterflow in a corridor requires dynamics which focusses more on the interaction. This could help to identify the relevant mechanisms in pedestrian dynamics and to understand human walking behaviour in the specific scenarios.

The presented model reproduces almost all characteristic effects of pedestrian motion. Especially for single-file motion, the good qualitative and quantitative agreement with experimental data for global as well as local measurements are rarely reached by other modelling approaches, including the original SHDV model. In addition, the model is highly flexible and can be easily applied and extended due to its modular structure. Until now, no model-based artefacts have been found, and the hybrid approach obviates numerical schemes to solve the model. Compared to acceleration- or other decision-based models, it provides an 'intrinsic' view on the agent rather than a 'bird's eye perspective' where the main influencing quantities are given externally. A pedestrian's decision is no longer considered as a 'black box' that outputs optimal motion, but as interplay of single decisions that rely on physical and psychological mechanisms.

For future work, the collision avoidance procedure can still be improved, especially for high-density situations. Simulating other scenarios could help to refine the modelled dynamics and give indications on the relevant quantities in these situations. As yet, the model considers a fully homogeneous crowd of pedestrians. Heterogeneities could be included in many ways by varying model parameters for the agent itself (radius, visual field, membership in a social group) or the dynamics. In the determination of speed, stochasticity could lead to a more heterogeneous response to a given distance-to-collision. Implementing this may lead to even more realistic results.

Bibliography

[1] E. D. Kuligowski and S. M. V. Gwynne. *The need for behavioral theory in evacuation modeling.* In: W. W. F. Klingsch, C. Rogsch, A. Schadschneider and M. Schreckenberg, Eds., *Pedestrian and Evacuation Dynamics 2008*, 721 – 732, Springer, Berlin, Heidelberg, 2010.

[2] I. von Sivers, A. Templeton, G. Köster, J. Drury and A. Philippides. *Humans do not always act selfishly: social identity and helping in emergency evacuation simulation.* Transp. Res. Proc. **2**, 585 – 593, 2014.

[3] I. von Sivers, A. Templeton, F. Künzner, G. Köster, J. Drury, A. Philippides, T. Neckel and H.-J. Bungartz. *Modelling social identification and helping in evacuation simulation.* Saf. Sci. **89**, 288 – 300, 2016.

[4] A. Templeton, J. Drury and A. Philippides. *From mindless mass to small groups: conceptualizing collective behavior in crowd modeling.* Rev. Gen. Psychol. **19**, 215 – 229, 2015.

[5] A. Sieben, J. Schumann and A. Seyfried. *Collective phenomena in crowds - where pedestrian dynamics need social psychology.* PLoS One **16**, e0177328, 2017.

[6] L. F. Henderson. *The statistics of crowd fluids.* Nature **229**, 381 – 383, 1971.

[7] R. L. Hughes. *The flow of large crowds of pedestrians.* Math. Comput. Simul. **53**, 367 − 370, 2000.

[8] S. P. Hoogendoorn, F. L. M. van Wageningen-Kessels, W. Daamen and D. C. Duives. *Continuum modelling of pedestrian flows: from microscopic principles to self-organised macroscopic phenomena.* Physica A **416**, 684 − 694, 2014.

[9] M. Fukui and Y. Ishibashi. *Jamming transition in cellular automaton models for pedestrians.* J. Phys. Soc. Jpn. **68**, 3738 − 3739, 1999.

[10] A. Schadschneider. *Cellular automaton approach to pedestrian dynamics.* In: M. Schreckenberg and S. D. Sharma, Eds., *Pedestrian and Evacuation Dynamics*, 75 − 86, Springer, Berlin, Heidelberg, 2002.

[11] C. Burstedde, K. Klauck, A. Schadschneider and J. Zittartz. *Simulation of pedestrian dynamics using a two-dimensional cellular automaton.* Physica A **295**, 507 − 525, 2001.

[12] D. Helbing and P. Molnár. *Social force model for pedestrian dynamics.* Phys. Rev. E **51**, 4282 − 4286, 1995.

[13] M. J. Seitz and G. Köster. *Natural discretization of pedestrian movement in continuous space.* Phys. Rev. E **86**, 046108, 2012.

[14] A. Garcimartín, J. M. Pastor, L. M. Ferrer, J. J. Ramos, C. Martín-Gómez and I. Zuriguel. *Flow and Clogging of a sheep herd passing through a bottleneck.* Phys. Rev. E **91**, 022808, 2015.

[15] I. Zuriguel, D. R. Parisi, R. C. Hidalgo, C. Lozano, A. Jando, P. A. Gago, J. P. Peralta, L. M. Ferrer, L. A. Pugnaloni, E. Clément, D. Maza, I. Pagonabarraga and A. Garcimartín. *Clogging transition of many-particle systems flowing through bottlenecks.* Sci. Rep. **4**, 7324, 2014.

[16] F. Kogler and S. H. L. Klapp. *Lane formation in a system of dipolar microswimmers.* Europhys. Lett. **110**, 10004, 2015.

[17] M. Rex and H. Löwen. *Lane formation in oppositely charged colloids driven by an electric field: Chaining and two-dimensional crystallization.* Phys. Rev. E **75**, 051402, 2007.

[18] T. Vissers, A. Wysocki, M. Rex, H. Löwen, C. P. Royall, A. Imhof and A. van Blaaderen. *Lane formation in driven mixtures of oppositely charged colloids.* Soft Matter **7**, 2352, 2011.

[19] T. Vicsek, A. Czirók, E. Ben-Jacob, I. Cohen and O. Shochet. *Novel type of phase transition in a system of self-driven particles.* Phys. Rev. Lett. **75**, 1226 – 1229, 1995.

[20] M. Muramatsu, T. Irie and T. Nagatani. *Jamming transition in pedestrian counter flow.* Physica A **267**, 487 – 498, 1999.

[21] J. Adrian, N. W. F. Bode, M. Amos, M. Baratchi, M. Beermann, M. Boltes, A. Corbetta, G. Dezecache, J. Drury, Z. Fu, R. Geraerts, S. M. V. Gwynne, G. Hofinger et al. *A glossary for research on human crowd dynamics.* Collective Dynamics **4**, 1 – 13, 2019.

[22] A. Schadschneider, W. Klingsch, H. Klüpfel, T. Kretz, C. Rogsch and A. Seyfried. *Evacuation dynamics: empirical results, modeling and applications.* In: R. A. Meyers, Ed., *Encyclopedia of Complexity and Systems Science*, 3142 – 3176. Springer, 2009.

[23] A. Schadschneider, D. Chowdhury and K. Nishinari. *Stochastic transport in complex systems: from molecules to vehicles.* Elsevier Science, 2010.

[24] A. Schadschneider, M. Chraibi, A. Seyfried, A. Tordeux and J. Zhang. *Pedestrian dynamics - from empirical results to modeling.* In: L. Gibelli and N. Bellomo, Eds., *Crowd Dynamics, Volume 1: Theory, Models and Safety Problems*, 63 – 102. Birkhäuser, 2018.

[25] H. Klüpfel. *Crowd dynamics phenomena, methodology, and simulation.* In: H. Timmermans, Ed., *Pedestrian Behavior: Models, Data Collection and Applications*, 215 – 244. Emerald Group Publishing Limited, 2009.

[26] U. Weidmann. *Transporttechnik der Fussgänger. Transporttechnische Eigenschaften des Fussgängerverkehrs (Literaturauswertung).* In: *Schriftenreihe des IVT Nr. 90, Zweite, ergänzte Auflage.* IVT, Institut für Verkehrsplanung, Transporttechnik, Strassen- und Eisenbahnbau ETH Zürich, 1993.

[27] A. Seyfried, M. Boltes, J. Kähler, W. W. F. Klingsch, A. Portz, T. Rupprecht, A. Schadschneider, B. Steffen and A. Winkens. *Enhanced empirical data for the fundamental diagram and the flow through bottlenecks.* In: W. W. F. Klingsch, C. Rogsch, A. Schadschneider and M. Schreckenberg, Eds., *Pedestrian and Evacuation Dynamics 2008*, 145 – 156, Springer, Berlin, Heidelberg, 2010.

[28] J. Zhang, W. W. F. Klingsch, A. Schadschneider and A. Seyfried. *Transitions in pedestrian fundamental diagrams of straight corridors and T-junctions.* J. Stat. Mech. **2011**, P06004, 2011.

[29] S. Hoogendoorn, W. Daamen and M. Campanella. *Self-organization and chaos in pedestrians flow: Experiments and modelling.* In: C. S. Skiadas, Ed., *Proceedings of CHAOS 2008*, 1 – 10. Technical University of Crete, 2008.

[30] M. Moussaïd, S. Garnier, G. Theraulaz and D. Helbing. *Collective information processing and pattern formation in swarms, flocks, and crowds.* Top. Cogn. Sci. **1**, 469 – 497, 2009.

[31] Pedestrian Dynamics Data Archive. *Evacuation, GymBay.* http://ped.fz-juelich.de/da/2014socialGroups, 2014.

[32] A. Seyfried, O. Passon, B. Steffen, M. Boltes, T. Rupprecht and W. W. F. Klingsch. *New insights into pedestrian flow through bottlenecks.* Transport Sci. **43**, 395 – 406, 2009.

[33] M. Bukáček, P. Hrabák and M. Krbálek. *Experimental analysis of two-dimensional pedestrian flow in front of bottlenecks.* In: M. Chraibi, M. Boltes, A. Schadschneider and A. Seyfried, Eds., *Traffic and Granular Flow '13*, 93 – 101, Springer, Cham, 2015.

[34] A. Winkens, T. Rupprecht, A. Seyfried and W. W. F. Klingsch. *Empirical study of pedestrians' characteristics at bottlenecks.* In: W. W. F. Klingsch, C. Rogsch, A. Schadschneider and M. Schreckenberg, Eds., *Pedestrian and Evacuation Dynamics 2008*, 263 – 268, Springer, Berlin, Heidelberg, 2010.

[35] A. Nicolas, S. Bouzat and M. N. Kuperman. *Pedestrian flows through a narrow door: effect of individual behaviours on the global flow and microscopic dynamics.* Transp. Res. B **99**, 30 – 43, 2017.

[36] A. Nicolas. *Fluctuations in pedestrian evacuation times: Going one step beyond the exit capacity paradigm for bottlenecks.* In: S. H. Hamdar, Ed., *Traffic and Granular Flow '17*, 357 – 364, Springer, Cham, 2019.

[37] H. C. Muir, D. M. Bottomley and C. Marrison. *Effects of motivation and cabin configuration on emergency aircraft evacuation behavior and rates of egress.* Int. J. Aviat. Psychol. **6**, 57 – 77, 1996.

[38] A. Garcimartín, I. Zuriguel, J. M. Pastor, C. Martín-Gómez and D. R. Parisi. *Experimental evidence of the "Faster is slower" effect.* Transp. Res. Proc. **2**, 760 – 767, 2014.

[39] C. Feliciani and K. Nishinari. *Pedestrian rotation measurement in bidirectional streams.* In: W. Song, J. Ma and L. Fu, Eds., *Pedestrian and Evacuation Dynamics 2016*, Collective Dynamics, 76 – 83, 2016.

[40] C. Feliciani and K. Nishinari. *Empirical analysis of the lane formation process in bidirectional pedestrian flow.* Phys. Rev. E **94**, 032304, 2016.

[41] J. Zhang, W. W. F. Klingsch, A. Schadschneider and A. Seyfried. *Ordering in bidirectional pedestrian flows and its influence on the fundamental diagram.* J. Stat. Mech. **2012**, P02002, 2012.

[42] Pedestrian Dynamics Data Archive. *Bidirectional Flow.* http://ped.fz-juelich.de/da/doku.php?id=corridor4, 2009.

[43] C. Appert-Rolland, J. Cividini, H.-J. Hilhorst and P. Degond. *Pedestrian flows: from individuals to crowds.* Transp. Res. Proc. **2**, 468 – 476, 2014.

[44] D. Helbing, A. Johansson and H. Z. Al-Abideen. *Dynamics of crowd disasters: An empirical study.* Phys. Rev. E **75**, 046109, 2007.

[45] A. Portz and A. Seyfried. *Analyzing stop-and-go waves by experiment and modeling.* In: R. D. Peacock, E. D. Kuligowski and J. D. Averill, Eds., *Pedestrian and Evacuation Dynamics*, 577 – 586, Springer, Boston, MA, 2011.

[46] A. Seyfried, B. Steffen, W. Klingsch and M. Boltes. *The fundamental diagram of pedestrian movement revisited.* J. Stat. Mech. **2005**, P10002, 2005.

[47] Y. Zhao, T. Lu, M. Li and L. Tian. *The self-slowing behavioral mechanism of pedestrians under normal and emergency conditions.* Phys. Lett. A **381**, 3149 – 3160, 2017.

[48] V. Ziemer, A. Seyfried and A. Schadschneider. *Congestion dynamics on pedestrian single-file-motion.* In: V. L. Knoop and W. Daamen, Eds., *Traffic and Granular Flow '15*, 89 – 96, Springer, Cham, 2016.

[49] A. Jelić, C. Appert-Rolland, S. Lemercier and J. Pettré. *Properties of pedestrians walking in line: Fundamental diagrams.* Phys. Rev. E **85**, 036111, 2012.

[50] R. Barlovic, L. Santen, A. Schadschneider and M. Schreckenberg. *Metastable states in cellular automata for traffic flow.* Eur. Phys. J. B **5**, 793 – 800, 1998.

[51] W. Lv, X. Wei and W. Song. *Experimental study on the interaction mechanism of cross-walking Pedestrians.* In: M. Chraibi, M. Boltes, A. Schadschneider and A. Seyfried, Eds., *Traffic and Granular Flow '13*, 219 – 226, Springer, Cham, 2015.

[52] D. R. Parisi, P. A. Negri and L. Bruno. *Experimental characterization of collision avoidance in pedestrian dynamics.* Phys. Rev. E **94**, 022318, 2016.

[53] M. Huber, Y.-H. Su, M. Krüger, K. Faschian, S. Glasauer and J. Hermsdörfer. *Adjustments of speed and path when avoiding collisions with another pedestrian.* PLoS One **9**, e89589, 2014.

[54] B. G. Silverman, N. I. Badler, N. Pelechano and K. O'Brien. *Crowd simulation incorporating agent psychological models, roles and communication*, 2005.

[55] C. Rogsch, M. Schreckenberg, E. Tribble, W. W. F. Klingsch and T. Kretz. *Was it panic? An overview about mass-emergencies and their origins all over the world for recent years.* In: W. W. F. Klingsch, C. Rogsch, A. Schadschneider and M. Schreckenberg, Eds., *Pedestrian and Evacuation Dynamics 2008*, 743 – 755, Springer, Berlin, Heidelberg, 2010.

[56] J. D. Sime. *Affiliate behaviour during escape to building exits.* J. Environ. Psychol. **3**, 21 – 41, 1983.

[57] A. R. Mawson. *Understanding mass panic and other collective responses to threat and disaster.* Psychiatry **68**, 95 – 113, 2005.

[58] L. Crociani, G. Vizzari and S. Bandini. *Adaptive tactical decisions in pedestrian simulation: a hybrid agent approach.* In: V. L. Knoop and W. Daamen, Eds., *Traffic and Granular Flow '15*, 257 – 264, Springer, Cham, 2016.

[59] C. Appert-Rolland. *Modeling of Pedestrians.* In: M. Chraibi, M. Boltes, A. Schadschneider and A. Seyfried, Eds., *Traffic and Granular Flow '13*, 3 – 12, Springer, Cham, 2015.

[60] L. F. Henderson. *On the fluid mechanics of human crowd motion.* Transp. Res. **8**, 509 – 515, 1974.

[61] R. L. Hughes. *A continuum theory for the flow of pedestrians.* Trans. Res. B **36**, 507 – 535, 2002.

[62] R. L. Hughes. *The flow of human crowds.* Annu. Rev. Fluid Mech. **35**, 169 – 182, 2003.

[63] L. Huang, S. C. Wong, M. Zhang, C.-W. Shu and W. H. Lam. *Revisiting Hughes' dynamic continuum model for pedestrian flow and the development of an efficient solution algorithm.* Trans. Res. B **43**, 127 – 141, 2009.

[64] A. Treuille, S. Cooper and Z. Popović. *Continuum crowds.* In: Association for Computing Machinery (ACM), Ed., *ACM Transactions on Graphics*, 25, 1160 – 1168, ACM, New York, 2006.

[65] S. P. Hoogendoorn, F. L. M. van Wageningen-Kessels, W. Daamen, D. C. Duives and M. Sarvi. *Continuum theory for pedestrian traffic flow: local route choice modelling and its implications.* Transp. Res. Proc. **7**, 381 – 397, 2015.

[66] P. Degond, C. Appert-Rolland, M. Moussaïd, J. Pettré and G. Theraulaz. *A hierarchy of heuristic-based models of crowd dynamic.* J. Stat. Phys. **152**, 1033 – 1068, 2013.

[67] K. Hirai and K. Tarui. *A simulation of the behaviour of a crowd in Panic.* In: IEEE Systems, Man and Cybernetics Society, Ed., *Proceeding of the 1975 International Conference on Cybernetics and Society*, 409 – 411, IEEE, New York, 1975.

[68] S. Okazaki. *A study of simulation model for pedestrian movement in architectural space, Part 1: Pedestrian movement by the application of magnetic models.* Transactions of Architectural Institute of Japan **283**, 111, 1979.

112

[69] S. Okazaki and S. Mathsushita. *A study of simulation model for pedestrian movement with evacuation and queuing.* In: R. A. Smith and J. F. Dickie, Eds., *Proceedings of the International Conference on Engineering for Crowd Safety*, Elsevier Science, Amsterdam, 1993.

[70] M. Chraibi, A. Seyfried and A. Schadschneider. *Generalized centrifugal-force model for pedestrian dynamics.* Phys. Rev. E **82**, 046111, 2010.

[71] W. J. Yu, R. Chen, L. Y. Dong and S. Q. Dai. *Centrifugal force model for pedestrian dynamics.* Phys. Rev. E **72**, 026112, 2005.

[72] M. Chraibi, M. Freialdenhoven, A. Schadschneider and A. Seyfried. *Modeling the desired direction in a force-based model for pedestrian dynamics.* In: V. V. Kozlov, A. P. Buslaev, A. S. Bugaev, M. V. Yashina, A. Schadschneider and M. Schreckenberg, Eds., *Traffic and Granular Flow '11*, 263 – 275, Springer, Berlin, Heidelberg, 2013.

[73] M. Chraibi. *Validated force-based modeling of pedestrian dynamics.* PhD thesis, Universität zu Köln, 2012.

[74] M. Chraibi, M. Boltes, A. Schadschneider and A. Seyfried, Eds. *Traffic and Granular Flow '13*, Springer, Cham, 2015.

[75] A. Schadschneider. *Noise-induced stop-and-go dynamics in pedestrian single-file locomotion.* Presentation, Conference 'Crowds: Models and Control', CIRM, Marseille, 2019.

[76] G. Köster, F. Treml and M. Gödel. *Avoiding numerical pitfalls in social force models.* Phys. Rev. E **87**, 063305, 2013.

[77] G. Köster and M. Gödel. *Implementation issues of force based pedestrian motion models.* In: M. Chraibi, M. Boltes, A. Schadschneider and A. Seyfried, Eds., *Traffic and Granular Flow '13*, 63 – 71, Springer, Cham, 2015.

[78] A. Schadschneider, C. Eilhardt, S. Nowak and P. R. Will. *Towards a calibration of the floor field cellular automaton*. In: R. D. Peacock, E. D. Kuligowski and J. D. Averill, Eds., *Pedestrian and Evacuation Dynamics*, 557 – 566, Springer, Boston, MA, 2011.

[79] V. Blue and J. Adler. *Cellular automata microsimulation of bidirectional pedestrian flow*. Transp. Res. Rec. **1678**, 135 – 141, 2000.

[80] A. Kirchner, K. Nishinari and A. Schadschneider. *Friction effects and clogging in a cellular automaton model for pedestrian dynamics*. Phys. Rev. E **67**, 056122, 2003.

[81] D. Yanagisawa, A. Tomoeda and K. Nishinari. *Conflicts at an exit in pedestrian dynamics*. In: W. W. F. Klingsch, C. Rogsch, A. Schadschneider and M. Schreckenberg, Eds., *Pedestrian and Evacuation Dynamics 2008*, 491 – 502, Springer, Berlin, Heidelberg, 2010.

[82] S. Sarmady, F. Haron and A. Z. Talib. *Simulation of pedestrian movement using fine grid cellular automata model*. In: *2010 12th International Conference on Computer Modelling and Simulation*, 428 – 433, IEEE, Cambridge, 2010.

[83] K. Yamamoto, S. Kokubo and K. Nishinari. *Simulation for pedestrian dynamics by real-coded cellular automata (RCA)*. Physica A **379**, 645 – 660, 2007.

[84] A. Kirchner, H. Klüpfel, K. Nishinari, A. Schadschneider and M. Schreckenberg. *Discretization effects and the influence of walking speed in cellular automata models for pedestrian dynamics*. J. Stat. Mech. **2004**, P10011, 2004.

[85] R.-Y. Guo. *Simulation of spatial and temporal separation of pedestrian counter flow through bottleneck*. Physica A **415**, 428 – 439, 2014.

[86] A. Tordeux, M. Chraibi and A. Seyfried. *Collision-free speed model for pedestrian dynamics.* In: V. L. Knoop and W. Daamen, Eds., *Traffic and Granular Flow '15*, 225 – 232, Springer, Cham, 2016.

[87] D. Helbing and P. Molnár. *Self-organization phenomena in pedestrian crowds.* In: F. Schweitzer, Ed., *Self-Organization of Complex Structures. From Individual to Collective Dynamics*, 569 – 577, Gordon and Breach, London, 1997.

[88] E. Kirik, A. Malyshev and E. Popel. *On the validation of a discrete-continuous model with bottleneck flow and computational artifacts.* In: M. Chraibi, M. Boltes, A. Schadschneider and A. Seyfried, Eds., *Traffic and Granular Flow '13*, 121 – 128, Springer, Cham, 2015.

[89] R.-Y. Guo and H.-J. Huang. *Formulation of pedestrian movement in microscopic models with continuous space representation.* Transp. Res. C **24**, 50 – 61, 2012.

[90] I. M. Sticco, F. E. Cornes, G. A. Frank and C. O. Dorso. *Beyond the faster is slower effect.* Phys. Rev. E **96**, 052303, 2017.

[91] L. Wang and Y. Jiang. *Escape dynamics based on bounded rationality.* Physica A **531**, 2019.

[92] F. E. V. G. Castro and J. P. Pabico. *Microsimulations of arching, clogging and bursty exit phenomena in crowd dynamics.* Philipp. Inf. Technol. J. **6**, 11 – 16, 2012.

[93] I. M. Sticco, G. A. Frank, F. E. Cornes and C. O. Dorso. *Fundamental diagram in the context of the Social Force Model.* arXiv:1812.10807, 2019.

[94] A. Portz and A. Seyfried. *Modeling Stop-and-Go Waves in Pedestrian Dynamics.* In: R. Wyrzykowski, J. Dongarra, K. Karczewski and J. Wasniewski, Eds., *Parallel Processing and Applied Mathematics. PPAM 2009. Lecture Notes in Computer Science*, 6068, 561 – 568. Springer, Berlin, Heidelberg, 2010.

[95] A. Seyfried, A. Portz and A. Schadschneider. *Phase coexistence in congested states of pedestrian dynamics.* In: S. Bandini, S. Manzoni, H. Umeo and G. Vizzari, Eds., *Cellular automata. ACRI 2010. Lecture Notes on Computer Science*, 6350, 496 – 505, Springer, Berlin Heidelberg, 2010.

[96] M. Chraibi and A. Seyfried. *Pedestrian dynamics with event-driven simulation.* In: W. W. F. Klingsch, C. Rogsch, A. Schadschneider and M. Schreckenberg, Eds., *Pedestrian and Evacuation Dynamics 2008*, 713 – 718, Springer, Berlin, Heidelberg, 2010.

[97] Q. Xu, B. Mao, X. Liang and J. Feng. *Simple cognitive heuristics applied to modeling pedestrian behavior dynamics.* Procedia Soc. Behav. Sci. **43**, 571 – 578, 2012.

[98] D. Zhang, H. Zhu, S. Hostikka and S. Qiu. *Pedestrian dynamics in a heterogeneous bidirectional flow: overtaking behaviour and lane formation.* Physica A **525**, 72 – 84, 2019.

[99] W. Lv, W.-G. Song, J. Ma and Z.-M. Fang. *A two-dimensional optimal velocity model for unidirectional pedestrian flow based on pedestrian's visual hindrance field.* In: *IEEE Transactions on Intelligent Transportation Systems*, 14, 1753 – 1763, 2013.

[100] M. Zhou, H. Dong, F.-Y. Wang, Q. Wang and X. Yang. *Modeling and simulation of pedestrian dynamical behavior based on a fuzzy logic approach.* Inf. Sci. **360**, 112 – 130, 2016.

[101] Y. Xiao, Z. Gao, Y. Qu and X. Li. *A pedestrian flow model considering the impact of local density: Voronoi diagram based heuristics approach.* Transp. Res. C **68**, 566 – 580, 2016.

[102] C. Eilhardt and A. Schadschneider. *Stochastic headway dependent velocity model for 1d pedestrian dynamics at high densities.* Transp. Res. Proc. **2**, 400 – 405, 2014.

[103] M. Chraibi, T. Ezaki, A. Tordeux, K. Nishinari, A. Schadschneider and A. Seyfried. *Jamming transitions in force-based models for pedestrian dynamics.* Phys. Rev. E **92**, 042809, 2015.

[104] A. Tordeux, M. Chraibi, A. Schadschneider and A. Seyfried. *Influence of the number of precedessors in interaction within acceleration-based flow models.* J. Phys. A **50**, 345102, 2017.

[105] A. Tordeux, A. Schadschneider and S. Lassarre. *Noise-induced stop-and-go dynamics.* In: S. H. Hamdar, Ed., *Traffic and Granular Flow '17*, 337 – 345. Springer, 2019.

[106] F. Dietrich, S. Disselnkötter and G. Köster. *How to get a model in pedestrian dynamics to produce stop and go waves.* In: V. L. Knoop and W. Daamen, Eds., *Traffic and Granular Flow '15*, 161 – 168, Springer, Cham, 2016.

[107] S. Nowak and A. Schadschneider. *A cellular automaton approach for lane formation in pedestrian counterflow.* In: V. V. Kozlov, A. P. Buslaev, A. S. Bugaev, M. V. Yashina, A. Schadschneider and M. Schreckenberg, Eds., *Traffic and Granular Flow '11*, 149 – 160, Springer, Berlin, Heidelberg, 2013.

[108] J. D. González, M. L. Sandoval and J. Delgado. *Social field model to simulate bidirectional pedestrian flow using cellular automata.* In: V. V. Kozlov, A. P. Buslaev, A. S. Bugaev, M. V. Yashina, A. Schadschneider and M. Schreckenberg, Eds., *Traffic and Granular Flow '11*, 197 – 206, Springer, Berlin, Heidelberg, 2013.

[109] K. Nishinari, Y. Suma, D. Yanagisawa, A. Tomoeda, A. Kimura and R. Nishi. *Toward smooth movement of crowds.* In: W. W. F. Klingsch, C. Rogsch, A. Schadschneider and M. Schreckenberg, Eds., *Pedestrian and Evacuation Dynamics 2008*, 293 – 308, Springer, Berlin, Heidelberg, 2010.

[110] J. Cristín, V. Méndez and D. Campos. *Universal scaling in bidirectional flows of self-avoiding agents.* arXiv:1901.10838v1, 2019.

[111] A. Festa, A. Tosin and M.-T. Wolfram. *Kinetic description of collision avoidance in pedestrian crowds by sidestepping.* Kinet. Relat. Models **11**, 491 – 520, 2018.

[112] A. Nakayama, K. Hasebe and Y. Sugiyama. *Instability of pedestrian flow and phase structure in a two-dimensional optimal velocity model.* Phys. Rev. E **71**, 036121, 2005.

[113] S. Nowak and A. Schadschneider. *Quantitative analysis of pedestrian counterflow in a cellular automaton model.* Phys. Rev. E **85**, 066128, 2012.

[114] F. Dietrich and G. Köster. *Gradient navigation model for pedestrian dynamics.* Phys. Rev. E **89**, 062801, 2014.

[115] J. Kwak, H.-H. Jo, T. Luttinen and I. Kosonen. *Jamming transitions induced by an attraction in pedestrian flow.* Phys. Rev. E **96**, 022319, 2017.

[116] M. J. Seitz, N. W. F. Bode and G. Köster. *How cognitive heuristics can explain social interactions in spatial movement.* J. R. Soc. Interface **13**, 20160439, 2016.

[117] N. Guo, H.-X. Liu, R. Jiang, B. Jia and M.-B. Hu. *Improving heuristics-based model to reproduce lane formation.* Int. J. Mod. Phys. C **29**, 1850069, 2018.

[118] W. Guo, X. Wang and X. Zheng. *Lane formation in pedestrian counterflows driven by a potential field considering following and avoidance behaviours.* Physica A **432**, 87 – 101, 2015.

[119] C. Eilhardt and A. Schadschneider. *Stochastic headway dependent velocity model and phase separation in pedestrian dynamics.* In: M. Chraibi, M. Boltes, A. Schadschneider and A. Seyfried, Eds., *Traffic and Granular Flow '13*, 281 – 289, Springer, Cham, 2015.

[120] C. Eilhardt. *Computer simulation of pedestrian dynamics at high densities.* PhD thesis, Universität zu Köln, 2014.

[121] M. Bando, K. Hasebe, A. Nakayama, A. Shibata and Y. Sugiyama. *Structure stability of congestion in traffic dynamics.* Jpn. J. Ind. Appl. Math. **11**, 203 – 223, 1994.

[122] M. Bando, K. Hasebe, A. Nakayama, A. Shibata and Y. Sugiyama. *Dynamical model of traffic congestion and numerical simulation.* Phys. Rev. E **51**, 1035 – 1042, 1995.

[123] K. Teknomo, Y. Takeyama and H. Inamura. *Microscopic pedestrian simulation model to evaluate "lane-like segregation" of pedestrian crossing.* In: *Proceedings of Infrastructure Planning Conference,* 24, 1 – 4, 2001.

[124] G. Baglietto and D. R. Parisi. *Continuous-space automaton model for pedestrian dynamics.* Phys. Rev. E **83**, 056117, 2011.

[125] Z.-M. Fang, W. Song, X. Liu, W. Lv, J. Ma and X. Xiao. *A continuous distance model (CDM) for the single-file pedestrian movement considering step-frequency and length.* Physica A **391**, 307 – 316, 2012.

[126] I. Karamouzas and M. Overmars. *A velocity-based approach for simulating human collision avoidance.* In: *Intelligent Virtual Agents*, 6356 of *LNAI*, 180 – 186. Springer, Berlin Heidelberg, 2010.

[127] M. Asano, T. Iryo and M. Kuwahara. *Microscopic pedestrian simulation model combined with a tactical model for route choice behaviour.* Transp. Res. C **18**, 842 – 855, 2010.

[128] D. C. Duives, W. Daamen and S. P. Hoogendoorn. *The influence of the interaction characteristics on the movement dynamics of pedestrians.* In: W. Song, L. Ma and L. Fu, Eds., *Pedestrian and Evacuation Dynamics 2016*, Collective Dynamics, 326 – 333, 2016.

[129] Y. Rahmati and A. Talebpour. *Learning-based game theoretical framework for modeling pedestrian motion.* Phys. Rev. E **98**, 032312, 2018.

[130] G. Antonini, M. Bierlaire and M. Weber. *Discrete choice models of pedestrian walking behavior.* Transp. Res. B **40**, 667 – 687, 2006.

[131] M. Moussaïd, D. Helbing and G. Theraulaz. *How simple rules determine pedestrian behavior and crowd disasters.* PNAS **108**, 6884 – 6888, 2011.

[132] J. Ondřej, J. Pettré, A.-H. Olivier and S. Donikian. *A synthetic-vision based steering approach for crowd simulation.* In: *ACM SIGGRAPH 2010 Papers*, SIGGRAPH '10, 123:1 – 123:9, ACM, New York, 2010.

[133] J. P. Costella. *Galilean antialiasing for virtual reality displays.* Technical report, School of Physics, The University of Melbourne, Parkville Vic. 3052, Australia, 1992.

[134] A. Turner and A. Penn. *Encoding natural movement as an agent-based dystem: an investigation into human pedestrian behaviour in the built environment.* Environment and Planning B **29**, 473 – 490, 2002.

[135] R. Bailo, J. A. Carrillo and P. Degond. *Pedestrian models based on rational behaviour.* In: L. Gibelli and N. Bellomo, Eds., *Crowd Dynamics, Volume 1*, 1, 259 – 292. Springer International Publishing, 2018.

[136] M. Bierlaire, G. Antonini and M. Weber. *Behavioral dynamics for pedestrians.* In: K. Axhausen, Ed., *Moving Through Nets: the Physical and Social Dimensions of Travel.* Elsevier, 2003.

[137] J. M. Usher, E. Kolstad and L. Strawderman. *Simulating pedestrian navigation behavior using a probabilistic model.* In: *Proceedings of the 2009 Industrial Engineering Research Conference*, 1634 – 1639, 2009.

[138] H. C. Braga, G. F. Moita and P. E. M. Almeida. *Simulation of people flow by a new fuzzy discrete automata model and an ergonomic approach.* In: V. L. Knoop and W. Daamen, Eds., *Traffic and Granular Flow '15*, 137 – 144, Springer, Cham, 2016.

[139] P. Hrabák, O. Ticháček and V. Sečkárová. *Estimation of discretised motion of pedestrians by the decision-making model.* In: V. L. Knoop and W. Daamen, Eds., *Traffic and Granular Flow '15*, 313 – 320, Springer, Cham, 2016.

[140] S. Bonneaud and W. H. Warren. *An empirically-grounded emergent approach to modeling pedestrian behavior.* In: U. Weidmann, U. Kirsch and M. Schreckenberg, Eds., *Pedestrian and Evacuation Dynamics 2012*, 625 – 638, Springer, Cham, 2014.

[141] F. Zanlungo, T. Ikeda and T. Kanda. *Social force model with explicit collision prediction.* Europhys. Lett. **93**, 68005, 2011.

[142] A. Johansson. *Constant-net-time headway as a key mechanism behind pedestrian flow dynamics.* Phys. Rev. E **80**, 026120, 2009.

[143] Y. Suma, D. Yanagisawa and K. Nishinari. *Anticipation effect in pedestrian dynamics: modeling and experiments.* Physica A **391**, 248 – 263, 2012.

[144] P. A. Thompson and E. W. Marchant. *A computer model for the evacuation of large building populations.* Fire Saf. J. **24**, 131 – 148, 1995.

[145] V. Schneider and R. Könnecke. *Egress route choice modelling - concepts and applications.* In: W. W. F. Klingsch, C. Rogsch, A. Schadschneider and M. Schreckenberg, Eds., *Pedestrian and Evacuation Dynamics 2008*, 619 – 625, Springer, Berlin, Heidelberg, 2010.

[146] G. C. Dachner and M. Kinateder. *Effects of visual information on decision making during way-finding in emergency and non-emergency situations.* In: W. Song, J. Ma and L. Fu, Eds., *Pedestrian and Evacuation Dynamics 2016*, Collective Dynamics, 185 – 189, 2016.

[147] J. van den Berg, S. Patil, J. Sewall, D. Manocha and M. Lin. *Interactive Navigation of Multiple Agents in Crowded Environments.* In: *Proceedings of the 2008 Symposium on Interactive 3D Graphics and Games*, I3D '08, 139 – 147, ACM, New York, 2008.

[148] M. Chraibi and D. Haensel. *Cognitive map routing.* In: S. El Yacoubi, J. Wąs and S. Bandini, Eds., *12th International Conference on Cellular Automata for Research and Industry, ACRI 2016*, 210 – 218, Springer, Cham, 2016.

[149] W. Shao and D. Terzoloulos. *Autonomous pedestrians.* In: K. Anjyo and P. Faloutsos, Eds., *Eurographics / ACM SIGGRAPH Symposium in Computer Animation*, 19 – 28, ACM, New York, 2005.

[150] W. Shao and D. Terzoloulos. *Autonomous pedestrians.* Graph. Models **69**, 246 – 274, 2007.

[151] E. Andresen, D. Haensel, M. Chraibi and A. Seyfried. *Wayfinding and cognitive maps for pedestrian models.* In: V. L. Knoop and W. Daamen, Eds., *Traffic and Granular Flow '15*, 249 – 256, Springer, Cham, 2016.

[152] E. Andresen, R. Zinke, G. Hofinger, M. Chraibi and A. Seyfried. *The impact of perception and wayfinding on pedestrian movements.* In: W. Song, J. Ma and L. Fu, Eds., *Pedestrian and Evacuation Dynamics 2016*, Collective Dynamics, 290 – 297, 2016.

[153] A. U. Kemloh Wagoum, A. Seyfried and S. Holl. *Modelling dynamic route choice of pedestrians to assess the criticality of building evacuation.* Adv. Complex Syst. **15**, 1250029, 2011.

[154] G. G. Løvås. *Models of wayfinding in emergency evacuations.* Eur. J. Oper. Res. **105**, 371 – 389, 1998.

[155] M. Nasir, C. O. Lim, S. Nahadandi and D. Creighton. *Prediction of pedestrians routes within a built envorinment in normal conditions.* Expert Syst. Appl. **41**, 4975 – 4988, 2014.

[156] P. M. Kielar, D. H. Biedermann, A. Kneidl and A. Borrmann. *A unified pedestrian routing model combining multiple graph-based navigation Methods.* In: V. L. Knoop and W. Daamen, Eds., *Traffic and Granular Flow '15*, 241 – 248, Springer, Cham, 2016.

[157] P. R. Will. *Simulation von Fußgängerströmen.* Staatsexamensarbeit, Universität zu Köln, 2009.

[158] G. Köster and B. Zönnchen. *Queuing at bottlenecks using dynamic floor field for navigation.* Transp. Res. Proc. **2**, 344 – 352, 2014.

[159] T.-Y. Tsai, S.-K. Wong, Y.-H. Chou and G.-W. Lin. *Directing virtual crowds based on dynamics adjustment of navigation fields.* Comput. Anim. Virtual Worlds **29**, e1765, 2018.

[160] Pedestrian Dynamics Data Archive. *Single File Movement, Rotunde.* http://ped.fz-juelich.de/da/2005singleFile, 2005.

[161] Pedestrian Dynamics Data Archive. *Single File Movement, Caserne [sic].* http://ped.fz-juelich.de/da/2006singleFile, DFG-Grant No. KL 1873/1-1, SE 1789/1-1, 2006.

[162] Pedestrian Dynamics Data Archive. *Evacuation, School WDG.* http://ped.fz-juelich.de/da/2014socialGroups, 2015.

[163] G. Chu and J. Sun. *The effect of pre-movement time and occupant density on evacuation time.* J. Fire Sci. **24**, 237 – 259, 2006.

[164] P. Å. Olsson and M. A. Regan. *A comparison between actual and predicted evacuation times.* Saf. Sci. **38**, 139 – 145, 2001.

[165] J. Zhang, W. Song and X. Xu. *Experiment and multi-grid modeling of evacuation from a classroom.* Physica A **387**, 5901 – 5909, 2008.

[166] D. Yanagisawa, H. Yamamoto, T. Ezaki and K. Nishinari. *Passing a narrow corridor: modelling body rotation by ellipse.* In: W. Song, J. Ma and L. Fu, Eds., *Pedestrian and Evacuation Dynamics 2016*, Collective dynamics, 213 – 219, 2016.

[167] W. H. Press, S. A. Teukolksy, W. T. Vetterling and B. P. Flannery. *Numerical Recipes: the Art of Scientific Computing.* Cambridge University Press, Third edition, 2007.

[168] B. Steffen and A. Seyfried. *Methods for measuring pedestrian density, flow, speed and direction with minimal scatter.* Physica A **389**, 1902 – 1910, 2010.

[169] G. Voronoi. *Nouvelles applications des paramètres continus à la théorie des formes quadratiques. Premier Mémoire. Sur quelques propriétés des formes quadratiques positives parfaites.* J. Reine Angew. Math. **133**, 97 – 178, 1907.

Parameters of the model

For reasons of clarity, following abbreviations are used: DTC - distance-to-collision, LF - lane formation, SHDV model - Stochastic Headway Dependent Velocity model [102, 119, 120], PT - probability transformation.

Parameter	Description	Value
α	Absolute angle	-
$\alpha_i(t)$	Direction of motion of pedestrian i	-
α_k	k-th angle in PT	-
α_{ia}	Interaction angle	-
α_n	Absolute perception angle of pedestrian n	-
α_n^{rel}	Relative perception angle of pedestrian n	-
α_{S}	Incline of SHDV model	$0.5 - 3.3\,1/\mathrm{s}$
α_{t}	Target direction	-
α_{t}'	Intermediate target direction	-
$\alpha_{\mathrm{t}}^{\mathrm{fin}}$	Final target angle	-
$\beta_1,\ \beta_2$	Viewing angle in wall perception	-
γ	Threshold of order parameter for LF	$3r/2$
$\delta,\ \delta_1,\ \delta_2$	Auxiliary angle	-
$\Delta\alpha_n$	Angular expanse of pedestrian n at one side	-
$\Delta\alpha_n^{\mathrm{tot}}$	Total angular expanse of pedestrian n	-

Parameter	Description	Value
Δi_k	Contribution of box k to the integral I	-
Δt	Time step	$0.1\,\mathrm{s}$, $0.3\,\mathrm{s}$
ρ_i	One-dimensional density of single-file motion	-
σ	Variance of Gaussian distribution	$0.05\,\mathrm{m}$
ϕ	Range of the visual field	$170°$
ϕ_i	Order parameter of pedestrian i for LF	-
Φ	Global order parameter for LF	-
a	Arbitrary angle	-
$a^\star$	Interaction angle in PT	-
$a_{\min}$, $a_{\max}$	Bonding angles for wall distance	-
B	Width of a (simulated) corridor	-
c	Normalisation constant in PT	-
d	Minimal distance pedestrian - wall	-
d, $d(a)$	DTC (for angle a)	-
d_c	Upper threshold of SHDV model	-
d_n	Distance to pedestrian n	-
d^p	DTC to pedestrians	-
d_S	Lower threshold of SHDV model	$0.03\,\mathrm{m}$, $0.1\,\mathrm{m}$
d_vf	Expanse of the visual field	$8.0\,\mathrm{m}$
d^w	DTC to walls	-
F	Area occupied by a pedestrian	-
$h_i(t)$	Headway of pedestrian i	-
i	Identification number of pedestrian i	$0,\dots,N-1$
I	Integral in PT	-
I'	Reduced integral in PT	-
K	Number of angles in PT - 1	-
L	Length of a (simulated) corridor	-
l_k, u_k	Lower, upper border of a box k	-
$l_{\min}^{\mathrm{all}}$	Minimum lower border of boxes $j > k$	-
$l_{\min}^{j}$	Min. lower border of overlapping boxes $j > k$	-
l_W	Length of a wall	-

Parameter	Description	Value
n	Id number of a non-active pedestrian	-
N	Number of pedestrians	-
N_{L}	Number of pedestrians with same walking direction	-
N_{O}	Number of pedestrians with opposite walking direction	-
o_{W}	Orientation of a wall	$0, \pi/2$
$p(a)$	Probability of angle a	-
p_k	Probability / height of box k	-
p_{W}	Position of a wall	-
p_0	Probability in slow-to-start rule of SHDV model	0.5, 0.6
p_1	Probability for strategy 0 in LF	0.5
p_2	Probability for strategy 1 in LF	$s_i(t)/(1.5v_{\max})$
r	Radius of a pedestrian	$0.15\,\mathrm{m}$
$s_i(t)$	Speed of pedestrian i	-
t	Time	-
t_{pre}	Pre-movement time	-
T_{evac}	Evacuation time	-
T_{sim}	Total simulation time	-
$u_{\max}^{\mathrm{all}}$	Maximum upper border of boxes $j < k$	-
$u_{\max}^{j}$	Maximum upper border of overlapping boxes $j < k$	-
$\boldsymbol{v}_i(t)$	Velocity of pedestrian i	-
v_i	Velocity of one-dimensional single-file motion	-
$v_{\max}, v_{\min}$	Maximum, minimum velocity of SHDV model	-
x	Uniform random deviate	-
$x_{\max}, x_{\min}$	Right, left end of a horizontal wall	-
$x_i(t), y_i(t)$	Current position of pedestrian i	-
$x_i^{\mathrm{a}}(t), y_i^{\mathrm{a}}(t)$	Anticipated position of pedestrian i	-
$x_{\mathrm{t},i}(t, x_i, y_i),$ $y_{\mathrm{t},i}(t, x_i, y_i)$	Target coordinates of pedestrian i	-
$y_{\max}, y_{\min}$	Upper, lower end of a vertical wall	-

Table A.1: Parameters of the model

Determination of Angles and Distances

B.1 Determination of Angles

In this section the calculation of two kinds of angles used in the model's perception phase is described in detail. First, the determination of the angles which border the range of the visual field covered by a wall is explained. Second, the interaction angle between the perceiving agent and another, detected pedestrian is introduced. It is also explained how this angle is transformed into a relative angle and how the angular range covered by the other pedestrian is calculated.

B.1.1 Viewing Angle in Wall Perception

When perceiving a wall a pedestrian determines the angular range of the visual field that is covered by the wall. This mainly includes the calculation of the angles under which the visual field intersects with the wall. This can only hold if the wall or parts of it are 'in sight', which means that the minimal distance d between the wall and the agent is equal or less the maximum visual range d_{vf}. This distance depends

on the pedestrian's relative position considering the agent's body extension: If the pedestrian is located directly besides wall, i.e. if

$$y_{\min} - r \leq y_i(t) \leq y_{\max} + r \tag{B.1}$$

for a vertical and

$$x_{\min} - r \leq x_i(t) \leq x_{\max} + r \tag{B.2}$$

for a horizontal wall (see Fig. B.1), the distance d is given by the absolute value of the difference of the wall's position p_{W} and the agent's respective coordinate. If the pedestrian is outside of the area where the wall is located, the minimal distance is then given by the distance between the pedestrian's position and the closest end of the wall. In short, this leads to

$$d = \begin{cases} \sqrt{(x_i - p_{\mathrm{W}})^2 + (y_i - y_{\min})^2} & : y_i < y_{\min} - r \\ |x_i - p_{\mathrm{W}}| & : y_{\min} - r \leq y_i \leq y_{\max} + r \\ \sqrt{(x_i - p_{\mathrm{W}})^2 + (y_i - y_{\max})^2} & : y_i > y_{\max} + r \end{cases} \tag{B.3}$$

for a vertical wall with position p_{W}, and an extension from $y_{\min}$ to $y_{\max}$; to

$$d = \begin{cases} \sqrt{(x_i - x_{\min})^2 + (y_i - p_{\mathrm{W}})^2} & : x_i < x_{\min} - r \\ |y_i - p_{\mathrm{W}}| & : x_{\min} - r \leq x_i \leq x_{\max} + r \\ \sqrt{(x_i - x_{\max})^2 + (y_i - p_{\mathrm{W}})^2} & : x_i > x_{\max} + r \end{cases} \tag{B.4}$$

for a horizontal wall.

If $(d - r) \leq d_{\mathrm{vf}}$ holds, the viewing angles are calculated. This is done in a simplified scenario: the wall is assumed to be infinitely long and the visual field to have a range of 2π. Then, the problem reduces to the determination of the two angles of intersection β_1 and β_2 of a line with a circle of radius d_{vf}. These angles are calculated absolutely with respect to the x-axis and depend on the relative position of the wall and the center of the circle which is basically the position of the pedestrian. Fig. B.1

(a) $o_{\mathrm{W}} = \frac{\pi}{2}$, $x_i > p_{\mathrm{W}}$

(b) $o_{\mathrm{W}} = \frac{\pi}{2}$, $x_i < p_{\mathrm{W}}$

(c) $o_{\mathrm{W}} = 0$, $y_i > p_{\mathrm{W}}$

(d) $o_{\mathrm{W}} = 0$, $y_i < p_{\mathrm{W}}$
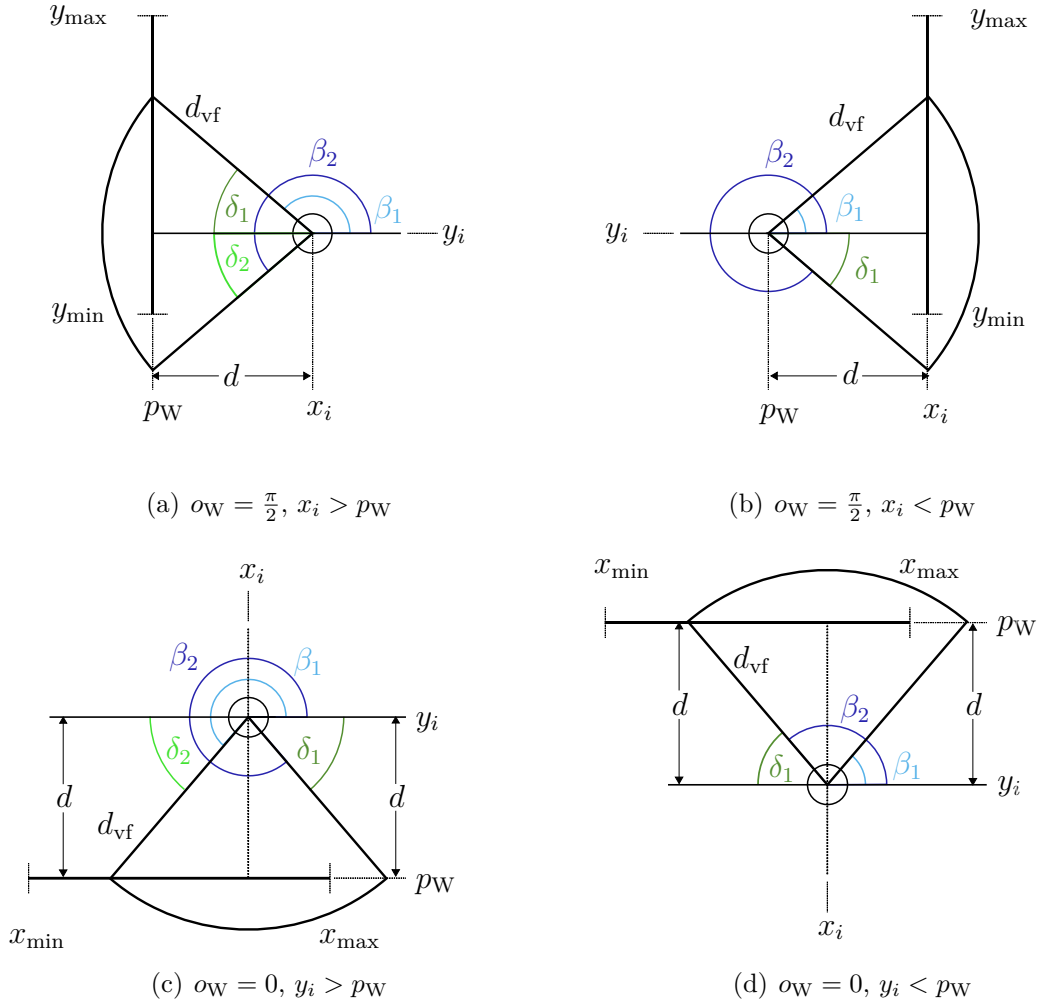
Figure B.1: The viewing angles β_1, β_2 depend on the wall's orientation and the relative position of the pedestrian.

shows the definition of the viewing angles β_1, β_2 for the different orientations of the pedestrian towards the wall. For simplicity reasons, it only displays the case when the agent stands by the wall, the calculation is the same for all other cases.

As can be seen from Fig. B.1(a), which represents a scenario with a vertical wall (case 1) and a pedestrian standing on the right, the viewing angles follow from

simple trigonometric considerations with the aid of auxiliary angles δ_1 and $\delta_2 = \delta_1$:

$$\beta_1^{1,\mathrm{r}} = \pi - \delta_1 = \pi - \arccos\left(\frac{d}{d_{\mathrm{vf}}}\right) = \pi - \arccos\left(\frac{x_i - p_{\mathrm{W}}}{d_{\mathrm{vf}}}\right), \tag{B.5}$$

$$\beta_2^{1,\mathrm{r}} = \pi + \delta_2 = \pi + \arccos\left(\frac{d}{d_{\mathrm{vf}}}\right) = \pi + \arccos\left(\frac{x_i - p_{\mathrm{W}}}{d_{\mathrm{vf}}}\right). \tag{B.6}$$

In the case of the pedestrian standing on the left (Fig. B.1(b)), the viewing angles can be determined by analogous trigonometric calculations using $\beta_1 = \delta_1 = \arccos\left(\frac{d}{d_{\mathrm{vf}}}\right)$:

$$\beta_1^{1,\mathrm{l}} = \arccos\left(\frac{d}{d_{\mathrm{vf}}}\right) = \arccos\left(\frac{p_{\mathrm{W}} - x_i}{d_{\mathrm{vf}}}\right), \tag{B.7}$$

$$\beta_2^{1,\mathrm{l}} = 2\pi - \delta_1 = 2\pi - \arccos\left(\frac{d}{d_{\mathrm{vf}}}\right) = 2\pi - \arccos\left(\frac{p_{\mathrm{W}} - x_i}{d_{\mathrm{vf}}}\right). \tag{B.8}$$

Relying on the symmetry properties of the arc cosine, $\arccos(-x) = \pi - \arccos(x)$, one can show that the expressions for both scenarios are equivalent since the sign of $(x_i - p_{\mathrm{W}})$ changes. Therefore, it is sufficient to give one, as done in Sec. 3.3.1. The calculations of the viewing angles for horizontal walls (0) run analogously. Using trigonometric considerations it follows for the situation depicted in Fig. B.1(c):

$$\beta_1^{0,\mathrm{a}} = \pi + \delta_2 = \pi + \arcsin\left(\frac{d}{d_{\mathrm{vf}}}\right) = \pi + \arcsin\left(\frac{y_i - p_{\mathrm{W}}}{d_{\mathrm{vf}}}\right), \tag{B.9}$$

$$\beta_2^{0,\mathrm{a}} = 2\pi - \delta_1 = 2\pi - \arcsin\left(\frac{d}{d_{\mathrm{vf}}}\right) = 2\pi - \arcsin\left(\frac{y_i - p_{\mathrm{W}}}{d_{\mathrm{vf}}}\right). \tag{B.10}$$

And analogously, one obtains for a pedestrian below a horizontal wall (Fig. B.1(d)):

$$\beta_1^{0,\mathrm{b}} = \arcsin\left(\frac{d}{d_{\mathrm{vf}}}\right) = \arcsin\left(\frac{p_{\mathrm{W}} - y_i}{d_{\mathrm{vf}}}\right), \tag{B.11}$$

$$\beta_2^{0,\mathrm{b}} = \pi - \delta_1 = \pi - \arcsin\left(\frac{d}{d_{\mathrm{vf}}}\right) = \pi - \arcsin\left(\frac{p_{\mathrm{W}} - y_i}{d_{\mathrm{vf}}}\right). \tag{B.12}$$

Again, the expression for both cases can be transferred into each other with the aid of the symmetry properties of the arc sine, $\arcsin(-x) = -\arcsin(x)$.

If $(d - r) \leq d_{\text{vf}}$ and at least one of the viewing angles β_1, β_2 calculated lies within the angular range of the visual field, the wall is perceived by the pedestrian. Since the angles are used later in the decision phase, they must be saved.

B.1.2 Angle Between x-axis and the Connecting Line Between Arbitrary Points in Space

At different stages during the decision-process a pedestrian has to calculate an absolute angle α towards a fixed, arbitrary point in space. This angle is basically defined as the angle enclosed by the connecting line between the point (x_i, y_i), which represents the position of pedestrian i, and the arbitrary point (x_j, y_j), and the x-axis. It is used in the model for the angle towards another pedestrian and for the angle towards the target (overall or intermediate). In order to facilitate later calculations, the angle should be positive and $|\alpha| \in [0, 2\pi)$. Therefore, the relative position must be considered.

Fig. B.2 shows the different orientations and the resulting angles α. Using again an auxiliary angle δ, the expression for α follows from trigonometric considerations. For the situations shown in Fig. B.2(a) and B.2(b) (the y-coordinates of the two points are equal) and Fig. B.2(c) and B.2(d) (equal x-coordinate), the angle α is easy to determine by reading out:

$$\alpha\left(x_i < x_j, y_i = y_j\right) = 0 \tag{B.13}$$

$$\alpha\left(x_i > x_j, y_i = y_j\right) = \pi \tag{B.14}$$

$$\alpha\left(x_i = x_j, y_i < y_j\right) = \frac{\pi}{2} \tag{B.15}$$

$$\alpha\left(x_i = x_j, y_i > y_j\right) = \frac{3\pi}{2} \tag{B.16}$$

133

(a) $x_i < x_j$, $y_i = y_j$ (b) $x_i > x_j$, $y_i = y_j$ (c) $x_i = x_j$, $y_i < y_j$

(d) $x_i = x_j$, $y_i > y_j$ (e) $x_i < x_j$, $y_i > y_j$ (f) $x_i > x_j$, $y_i < y_j$

(g) $x_i > x_j$, $y_i > y_j$ (h) $x_i < x_j$, $y_i > y_j$
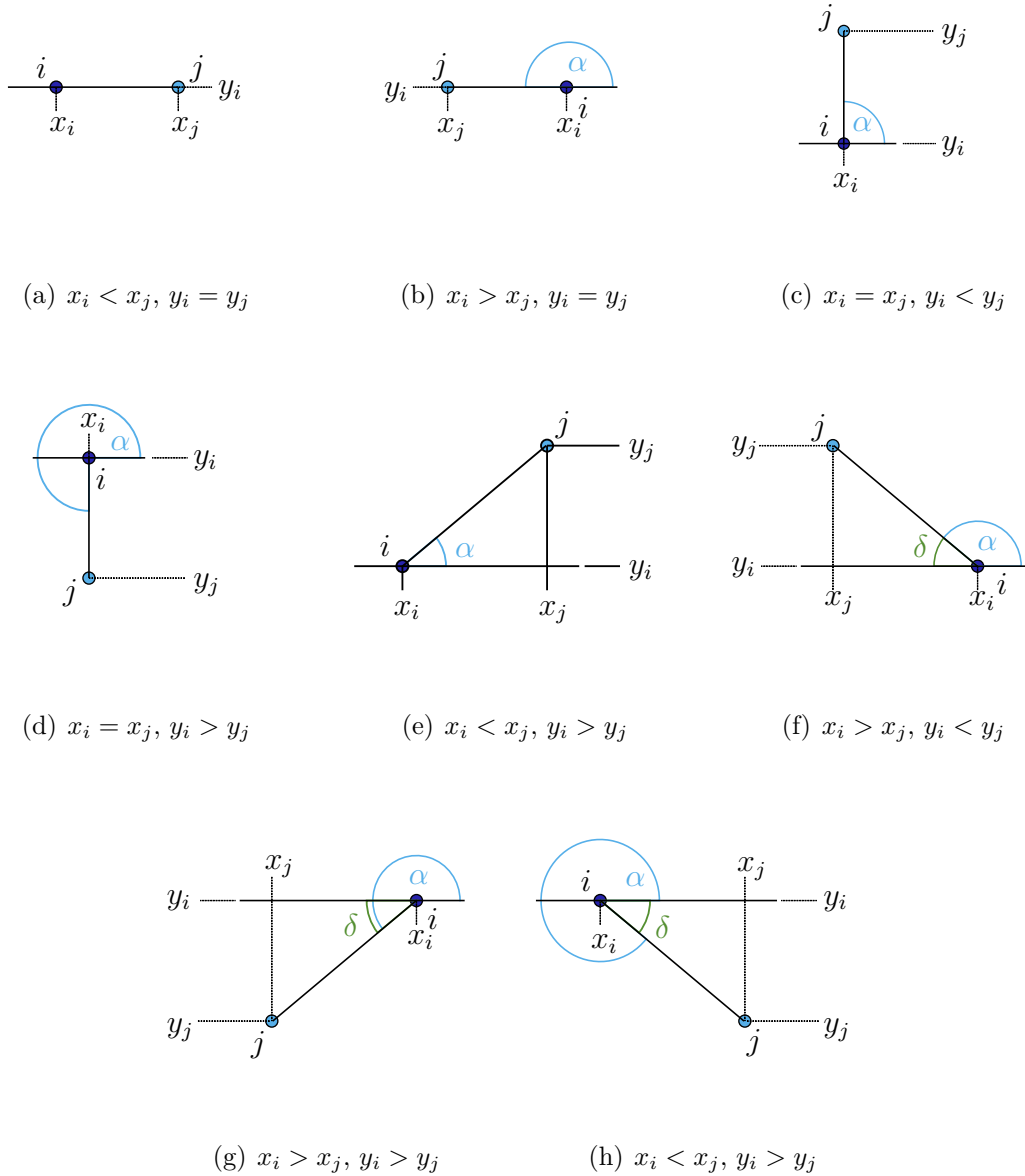
Figure B.2: The angle between the connecting line of two points in space and the x-axis depends on the relative position and follows from trigonometric considerations.

The angle for $x_i < x_j$ and $y_i < y_j$ is given by simple geometric considerations, see Fig. B.2(e):

$$\alpha\left(x_i < x_j, y_i < y_j\right) = \arctan\left(\frac{y_j - y_i}{x_j - x_i}\right) \tag{B.17}$$

As shown in Fig. B.2(f), for $x_i > x_j$ the same considerations as above can be made by using the auxiliary angle δ:

$$\alpha\left(x_i > x_j, y_i < y_j\right) = \pi - \delta = \pi - \arctan\left(\frac{y_j - y_i}{x_i - x_j}\right) \tag{B.18}$$

The expression for the situation shown in Fig. B.2(g) can either be derived by the same trigonometric considerations using δ as in the upper case or just by using the symmetry properties of the arc tangent, $\arctan(-x) = -\arctan(x)$ with Eq. (B.18):

$$\alpha\left(x_i > x_j, y_i > y_j\right) = \pi + \delta = \pi + \arctan\left(\frac{y_i - y_j}{x_i - x_j}\right) \tag{B.19}$$

And it follows analogously for the situation shown in Fig. B.2(h):

$$\alpha\left(x_i < x_j, y_i > y_j\right) = 2\pi - \delta = 2\pi - \arctan\left(\frac{y_i - y_j}{x_j - x_i}\right) \tag{B.20}$$

B.1.3 Transformation from Absolute to Relative Perception Angle

In case the angle α, as described in Sec. B.1.2, is used during the perception of other pedestrians, it has to be transformed into a relative angle with respect to the direction of motion α_i of the perceiving pedestrian i. The relative angle α_n^{rel} displays, unlike the (absolute) angle α_n, the relative orientation of the perceived agent n. This is shown in Fig. B.3: the relative angle α_n^{rel} is always defined to start from the direction of motion of pedestrian i, α_i, and to open towards the connecting line under the angle α_n. As a consequence, it opens into different directions according to the relative positions of the two pedestrians (see Fig. B.3(a) and B.3(b)).
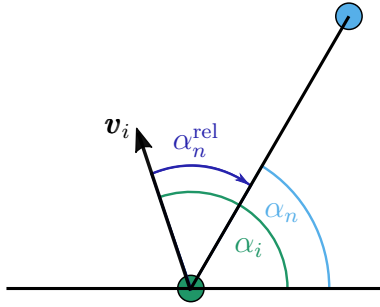
(a) Pedestrian on the right, $\alpha_{\text{rel}} < 0$
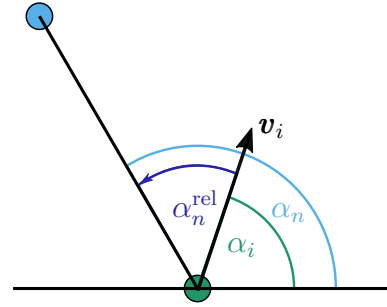
(b) Pedestrian on the left, $\alpha_{\text{rel}} > 0$
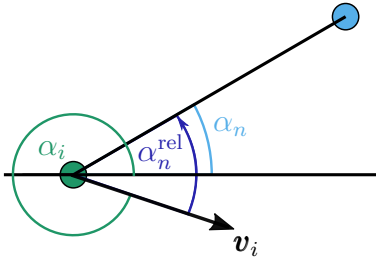
(c) Inner relative angle, $\alpha_{\text{rel}} > 0$
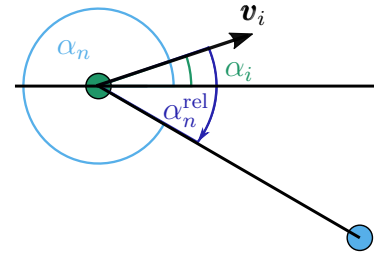
(d) Inner relative angle, $\alpha_{\text{rel}} < 0$

Figure B.3: The relative angle is defined by the difference of α and α_i. Its sign states the relative position of the agents.

Using the mathematical direction of rotation as a basis, the relative angle becomes a signed quantity: an angle that opens along the direction of rotation should be positive, an angle opening into the opposite direction negative. That means that a pedestrian located on the left of the perceiving agent has a positive relative perception angle, whereas seeing a pedestrian on the right results in a negative relative perception angle. While the absolute angle lies between 0 and 2π, the relative angle then satisfies $\alpha_n^{\text{rel}} \in [-\pi, \pi]$, where $\alpha_n^{\text{rel}} \in [-\pi, 0)$ describes the agent's

right-hand side, and $\alpha_n^{\text{rel}} \in (0, \pi]$ the *left*-hand side. $\alpha_n^{\text{rel}} = 0$ represents that the pedestrian is perceived straight ahead.

In most cases, the absolute value of the relative angle is given by the difference between absolute perception angle and the direction of motion, which can be easily seen in Fig. B.3(a) and B.3(b):

$$|\alpha_n^{\text{rel}}| = |\alpha_n - \alpha_i| \tag{B.21}$$

In order to include the sign of the relative angle it can then be defined as

$$\alpha_n^{\text{rel}} = \alpha_n - \alpha_i \tag{B.22}$$

which is positive if the pedestrian is on the left $(\alpha_n > \alpha_i)$ and negative for a pedestrian standing on the right $(\alpha_n < \alpha_i)$. It should be noted, however, that the relative angle is defined as the angle enclosed by the direction of motion and the connecting line between the two pedestrians. Therefore, its absolute value should not be larger than π, as it also follows from its definition as a signed quantity. Then, the expressions given in Eq. (B.21) and (B.22) cannot hold for all situations, see e.g. Fig. B.3(c) and B.3(d). Here, one of the angles is larger than $3\pi/2$, while the other is smaller than $\pi/2$. The difference $|\alpha_n - \alpha_i|$ is hence larger than π and the angle must be corrected by 2π:

$$\alpha_n^{\text{rel}} = \begin{cases} \alpha_n - \alpha_i + 2\pi & > 0 \quad : \alpha_n - \alpha_i < -\pi, \\ \alpha_n - \alpha_i - 2\pi & < 0 \quad : \alpha_n - \alpha_i > \pi. \end{cases} \tag{B.23}$$

Taken together, it follows for the relative perception angle:

$$\alpha_n^{\text{rel}} = \begin{cases} \alpha_n - \alpha_i + 2\pi & : \alpha_n - \alpha_i < -\pi, \\ \alpha_n - \alpha_i - 2\pi & : \alpha_n - \alpha_i > \pi \\ \alpha_n - \alpha_i & : \text{else.} \end{cases} \tag{B.24}$$

B.1.4 Angular Extension During Perception of Pedestrians

In the last step of the perception of another pedestrian n the angular range that is covered by it has to be determined. The general idea is schematically shown in Fig. B.4(a). Due to its body extension a pedestrian occupies a certain area within the visual field. Combined with the relative distance towards the perceiving agent this area can be described as a range of angles with respect to the pedestrian's position. Additionally, the perceiving agent also has a body extension that must be considered: the set of all directions that would lead to a collision of the pedestrians' bodies constitute the angular range that is covered by the presence of the other pedestrian in the agent's visual field (shaded in green in Fig. B.4(a)). It is given by the interval $[\alpha_n^{\mathrm{rel}} - \Delta\alpha_n, \alpha_n^{\mathrm{rel}} + \Delta\alpha_n]$ with $\Delta\alpha_n$ being the maximum angular distance that would lead to a collision at one side. Since the relative angle α_n^{rel} has been determined previously, it remains to calculate the expanse $\Delta\alpha_n$.

From Fig. B.4 it can be seen that $\Delta\alpha_n$ depends on the relative distance d_n between pedestrian i and n and the pedestrians' radius r. In order to determine the covered angular range one needs the spatial extension of pedestrian n perpendicular to the connecting line between the two agents. Since a pedestrian is modelled as a circle this extension varies along the connecting line. At the closest point the pedestrian seems to be point-like, whereas it displays its maximum extension $2r$ at the centre. In terms of perception and interaction it shall now be assumed that a pedestrian's diameter $2r$ holds for the entire body. This simplification is basically an approximation of a pedestrian's body area as a square whose edges are perpendicular to the connecting line. It is shown in Fig. B.4(b): both pedestrians are approximated as squares whose facing edges are parallel to each other and perpendicular to the connecting line. The distance between both agents is determined by the distance between the closest edges of the respective squares and is given by d as defined above for the entire body extension. Of course this approximation leads to an overestimation of the body extension F which amounts to just under 30%:

$$\frac{F_{\mathrm{square}} - F_{\mathrm{circle}}}{F_{\mathrm{circle}}} = \frac{(2r)^2 - \pi r^2}{\pi r^2} = \frac{4r^2 - \pi r^2}{\pi r^2} = \frac{4 - \pi}{\pi} \approx 27.32\,\%. \qquad \text{(B.25)}$$

(a) General idea of the angular coverage.

(b) Simplified scenario for the derivation.

Figure B.4: The angular range covered by another pedestrian describes the set of all directions that would lead to a collision of the pedestrians.

Nevertheless, there are several reasons that are indicative that this assumption is reasonable and has no falsifying influence on the dynamic of the pedestrians: the exact shape of a pedestrian is only roughly approximated when using a circle and could be represented more exactly by more complex shapes like an ellipse (see e.g. [70] and references therein). Temporarily representing the pedestrian as a square therefore should not have a large impact on the general dynamics. More importantly, it can be assumed that the most significant component of a body's extension during the perception of the angular coverage is the maximum range. Thirdly, the angular coverage only considers the actual expanse of the body without any need for personal space or 'safety' distance. It might be possible that the additional space from the square approximation contributes to some kind of private space that is unconsciously considered by the perceiving agent.

Fig. B.4(b) shows the simplified scenario. The perceiving agent i and the perceived pedestrian n are approximated as squares with an edge length of $2r$. The closest edges are relevant for further considerations. Their distance is given by d_n as defined

in Eq. (3.4),

$$d_n = \sqrt{(x_i - x_n)^2 + (y_i - y_n)^2} - 2r. \tag{B.26}$$

At first, the angular expanse of pedestrian n at one side is considered. It is given by the set of all angles which would lead to a collision of the two bodies. It is bounded by the maximum angle $\Delta\alpha_n$, the angle under which a collision only just occurs. This maximum angle is given when assuming that the corner of the squares (the ends of the closest edges) touch. In Fig. B.4(b) this is indicated by the grey 'passing' line: the agents i and n would only just collide, if the upper left corner of i touches the lower right corner of n while passing. Angles that are smaller than $\Delta\alpha_n$ would therefore lead to a collision, chosing a larger angle would lead to passing without contact. How to determine the maximum angular range $\Delta\alpha_n$ becomes clearer if the grey passing line is shifted by r along the square's edge: it can then be seen that $\Delta\alpha_n$ is given by simple trigonometry:

$$\Delta\alpha_n = \arctan\left(\frac{2r}{d_n}\right). \tag{B.27}$$

Since this is a symmetric problem, the same argumentation holds for the other side and the total angular range of the visual field of pedestrian i that is covered by the pedestrian n is given by

$$\Delta\alpha_n^{\text{tot}} = 2\Delta\alpha_n = 2\arctan\left(\frac{2r}{d_n}\right), \tag{B.28}$$

with the minimal distance d_n between agent i and n.

B.2 Distance-to-Collision

The distance-to-collision appears at many stages during the decision phase. It is determined either towards walls or other pedestrians in a given, arbitrary direction. Both cases are described in the following sections.

B.2.1 Distance-to-Collision to Walls

The distance-to-collision is one of the main quantities of the model. During the navigation within the environment, it is necessary to determine the distance-to-collision under an arbitrary angle to a wall. In order to get the minimum distance-to-collision in a given scenario, a pedestrian calculates the distance to all perceived walls and takes the smallest value as its headway. In the following the determination of the distance-to-collision $d(a)$ under a given angle a to an arbitrary wall is described in detail.

During the perception phase, the agent has already determined the viewing angles β_1 and β_2 (let $\beta_1 < \beta_2$ w.l.o.g.) that border the range of the visual field covered by the wall. Only within this range a wall is detected. As a first rough presorting it therefore has to be assessed whether the direction a lies within the covered range. For most cases, the difference between the two viewing angles does not exceed π except for the pedestrian standing on the left side of a vertical wall. As the viewing angles are absolutely given with respect to the x-axis, it holds that $\beta_1 < \pi/2$ and $\beta_2 > 3\pi/2$ in this case. Considering this, the first criterion if a wall is detected sums up to

$$\begin{cases} \beta_1 \leq a \leq \beta_2 & : \beta_2 - \beta_1 < \pi, \\ a \leq \beta_1 \ \vee \ \beta_2 \leq a & : \beta_2 - \beta_1 > \pi. \end{cases} \tag{B.29}$$

The next steps in the derivation are exemplarily made for the situation of a pedestrian i standing on the right of a vertical wall ($o_{\mathrm{W}} = \pi/2$, $x_i > p_{\mathrm{W}}$) as shown in Fig. B.5. The calculations for all other cases work analogously.

The distance-to-collision $d(a)$ for a given wall has a finite value only if the direction a directly points at that wall. In addition, the finite length of a wall that was neglected during the perception phase has to be considered: if a points past the wall, the distance-to-collision also diverges. In the model any infinite distance-to-collision is set to the maximum visual range d_{vf}. Therefore, in a second step the angular range $[a_{\min}, a_{\max}]$ has to be determined in which a headway would have a finite value. The scenario is shown in Fig. B.5(a) to B.5(c). $a_{\min}$ and $a_{\max}$ are

(a) Pedestrian above, $y_i > y_{\mathrm{max}}$

(b) Pedestrian below, $y_i < y_{\mathrm{min}}$

(c) Pedestrian right beside, $y_{\mathrm{min}} < y_i < y_{\mathrm{max}}$

(d) Determination of distance-to-collision d
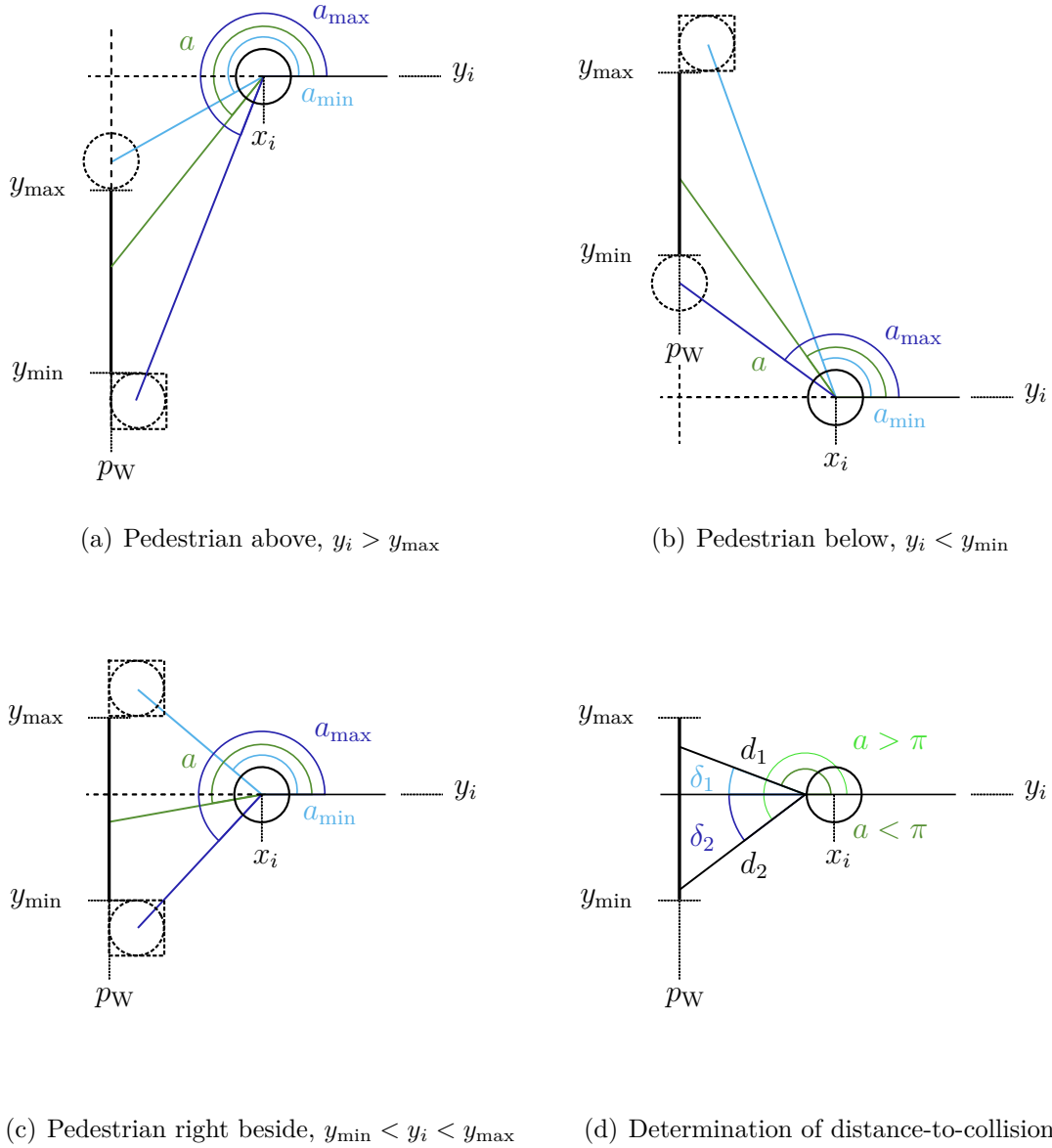
Figure B.5: The distance-to-collision d is finite, if $a_{\mathrm{min}} \leq a \leq a_{\mathrm{max}}$ (see (a)-(c)), and can be calculated using trigonometry (see (d)).

the two angles that bound, under consideration of the pedestrian's body extension, the area which would lead to a finite distance-to-collision. There are three possible

relative positions of the agent with respect to the wall: the agent stands beside, $y_{\min} - r \le y_i \le y_{\max} + r$, above, $y_i > y_{\max} + r$, or below the wall, $y_i < y_{\min} - r$. For each of these relative positions the bounding angles can be determined by geometric relations assuming that the closest point of the pedestrian touches the upper or lower end of the wall, respectively. This point on the periphery of the circles that represents the pedestrian is, however, not easily determined since it mostly depends on the angle under which the agents passes the wall (except if the agent goes by the wall without being right beside it at some time, e.g. if it is located and stays above the wall). Therefore, the simplification of Sec. B.1.4 is again used which approximates the agents temporarily as a square. In doing so the closest point on the pedestrian's circumference to the wall can be easily found and used for the calculations. Fig. B.5(a) shows the scenario of the agent standing above. It includes the geometrical considerations that help at determining the bounding angles with the aid. From the figure it follows that

$$a^{\mathrm{a}}_{\min} = \pi + \delta = \pi + \arctan\left(\frac{y_i - (y_{\max} + r)}{x_i - p_{\mathrm{W}}}\right) = \pi + \arctan\left(\frac{y_i - y_{\max} - r}{x_i - p_{\mathrm{W}}}\right) \quad \text{(B.30)}$$

and, accordingly,

$$a^{\mathrm{a}}_{\max} = \pi + \delta = \pi + \arctan\left(\frac{y_i - (y_{\min} - r)}{x_i - p_{\mathrm{W}} - r}\right) = \pi + \arctan\left(\frac{y_i - y_{\min} + r}{x_i - p_{\mathrm{W}} - r}\right). \quad \text{(B.31)}$$

The same considerations can be done for an agent standing beside or below, but it can be shown that the results sum up to similar expressions as above using the symmetry properties of the arc tangent if the differences $y_i - (y_{\max} + r)$ or

$y_i - (y_{\mathrm{min}} - r)$ change the sign, see e.g.

$$
\begin{aligned}
a_{\mathrm{min}}^{\mathrm{bel}} = \pi - \delta &= \pi - \arctan\left(\frac{(y_{\mathrm{max}} + r) - y_i}{x_i - p_{\mathrm{W}} - r}\right) \\
&= \pi + \arctan\left(\frac{y_i - (y_{\mathrm{max}} + r)}{x_i - p_{\mathrm{W}} - r}\right) \\
&= \pi + \arctan\left(\frac{y_i - y_{\mathrm{max}} - r}{x_i - p_{\mathrm{W}} - r}\right).
\end{aligned}
\tag{B.32}
$$

If $a_{\mathrm{min}} \leq a \leq a_{\mathrm{max}}$ holds, the headway $h_i(a)$ is finite and can be calculated. For that, the scenario is exemplarily depicted in Fig. B.5(d) with a pedestrian that stands beside the wall. The two cases shown here, $a < \pi$ and $a \geq \pi$, describe the same situations as if the agent stood below and above the wall, respectively. Later it can be shown that both results can be reduced to one single expression. First, we consider $a < \pi$. Using the auxiliary angle $\delta_1 = \pi - a$, $d(a)$ can be derived by trigonometric considerations. It should be noted that the pedestrians' body extension has to be considered explicitly. Therefore, one does not regard the centre of the circle as the starting point for h, but the point at the edge of the circle that is closest to the wall, since this site would be the first point that collides with the wall. In doing so, the respective coordinate has to be reduced by r:

$$
\begin{aligned}
&\cos(\delta_1) = \frac{(x_i - r) - p_{\mathrm{W}}}{d(a)} \\
\Leftrightarrow \quad &d(a) = \frac{x_i - p_{\mathrm{W}} - r}{\cos(\delta_1)} = \frac{x_i - p_{\mathrm{W}} - r}{\cos(\pi - a)} \\
\Leftrightarrow \quad &d(a) = -\frac{x_i - p_{\mathrm{W}} - r}{\cos(a)}
\end{aligned}
\tag{B.33}
$$

where it was used that $\cos(\pi - x) = \cos(\pi)\cos(x) + \sin(x)\sin(\pi) = -\cos(x)$.

Accordingly, the derivation for the case $a \geq \pi$ follows as

$$\cos(\delta_2) = \frac{(x_i - r) - p_W}{d(a)}$$

$$\Leftrightarrow \quad d(a) = \frac{x_i - p_W - r}{\cos(\delta_2)} = \frac{x_i - p_W - r}{\cos(a - \pi)}$$

$$\Leftrightarrow \quad d(a) = -\frac{x_i - p_W - r}{\cos(a)} \tag{B.34}$$

using $\cos(a - \pi) = \cos(\pi - a) = -\cos(a)$. Because of $\arctan(x) \in (-\pi/2, \pi/2)$, it must hold that $a_{\min}, a_{\max} \in (\pi/2, 3\pi/2)$. It was required that $a_{\min} \leq a \leq a_{\max}$, therefore it must also hold that $a \in (\pi/2, 3\pi/2)$. From that it follows, that $\cos(a) < 0$ and the expression for the distance-to-collision d can be rewritten as

$$d(a) = \left| \frac{x_i - p_W - r}{\cos(a)} \right|. \tag{B.35}$$

If $a < \frac{\pi}{2}$ or $a > 3\pi/2$, the angle does not point directly at the wall and $d(a)$ is infinite or set to d_{vf}. For $a = \pi/2$, $d(a)$ is finite only if the pedestrian stands in line and below the wall, $x_i = p_W$ and $y_i < (y_{\min} - r)$. Then, the distance is given by

$$d\left(a = \frac{\pi}{2}\right) = y_{\min} - y - r. \tag{B.36}$$

Similar, for $a = 3\pi/2$ d is finite if $x_i = p_W$ and $y_i > (y_{\max} + r)$ and given by

$$d\left(a = \frac{3\pi}{2}\right) = y_i - y_{\max} - r. \tag{B.37}$$

The calculations for the other three cases work analogously, using the relations

$$\cos(2\pi - x) = \cos(2\pi)\cos(x) + \sin(x)\sin(2\pi) = \cos(x),$$
$$\sin(\pi - x) = \sin(\pi)\cos(x) - \cos(\pi)\sin(x) = \sin(x),$$
$$\sin(x - \pi) = -\sin(\pi - x) = -\sin(x), \tag{B.38}$$
$$\sin(2\pi - x) = \sin(2\pi)\cos(x) - \cos(2\pi)\sin(x) = \sin(x).$$

For $o_W = \pi/2$, but $x_i < p_W$ (vertical wall with pedestrian standing on the left), the two angles that bound the wall area are given by

$$a_{\min}^{\mathrm{ab}} = 2\pi - \arctan\left(\frac{y_i - y_{\min} + r}{p_W - x_i - r}\right),$$

$$a_{\max}^{\mathrm{ab}} = 2\pi - \arctan\left(\frac{y_i - y_{\max} - r}{p_W - x_i}\right) \tag{B.39}$$

for $y_i > (y_{\max} + r)$, for $y_i < (y_{\min} - r)$ it is

$$a_{\min}^{\mathrm{bel}} = \arctan\left(\frac{y_{\min} - y_i - r}{p_W - x_i}\right),$$

$$a_{\max}^{\mathrm{bel}} = \arctan\left(\frac{y_{\max} - y_i + r}{p_W - x_i - r}\right) \tag{B.40}$$

and for $y_{\min} \leq y_i \leq y_{\max}$

$$a_{\min}^{\mathrm{by}} = \arctan\left(\frac{y_{\max} - y_i + r}{p_W - x_i - r}\right),$$

$$a_{\max}^{\mathrm{by}} = 2\pi - \arctan\left(\frac{y_i - y_{\min} + r}{p_W - x_i - r}\right). \tag{B.41}$$

For all cases, the distance-to-collision is given by

$$d(a) = \frac{p_W - x - r}{\cos(a)}. \tag{B.42}$$

It should be noted that in case of $y_{\min} \leq y_i \leq y_{\max}$, $d(a)$ is finite if

$$a \leq a_{\min} \lor a_{\max} \leq a. \tag{B.43}$$

For horizontal walls, $o_W = 0$, the three possible relative positions of a pedestrian are on the right ($x_i > x_{\max} + r$) or the left side of the wall ($x_i < x_{\min} - r$) and right beside it ($x_{\min} - r \leq x_i \leq x_{\max} + r$). If the agent stands, additionally, above the

wall, $y_i > p_\mathrm{W}$, the bounding angles are given by

$$a^\mathrm{r}_\mathrm{min} = \pi + \arctan\left(\frac{y_i - p_\mathrm{W} - r}{x - x_\mathrm{min} + r}\right),$$
$$a^\mathrm{r}_\mathrm{max} = \pi + \arctan\left(\frac{y_i - p_\mathrm{W}}{x_i - x_\mathrm{max} - r}\right); \tag{B.44}$$

$$a^\mathrm{l}_\mathrm{min} = 2\pi - \arctan\left(\frac{y_i - p_\mathrm{W}}{x_\mathrm{min} - x - r}\right),$$
$$a^\mathrm{l}_\mathrm{max} = 2\pi - \arctan\left(\frac{y_i - p_\mathrm{W} - r}{x_\mathrm{max} - x + r}\right); \tag{B.45}$$

$$a^\mathrm{by}_\mathrm{min} = \pi + \arctan\left(\frac{y_i - p_\mathrm{W} - r}{x_i - x_\mathrm{min} + r}\right),$$
$$a^\mathrm{by}_\mathrm{max} = 2\pi - \arctan\left(\frac{y_i - p_\mathrm{W} - r}{x_\mathrm{max} - x + r}\right), \tag{B.46}$$

and correspondingly the distance-to-collision follows as

$$d(a) = -\frac{y_i - p_\mathrm{W} - r}{\sin(a)}. \tag{B.47}$$

The last case represents a pedestrian standing below a wall and the results are given by

$$a^\mathrm{r}_\mathrm{min} = \pi - \arctan\left(\frac{p_\mathrm{W} - y_i}{x_i - x_\mathrm{max} - r}\right),$$
$$a^\mathrm{r}_\mathrm{max} = \pi - \arctan\left(\frac{p_\mathrm{W} - y_i - r}{x_i - x_\mathrm{min} + r}\right); \tag{B.48}$$

$$a^\mathrm{l}_\mathrm{min} = \arctan\left(\frac{p_\mathrm{W} - y_i - r}{x_\mathrm{max} - x_i + r}\right),$$
$$a^\mathrm{l}_\mathrm{max} = \arctan\left(\frac{p_\mathrm{W} - y_i}{x_\mathrm{min} - x_i - r}\right); \tag{B.49}$$

$$a^\mathrm{by}_\mathrm{min} = \arctan\left(\frac{p_\mathrm{W} - y_i - r}{x_\mathrm{max} - x_i + r}\right),$$
$$a^\mathrm{by}_\mathrm{max} = \pi - \arctan\left(\frac{p_\mathrm{W} - y_i - r}{x_i - x_\mathrm{min} + r}\right), \tag{B.50}$$

with the respective distance-to-collision

$$d(a) = \frac{p_{\mathrm{W}} - y_i - r}{\sin(a)}. \tag{B.51}$$

For $a = 0$ and $a = \pi$, the distance-to-collision diverges except for the special case that $y_i = p_{\mathrm{W}}$. Then, for $x_i < x_{\min} - r$, the distance-to-collision is given by

$$d(a = 0) = x_{\min} - x_i - r, \tag{B.52}$$

and for $x_i > x_{\max} + r$ it is

$$d(a = \pi) = x_i - x_{\max} - r. \tag{B.53}$$

B.2.2 Distance-to-Collision to Pedestrians

The distance-to-collision $d(a)$ towards pedestrians in an arbitrary direction a mainly relies on the relative distance to any pedestrian as determined during the perception phase and defined in Eq. (3.4). If a lies within an angular range that is covered by an agent n, the respective distance-to-collision shall be given by the distance to this agent, d_n. On the other side, in free ranges the distance-to-collision is restricted by the maximum visual range d_{vf}. As a pedestrian n is perceived only if $d_n \leq d_{\mathrm{vf}}$, the presence of agents standing farther afield would not be detected. Therefore, the minimum distance-to-collision for these ranges can be set to d_{vf}. Giving a relatively to the direction of motion α_i of the acting pedestrian i, the distance-to-collision is then defined as the minimum distance towards pedestrians into this direction,

$$d(a) = \begin{cases} \min_{n} d_n & : \alpha_n^{\mathrm{rel}} - \Delta\alpha_n \leq a \leq \alpha_n^{\mathrm{rel}} + \Delta\alpha_n, \\ d_{\mathrm{vf}} & : \text{else.} \end{cases} \tag{B.54}$$

Here, the distance d_n is used as distance-to-collision for the entire angular range that is covered by the respective agent n. However, by definition, d_n is the minimum distance between the pedestrians n and i and was determined along the directly

connecting line between the agents' positions. As soon as a deviates from this connecting line, the actual distance along this direction is given by

$$\tilde{d}(a) = \frac{d_n}{\cos\left(|a - \alpha_n^{\text{rel}}|\right)}, \tag{B.55}$$

so that $d(a)$ as stated above is underestimated by the factor $1/\cos\left(|a - \alpha_n^{\text{rel}}|\right)$. This discrepancy is not significant for small deviations $|a - \alpha_n^{\text{rel}}| \to 0$ or short distances, $d_n \to 0$. That it is also negligible for large distances as can be seen when considering the maximum deviation, $|a - \alpha_n^{\text{rel}}| = \Delta\alpha_n = \arctan\left(2r/d_n\right)$, and

$$\begin{aligned}
\tilde{d}(a) &= \frac{d_n}{\cos\left(|a - \alpha_n^{\text{rel}}|\right)} \\
&= \frac{d_n}{\cos\left(\arctan\left(\frac{2r}{d_n}\right)\right)} \\
&= d_n\sqrt{1 + \left(\frac{2r}{d_n}\right)^2}
\end{aligned} \tag{B.56}$$

using $\cos\left(\arctan(x)\right) = 1/\sqrt{1 + x^2}$. For $d_n \gg 2r$ it then holds that $\tilde{d}_n \to d_n$. For other distances d_n, there is no formal justification for neglecting the deviation. Nevertheless, there are reasons that may legitimise the assumption $\tilde{d} = d_n$ with regard to modelling pedestrian dynamics. Modelling-wise, this approximation facilitates the determination of the interaction angle significantly. As will be seen in Sec. B.3, the calculation of the probability function $P(a)$ and the respective interaction angle highly benefits from $d(a)$ being a piecewise constant function in a. Since the model should be developed as realistic as possible while being as simple as possible, it might be reasonable to make this simplification as a first measure and assess the results. Considering the nature of the particles modelled, one may take into account uncertainties of the human behaviour. At several points in the model it was referred to the uncertainty of human decisions. Stochastic elements are explicitly included to cover this, e.g. during the determination of the target or interaction angle. Restricting an agent's perception of a pedestrian to the minimal distance

without further distinction over its extension may join the ranks of these considerations. Neglecting that the distance-to-collision increases slightly towards the 'edges' of an opponent may cover an pedestrian's inaccuracies and misjudgements during its perception. Regarding the perceived pedestrian, the distance-to-collision as above does not include any personal space or safety distance or other extensions due to additional body rotation or arm movements. A more rough determination could represent that the amount of occupied space may slightly change from time to time.

B.3 Probability Distribution for Collision Avoidance and Interaction Angle

During the decision phase, an agent has to determine a preferred direction in terms of collision avoidance. As described in Sec. 3.4.2, this decision relies mainly on the distances-to-collision that have been determined in the previous perception phase. Each angle within the visual field $a \in [-\phi, \phi]$ - a is given relatively to the agent's direction of motion - is assigned a probability $p(a)$ that follows from the quotient of the distance-to-collision into direction a, $d(a)$, and the maximum visual range d_{vf},

$$p(a) = \begin{cases} \frac{1}{c} \frac{d(a)}{d_{\mathrm{vf}}} & : |a| \leq \phi, \\ 0 & : \text{else} \end{cases} \tag{B.57}$$

with the normalisation constant

$$c = \int_{-\phi}^{\phi} p(a)\, \mathrm{d}a. \tag{B.58}$$

and

$$d(a) = \begin{cases} \min_{n} d_n & : \alpha_n^{\mathrm{rel}} - \Delta\alpha_n \leq a \leq \alpha_n^{\mathrm{rel}} + \Delta\alpha_n, \\ d_{\mathrm{vf}} & : \text{else}. \end{cases} \tag{B.59}$$

$p(a)$ is maximum for all directions that point to an angular range that is not covered by a pedestrian. In this case the minimum distance-to-collision is only restricted by the maximum visual range and can therefore be set to d_{vf}. On the other side, the probability is decreased for angles that point towards one or more pedestrians correspondingly to the distance-to-collision measured along the direction. If an angle points towards multiple pedestrians, the minimum of all distances is taken as final distance-to-collision. Based on this, $p(a)$ is as an angular probability distribution for collision avoidance. The decision of the pedestrian in terms of interaction is then modelled by calculating the interaction angle α_{ia} as drawn from this distribution.

B.3.1 General Approach

Calculating the interaction angle α_{ia} based on the probability distribution $p(a)$ basically means to draw a random number from an arbitrary probability function. The explanation of the general numerical approach to this problem follows the derivation in [167] (Chapter 7.3.1 and 7.3.2, pp. 361 - 363).
The determination of a random variable drawn from an arbitrary distribution corresponds numerically to the transformation of a uniformly distributed into an arbitrarily distributed deviate. Let x be a uniform deviate between 0 and 1 with the corresponding probability distribution

$$p(x)\mathrm{d}x = \begin{cases} \mathrm{d}x & : 0 \leq x < 1 \\ 0 & : \text{else.} \end{cases} \tag{B.60}$$

Further, let $y(x)$ be a given, arbitrary function of x. The transformation law of probabilities then displays how to determine the probability distribution $p(y)$ subject to the distribution $p(x)$:

$$|p(y)\mathrm{d}y| = |p(x)\mathrm{d}x|$$

$$\Rightarrow \quad p(y) = p(x)\left|\frac{\mathrm{d}x}{\mathrm{d}y}\right|. \tag{B.61}$$

In a second step, let $p(y) = f(y)$ be an arbitrary, given probability distribution with $f(y)$ being a positive and normalised function. With the aid of this and Eq. (B.60), the expression (B.61) then reduces to

$$f(y) = \frac{\mathrm{d}x}{\mathrm{d}y}. \tag{B.62}$$

Using the antiderivative of $f(y)$, $F(y)$, and its inverse function $F^{-1}(y)$, it follows that

$$x = F(y) \tag{B.63}$$

and respectively

$$y(x) = F^{-1}(x). \tag{B.64}$$

That indicates that the arbitrarily distributed variable $y(x)$ can be determined as a function of x if the function F^{-1} is calculable.

As it can be seen from Fig. B.6, the relations B.63 and B.64 can be interpreted in a geometric way. Knowing that

$$F(y) = \int_0^y f(y')\mathrm{d}y' \tag{B.65}$$

displays the area under the curve of $f(y) = p(y)$ to the left of y, $x = F(y)$ can be understood as the fraction of the entire area under the curve that belongs to values smaller than y. The total integral is, as stated in the assumption above, equal to one. This can be used for the determination of y for a given x: having drawn a uniform variable $x \in [0, 1]$, y can be calculated by finding the value for which the area under the curve corresponds to x.

This geometric approach is used in the model to determine the interaction angle. The probability distribution $p(a)$ is a positive and normalised function and therefore obeys the assumptions made above. In the model process, the normalisation constant c is calculated and a uniform random deviate x generated. Afterwards, the interaction angle α_{ia} is determined as the value of a for which the area under the curve $p(a)$ is equal to x.
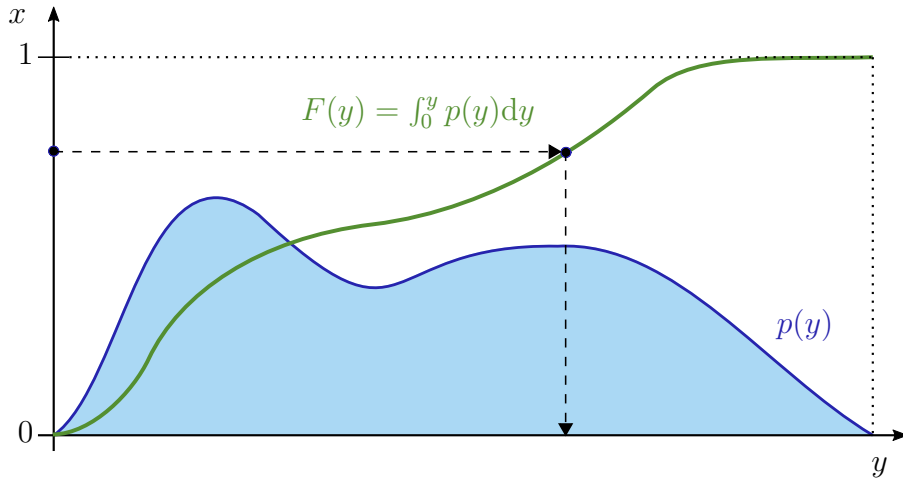
Figure B.6: Given a uniform deviate x, the random variable y with probability distribution $p(y)$ can be calculated as the value of the inverse function F^{-1} at x. It corresponds to the value for which the area under the curve of $p(y)$ is equal to x (after [167], pp. 363).

B.3.2 Calculation of the Normalisation Constant

The calculation of the normalisation constant is basically the determination of the integral

$$c = \int_{-\phi}^{\phi} p(a)\, \mathrm{d}a, \tag{B.66}$$

and relies on some specific properties of the probability function $p(a)$ as it is shown in Fig. B.7. The distribution is only defined for angles within the visual field that are given relatively to the acting pedestrian's direction of motion, $a \in [-\phi, \phi]$. In order to facilitate subsequent calculations, a shall be shifted for now by ϕ so that the domain of definition changes to $a \in [0, 2\phi]$. Following from its definition, $p(a)$ is equal to one for all angular ranges that are not covered by a pedestrian[1]. For each agent that was perceived, the probability reduces to the respective value $p(\alpha_k) = d_k/d_{\mathrm{vf}}$ for the entire angular range that is covered due to the agent's body extension, the interval $[\alpha_k - \Delta\alpha_k, \alpha_k + \Delta\alpha_k]$. It should be noted that the index k

---

[1]Here, $p(a)$ is not yet normalised.
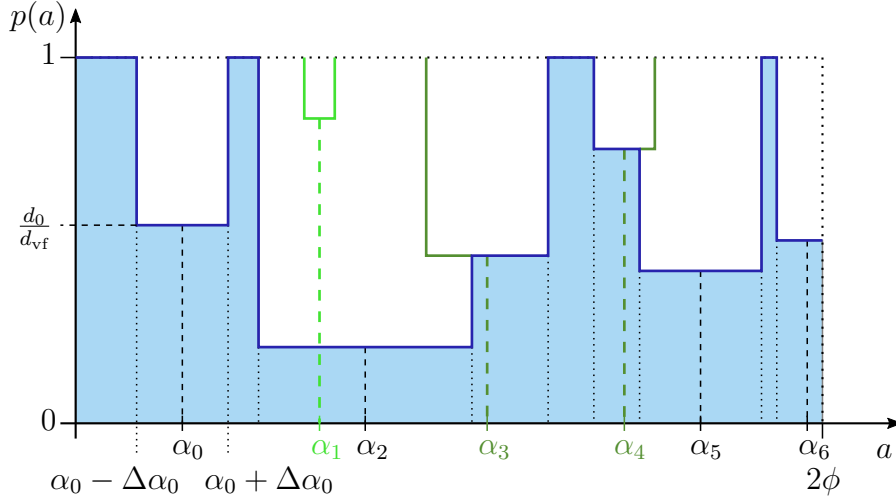
Figure B.7: The function $p(a)$ (dark blue) is a piecewise constant function. It is 1 for free areas and reduced to the corresponding probability in covered ranges (see e.g. α_0). Since the minimum distance is significant, some pedestrians are totally (light green) or partially (dark green) covered by others, and do not (fully) contribute to the function. During the transformation the effective integral (shaded blue area) has to be determined.

at this point does *not* represent the pedestrian's id number. Here, the interaction angles are numbered consecutively when arranged according to size.

For determining the effective (not normalised) probability distribution one has to consider that multiple pedestrians may stand behind one another within the visual field. In this case, the angular ranges covered by the agents overlap. In terms of collision avoidance, the minimum distance for each angle is needed. In other words, pedestrians that are screened from sight by other agents do not contribute to the collision avoidance decision. For the time being, it will be distinguished between total and partial screening. If two pedestrians overlap totally (see Fig. B.7, α_1, bright green), the agent standing farther afield is totally neglected for the probability distribution. For partial coverage ($\alpha_{3,4}$, dark green) the rear pedestrian only contributes for the angular range that does not overlap with the other agent. This effect is intensified by the reciprocal relation between angular extension and

distance-to-collision, $2\Delta\alpha_k = \arctan\left(2r/d_k\right)$ so that nearer pedestrians cover a larger angular range of the visual field.

Taking into account partial or total overlaps of some interaction angles, the probability function $p(a)$ is constructed. For the determination of the normalisation constant, the integral of $p(a)$ over the entire visual field has to be calculated. As it can be seen from Fig. B.7, the integral (shaded blue area) can be regarded as composited by several rectangles or boxes. Each angle contributes a rectangle with a lowered height corresponding to the probability, areas that are not covered are represented by rectangles of height 1. Coverage of multiple pedestrians leads to overlapping of different boxes that follow from the respective widths and relative heights. As described above, rectangles with a smaller height always dominate when overlapping. Parts of boxes that are screened do not contribute to the effective integral. This geometric approach can be used for the numerical calculation of the integral by consecutively adding up the surface areas of all contributing rectangles. Let $\{a_0, \ldots, \alpha_k, \ldots, \alpha_K\}$ be the set of all $K+1$ interaction angles with $\alpha_0 \leq \alpha_1 \leq \ldots \alpha_{K-1} \leq \alpha_K$. The range of extension assigned to each angle α_k is given by $2\Delta\alpha_k = 2\arctan\left(2r/d_k\right)$ and the respective probability by $p_k = d_k/d_{\mathrm{vf}}$. The lower and upper border (in a) of the rectangle k around the interaction angle α_k are, regardless of any overlaps, then given by

$$l_k = \max\left(\alpha_k - \Delta\alpha_k, 0\right), \tag{B.67}$$

$$u_k = \min\left(\alpha_k + \Delta\alpha_k, 2\phi\right), \tag{B.68}$$

respectively, whereby the angles remain restricted to the visual field, $a \in [0, 2\phi]$. In general, the box k can overlap with rectangles belonging to smaller angles α_j, $j < k$, or larger ones with $j > k$. Let

$$l_{\mathrm{min}}^{\mathrm{all}} = \min_{j > k}\left\{l_j | u_j > u_k\right\} \tag{B.69}$$

be the minimum lower border of all boxes j on the right from box k $(j > k)$ whose upper border u_j is larger than the upper border of box k, u_k. If $u_j < u_k$,

while keeping in mind that $\alpha_j > \alpha_k$, the width of box j must be so small that it is fully covered by the rectangle k (see e.g. Fig. B.7, α_1, bright green). In this case it does not influence the contribution of the rectangle k and can be neglected. Correspondingly, let

$$u_{\max}^{\text{all}} = \max_{j<k} \left\{ u_j | l_j < l_k \right\} \tag{B.70}$$

be the maximum upper border of all rectangles on the left of box k. The rectangle k is not overlapped if

$$u_{\max}^{\text{all}} < l_k \quad \wedge \quad l_{\min}^{\text{all}} > u_k, \tag{B.71}$$

that means if neither boxes from 'below' / 'left' ($j < k$) nor from 'above' / 'right' ($j > k$) intersect with the rectangle representing α_k. In contrast, it is completely screened if

$$u_{\max}^{\text{all}} > u_k \quad \vee \quad l_{\min}^{\text{all}} < l_k, \tag{B.72}$$

i.e. if there is at least one rectangle for $j < k$ whose upper border u_j exceeds the upper border of k, u_k, or, for $j > k$, at least one box whose lower border l_j is smaller than the lower border l_k. For e.g. $u_{\max}^{\text{all}}$ only those rectangles are considered whose lower border lies outside from box k. So, if $u_{\max}^{\text{all}} > u_k$, the corresponding rectangle must have a larger extension than the box k. Because of the reciprocal relation between the extension $2\Delta\alpha_j$ and p_j it must have a smaller probability and is therefore dominant towards the rectangle k and screens it completely. The analogous consideration holds for $j > k$.

Two rectangles k and $j < k$ overlap partially, if $l_k < u_j < u_k$. Whether the box j influences the contributing surface area of k depends on the corresponding probabilities p_j and p_k. Let

$$u_{\max}^j = \max_{j<k} \left\{ u_j | l_j < l_k, p_j \le p_k \right\} \tag{B.73}$$

be the maximum upper border of all boxes $j < k$ whose lower border lies outside the box k and whose probability p_j is equal to or less p_k. Partial overlapping of the rectangle k by a box corresponding to a smaller angle α_j that influences the

effective area of box k is then given if

$$l_k < u_{\max}^j < u_k. \tag{B.74}$$

Analogously, using the minimum lower border of all rectangles $j > k$ with the upper border outside the box and a lower probability,

$$l_{\min}^j = \min_{j>k} \{l_j | u_j > u_k, p_j < p_k\}, \tag{B.75}$$

partial screening of the box k by a larger angle is given if

$$l_k < l_{\min}^j < u_k. \tag{B.76}$$

Of course a box can be screened from both sides. In case that

$$l_{\min}^j \leq u_{\max}^j \tag{B.77}$$

holds, each overlapping again intersects, and as a result the rectangle of k is totally covered.

Based on this, the integral of $p(a)$ can be determined by consecutively adding up the area of the box of each interaction angle. The overall integral I is composed of the contributions of every angle k, Δi_k, plus contributions from the 'left' and 'right' end', for $a < l_0$ and $a > u_K$,

$$I = \Delta i_{\text{left}} + \sum_{k=0}^{K} (\Delta i_k) + \Delta i_{\text{right}}. \tag{B.78}$$

Rectangles of height 1, representing a free angular range, are co-considered with the rectangle for the next smallest angle, that means that is directly attached on the left of the considered box. Therefore, they are not explicitly displayed in Eq. (B.78). For the first angle α_0 screening 'from the left' is not possible. Fig. B.8 shows the four remaining cases of screening for α_0: in case of a total overlap (Fig. B.8(a)), the

(a) First angle, total overlap   (b) First angle, partial overlap   (c) First angle, overlapping

(d) First angle, no overlap   (e) k-th angle, total overlap   (f) k-th angle, partial overlap
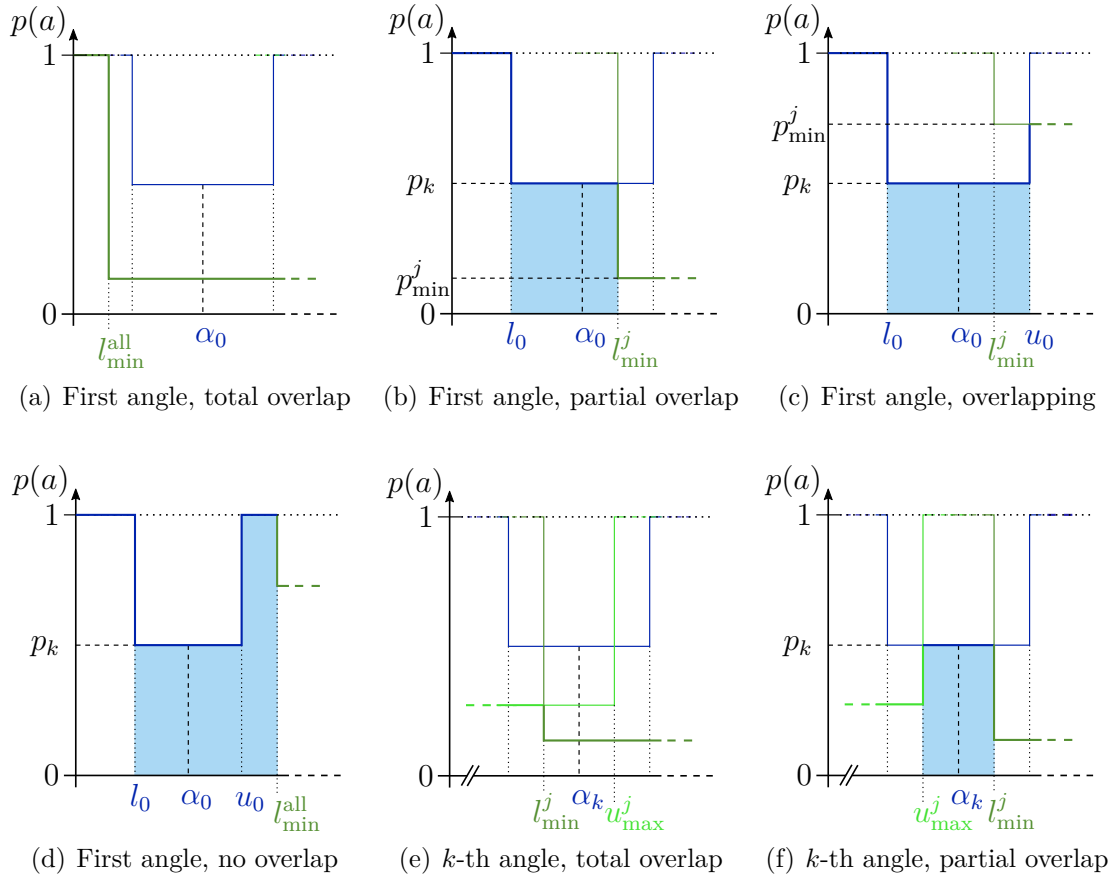
Figure B.8: The area contributing to the integral for each angle (blue) depends on the screening of the respective rectangle. For the first angle, total partial and no screening is shown. The two special cases for the k-th angle due to screening on both sides are displayed in (e) and (f).

angle does not contribute to the integral. Partial overlapping as described above is shown in Fig. B.8(b), where the effective area is represented by the blue-shaded area. The contribution of α_0 in the case of no overlapping (see Fig. B.8(d)) involves the actual rectangle plus the following box of height 1. This additional area is not included if the box 0 partially overlaps with another rectangle which has a larger height, as shown in Fig. B.8(c). In sum, the contribution of the first angle α_0 is

given by

$$
\Delta i_0 = \begin{cases}
0 & : l_{\min}^{\text{all}} \leq l_0 \\
\left(l_{\min}^j - l_0\right) p_0 & : l_0 < l_{\min}^j \leq u_0, \ p_{\min}^j < p_0 \\
(u_0 - l_0) \, p_0 & : l_0 < l_{\min}^j \leq u_0, \ p_{\min}^j \geq p_0 \\
(u_0 - l_0) \, p_0 + \left(l_{\min}^{\text{all}} - u_0\right) & : l_{\min}^{\text{all}} > u_0,
\end{cases}
\tag{B.79}
$$

describing total and partial screening, overlapping without screening of box 0 and no overlap, respectively.

The box of the last angle α_K can only be screened 'from the left'. The different cases are shown in Fig. B.9(a) to B.9(c). Since the borders of the integral are considered separately, there is no contribution of a potential box of height 1 in this case and the area of the box of α_K follows as

$$
\Delta i_K = \begin{cases}
0 & : u_{\max}^{\text{all}} \geq u_K \\
(u_K - u_{\max}^j) \, p_K & : l_K < u_{\max}^j \leq u_K, \ p_{\max}^j < p_K \\
(u_K - l_K) \, p_K & : u_{\max}^{\text{all}} < l_K
\end{cases}
\tag{B.80}
$$

for total, partial and no overlap, respectively.

Considering the angles α_k with $0 < k < K$, the effective area can be displayed by the combination of the results for the first and the last angle plus the two cases of partial overlapping from both sides. As described above, this kind of screening can lead to no contribution from the rectangle k, see Fig. B.8(e), or a reduced area as shown in Fig. B.8(f).

The combined result for α_k is then

$$
\Delta i_k = \begin{cases}
0 & : \quad u_{\max}^{\text{all}} \geq u_k \;\vee\; l_{\min}^{\text{all}} \leq l_k \\[1ex]
(u_k - l_k)\, p_k & : \quad u_{\max}^{\text{all}} < l_k \;\wedge\; l_k < l_{\min}^{\text{all}} \leq u_k \\
& \qquad \wedge\; p_{\min}^{j} \geq p_k \\[1ex]
(u_k - l_k)\, p_k + \left(l_{\min}^{\text{all}} - u_k\right) & : \quad u_{\max}^{\text{all}} < l_k \;\wedge\; l_{\min}^{\text{all}} > u_k \\[1ex]
(u_k - u_{\max}^{j})\, p_k & : \quad l_k < u_{\max}^{j} < u_k \;\wedge\; p_{\max}^{j} < p_k \\
& \qquad \wedge\; l_k < l_{\min}^{\text{all}} \leq u_k \;\wedge\; p_{\min}^{j} \geq p_k \\[1ex]
(u_k - u_{\max}^{j})\, p_k + \left(l_{\min}^{\text{all}} - u_k\right) & : \quad l_k < u_{\max}^{j} < u_k \;\wedge\; p_{\max}^{j} < p_k \\
& \qquad \wedge\; l_{\min}^{\text{all}} > u_k \\[1ex]
\left(l_{\min}^{j} - l_k\right) p_k & : \quad u_{\max}^{\text{all}} < l_k \;\wedge\; l_k < l_{\min}^{j} \leq u_k \\
& \qquad \wedge\; p_{\min}^{j} < p_k \\[1ex]
0 & : \quad l_k < u_{\max}^{j} < u_k \;\wedge\; p_{\max}^{j} < p_k \\
& \qquad \wedge\; l_k < l_{\min}^{j} < u_k \;\wedge\; p_{\min}^{j} < p_k \\
& \qquad \wedge\; u_{\max}^{j} \geq l_{\min}^{j} \\[1ex]
\left(l_{\min}^{j} - u_{\max}^{j}\right) p_k & : \quad l_k < u_{\max}^{j} < u_k \;\wedge\; p_{\max}^{j} < p_k \\
& \qquad \wedge\; l_k < l_{\min}^{j} \leq u_k \;\wedge\; p_{\min}^{j} < p_k \\
& \qquad \wedge\; u_{\max}^{j} < l_{\min}^{j}
\end{cases}
\tag{B.81}
$$

This describes total screening from either left or right, no overlap on the left but partial overlap on the right with a smaller p_k (leading to no contribution of a box of height 1), no overlap right nor left, partial screening left and k overlaps on the right with the smaller probability, partial overlap left and no overlap right, no overlap left but partial overlap right, total overlap due to intersecting screening from both sides and overlaps from both sides without intersection, respectively.

Last, the contribution of the rectangles at the end of the integral have to be considered. For the left marginal box as shown in Fig. B.9(d) and B.9(e) the definition of $l_{\min}^{\text{all}}$ is slightly changed to

$$
l_{\min}^{\text{all}} = \min_{j} l_j
\tag{B.82}
$$

(a) Last angle, total overlap   (b) Last angle, partial overlap   (c) Last angle, no overlap

(d) Left marginal box   (e) No left marginal box   (f) Right marginal box
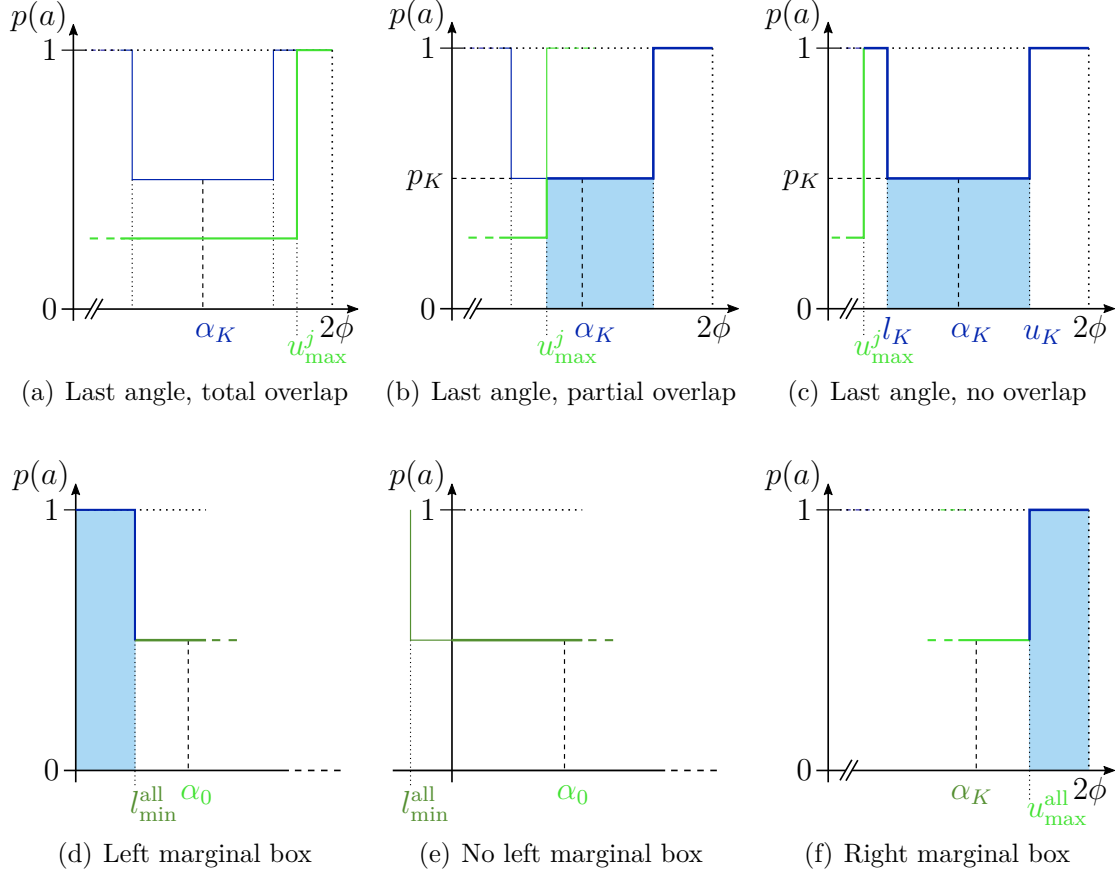
Figure B.9: The last angle can also be totally, partially or not screened depending on the probabilities and box widths. Contributions at the edges of the integral are finite if none of the boxes exceed the bounds of the integral.

describing just the minimal lower border of all rectangles. There is a finite contribution by the left margin to the integral if this minimum is not below the lower bound of integration:

$$\Delta i_{\text{left}} = \begin{cases} l_{\min}^{\text{all}} & : l_{\min}^{\text{all}} > 0 \\ 0 & : l_{\min}^{\text{all}} \leq 0. \end{cases} \tag{B.83}$$

In particular, there is no left margin box if at least one of the interaction angles α_k is less than zero.

Analogously, for a potential margin box it holds that

$$u_{\text{max}}^{\text{all}} = \max_j u_j. \tag{B.84}$$

If this maximum of all upper borders exceeds the upper bound of integral 2ϕ, there is no finite contribution by the right margin to the integral,

$$\Delta i_{\text{right}} = \begin{cases} 2\phi - u_{\text{max}}^{\text{all}} & : u_{\text{max}}^{\text{all}} < 2\phi \\ 0 & : u_{\text{max}}^{\text{all}} \geq 2\phi. \end{cases} \tag{B.85}$$

It should be noted that, if the box of the last angle α_K is totally screened by another rectangle, the right margin box is already included in the contribution of the screening rectangle. Moreover, for $K = 1$ the entire integral is described by the contribution of the left margin and the first angle. For $K = 2$ it is sufficient to consider both margins, and the first and the last angle.

B.3.3 Calculation of the Interaction Angle

As previously described in Sec. B.3.1, the determination of the new interaction angle requires the calculation of the value of a, referred to as $a^\star$, for which the area under the curve $p(a)$ to the left of $a^\star$ corresponds to a given, uniform random deviate x, providing that $p(a)$ is normalised. This can be expressed as

$$x = \frac{1}{c} \int_0^{a^\star} p(a)\mathrm{d}a \tag{B.86}$$

with the normalisation constant c as defined in Eq. (B.66) and derived in Sec. B.3.2. Using that c corresponds to the total integral I, Eq. (B.86) can be written as

$$I' \equiv cx = \int_0^{a^\star} p(a)\mathrm{d}a \tag{B.87}$$

and one has to derive the value $a^\star$ for that the area under the curve $p(a)$ is equal to the reduced integral I'. Following the integration method as described in Sec. B.3.2, it is possible to sequentially calculate the integral until $a^\star$ is found. In doing so, it is crucial to start with the contribution of the left margin box and to consider each angle according to size. Every contribution Δi is individually added up to the fraction ΔI of the entire integral that has been determined so far. If the sum of both exceeds the given value of the integral, $\Delta I + \Delta i \leq I'$, $a^\star$ must lie within the rectangle described by Δi. Then, using a simple conversion, the final value for $a^\star$ can be calculated.

Fig. B.10 exemplarily shows some of the possible values for $a^\star$ within the different rectangles. The integral that was already determined is shown by the area shaded in light blue, the mid-blue area displays the contribution that is considered in this particular iteration.

If the area of the left marginal box already exceeds the wanted value of the integral (see Fig. B.10(a)),

$$\Delta i_{\text{left}} \geq I', \tag{B.88}$$

the new interaction angle is easily found:

$$I' = (a^\star - 0) \cdot 1 = a^\star. \tag{B.89}$$

The first angle only can be screened from the right, and the partial overlap does not influence the determination of the interaction angle. However, the contribution of the actual rectangle 0 and, if existing, a following box of height 1 must be considered separately. Fig. B.10(b) and B.10(c) show the two different cases.

First, $a^\star$ lies within the rectangle 0 if

$$\Delta I + (u_0 - l_0)p_o \geq I' \quad \vee \quad \Delta I + (l_{\text{min}}^j - l_0)p_o \geq I' \tag{B.90}$$
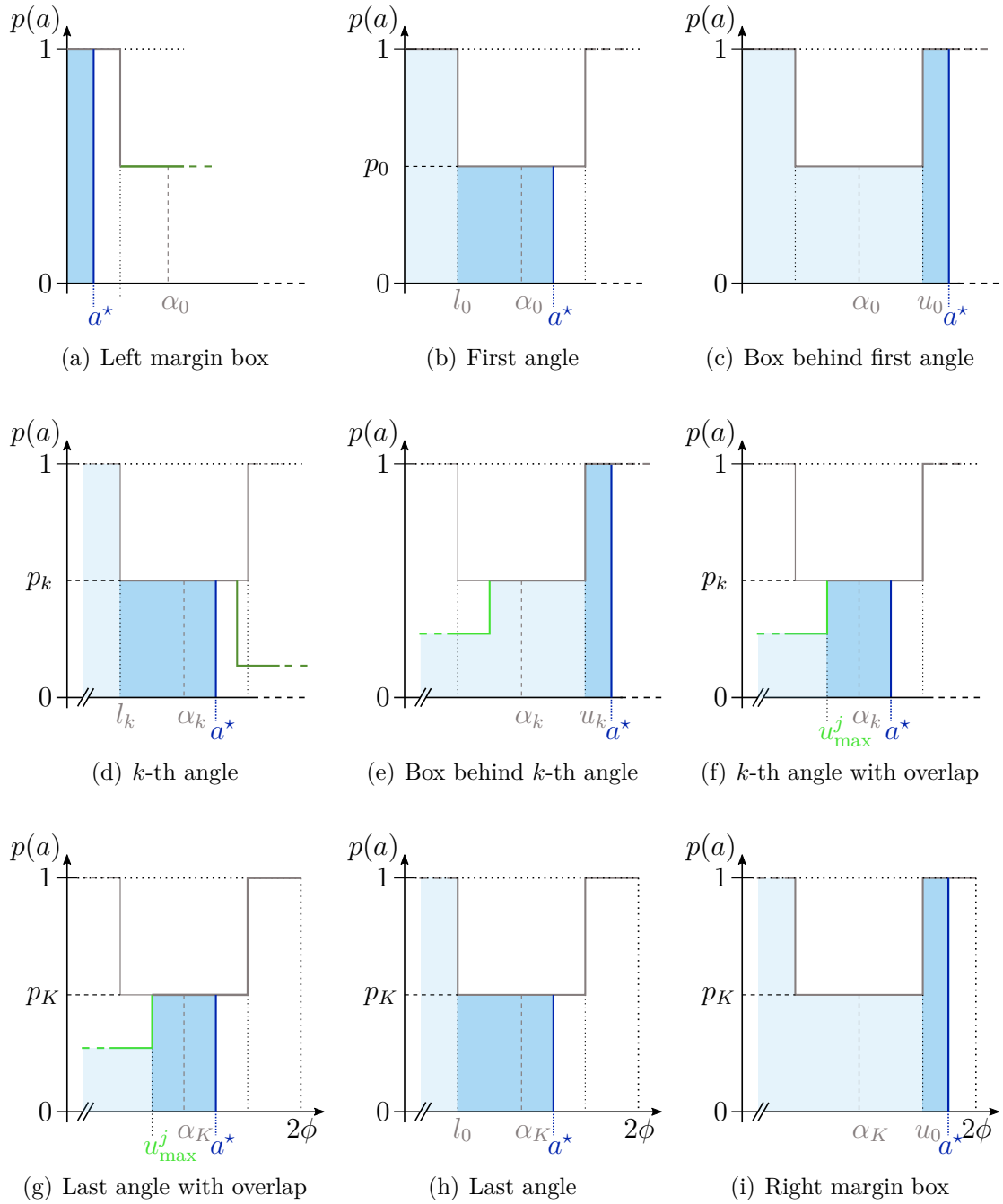
Figure B.10: For the determination of the interaction angle $a^\star$ the sum of the contribution of the considered box (mid-blue) and the previously calculated area (light blue) must correspond to the reduced integral $I' = xI$.

for either no or partial overlap. Then it follows that

$$I' = \Delta I + (a^\star - l_0)\, p_0$$

$$\Leftrightarrow \quad a^\star = \frac{1}{p_0}\left(I' - \Delta I\right) + l_0 \tag{B.91}$$

Second, if $a^\star$ is within the following box of height 1,

$$\Delta I + \left(l_{\min}^{\text{all}} - u_o\right) \geq I', \tag{B.92}$$

the derivation changes to

$$I' = \Delta I + (a^\star - u_0)$$

$$\Leftrightarrow \quad a^\star = I' - \Delta I + u_0. \tag{B.93}$$

Here, ΔI already includes the contribution of box 0. The further derivations work analogously. For the k-th angle, there are three different cases since overlapping from the right can be neglected: the interaction angle lies within box k if

$$\Delta I + (u_k - l_k)\, p_k \geq I' \quad \vee \quad \Delta I + \left(l_{\min}^{j} - l_k\right) p_k \geq I', \tag{B.94}$$

in the following box with height 1 if

$$\Delta I + \left(l_{\min}^{\text{all}} - u_k\right) \geq I', \tag{B.95}$$

or in the box k under consideration of its partial screening if

$$\Delta I + \left(u_k - u_{\max}^{j}\right) p_k \geq I' \quad \vee \quad \Delta I + \left(l_{\min}^{j} - u_{\max}^{j}\right) p_k \geq I'. \tag{B.96}$$

Then the new interaction angle is

$$
a^\star = \begin{cases}
\frac{1}{p_k}\left(I' - \Delta I\right) + l_k & : a^\star \text{ in box } k \\
I' - \Delta I + u_k & : a^\star \text{ in box } k \text{ with height } 1 \\
\frac{1}{p_k}\left(I' - \Delta I\right) + u^j_{\max} & : a^\star \text{ in box } k \text{ with overlap}
\end{cases}
\tag{B.97}
$$

For the last angle α_K the condition for $a^\star$ being in the box K is given by

$$
a^\star \text{ in box if } \begin{cases}
\Delta I + \left(u_K - u^j_{\max}\right) p_K \geq I' & : \text{ overlap} \\
\Delta I + \left(u_K - l_K\right) p_K \geq I' & : \text{ no overlap,}
\end{cases}
\tag{B.98}
$$

see Fig. B.10(g) and B.10(h). The corresponding interaction angle follows as

$$
a^\star = \begin{cases}
\frac{1}{p_K}\left(I' - \Delta I\right) + u^j_{\max} & : \text{ overlap} \\
\frac{1}{p_K}\left(I' - \Delta I\right) + l_K & : \text{ no overlap.}
\end{cases}
\tag{B.99}
$$

For the right margin box, if existing, the consideration is as easy as for the left margin and the interaction angle is simply given by

$$
a^\star = I' - \Delta I + u^{\text{all}}_{\max}.
\tag{B.100}
$$

The final angle $a^\star$ is limited to the bounds of the integration and therefore lies within the visual field. However, all angles α_k were shifted by ϕ at the beginning, so the interaction angles must therefore be corrected by $-\phi$ so that $a^\star \in [-\phi, \phi]$.

APPENDIX C

Determination of Density and Velocity

In pedestrian dynamics, density, velocity and flow are the main observables. Their values, development in time and relation act as the basis for the description and understanding of pedestrian walking behaviours. However, the definition or measurement method of these quantities severely influence the outcome (see e.g. [27, 168]). This should be kept in mind when investigating pedestrian dynamics quantitatively.

In Sec. 4.2, the fundamental diagram or velocity-density relation of pedestrian single-file motion is determined for simulations and experiments. In doing so, two different approaches are used: the global fundamental diagram describes the dynamics of the entire system by using averaged quantities. The local diagram considers individual motion and local quantities. Hereby, several density and velocity concepts are used that are explained in greater detail in the following.

C.1 Global Fundamental Diagram

In the simulations, the global definitions of density and velocity are chosen in an intuitive way. The global density is defined as the number of participants N divided by the corridor length L,

$$\rho_g^s = \frac{N}{L}, \tag{C.1}$$

whereas the global velocity is given as the speed parallel to the direction of the corridor (in this case this is given by the x-component of the pedestrian's speed) averaged over time T, the number of runs R and the number of people N. This results in

$$v_g^s = \frac{1}{R} \sum_{\text{run}=1}^{R} \frac{1}{T-T'} \sum_{t=T'}^{T} \frac{1}{N} \sum_{i=1}^{N} s_i^x(t)$$
$$= \frac{1}{R(T-T')N} \sum_{\text{runs},t,i} s_i^x(t), \tag{C.2}$$

where T is the total simulation time, and T' the time at which the measurement starts. Since the system has to be in a stationary state in order to obtain reliable results, the measurement of the averaged velocity should not start until T'. The choice of T' depends on the system size.

For the experimental data these definitions have to be slightly adapted. In both laboratory experiments, the data acquisition is not done within the entire system but restricted to a certain measurement area. Because of that, the determination of the global density as described above becomes problematic. Especially for a small total number of pedestrians, the global density displays large fluctuations if an agent is entering or exiting the measurement region [46]. Therefore, a reviewed concept of the global density is used, the Θ-density. This density was first introduced by Seyfried et al. [46] and used and extended in [45, 95, 120]. In the following, the definition of the Θ-density as used in the work of Eilhardt [120] is applied.

The density Θ_i of a pedestrian i is defined as the fraction of the distance between the agent i and its predecessor $i+1$ that lies within the measurement area. It is

therefore comparable to the fraction of the Voronoi cell of pedestrian i with the measurement region[1]. Let $x_{i,i+1} = x_{i+1} - x_i$ be the distance between pedestrians i and $i+1$ (along the x direction) and $L_{i,i+1}$ the space between i and $i+1$ within the measurement area, then the Θ-density is given by

$$\Theta_i = \frac{L_{i,i+1}}{x_{i,i+1}} \tag{C.3}$$

Therewith, a 'momentary density' [46] can be defined as

$$\rho(t) = \frac{\sum_{i=1}^{N} \Theta_i(t)}{L_m} \tag{C.4}$$

which gives the current global density within the measurement region of length L_m. Each pedestrian can then be assigned an individual global density ρ_i by averaging over the time the agent was walking within the measurement area,

$$\rho_i = \frac{1}{t_{\text{out}}^i - t_{\text{in}}^i} \int_{t_{\text{in}}^i}^{t_{\text{out}}^i} \rho(t), \tag{C.5}$$

where t_{in}^i is the time pedestrian i entered the measurement area, and t_{out}^i the time the agent left it.

The corresponding global velocity is given by the average speed of the pedestrian i within the measurement area,

$$v_i = \frac{L_m}{t_{\text{out}}^i - t_{\text{in}}^i}. \tag{C.6}$$

Even for the experimental data, care has to be taken that the system is in an almost stationary state and that additional influences and mechanisms at the start and the end of the experimental runs are mainly excluded. Therefore, for a constant number of pedestrians within the systems, the global density should also be nearly constant during the measurement.

---

[1]For more information on the concept of Voronoi cells and the corresponding density, see C.2.

C.2 Local Fundamental Diagram

A commonly used concept for a local density in pedestrian dynamics is based on Voronoi diagrams [169]. For a set of positions $\{\boldsymbol{p}_1, \ldots, \boldsymbol{p}_n\}$ a Voronoi diagram can be determined. It consists of cells c_i each of which is assigned to one of the positions, or pedestrians, respectively. A Voronoi cell c_i of a pedestrian i contains the set of all points in space that is closer to this agent than to any other. The size of all cells A_i can be used to define a density distribution

$$\rho(\boldsymbol{x}) = \sum_i \rho_i(\boldsymbol{x}) \quad \text{with} \quad \rho_i(\boldsymbol{x}) = \begin{cases} \frac{1}{A_i} & : \boldsymbol{x} \in c_i \\ 0 & : \text{else.} \end{cases} \tag{C.7}$$

Descriptively, that means that the reciprocal of the size of a Voronoi cell c_i, $1/A_i$, gives the local density for a pedestrian i.

Of course, the Voronoi density can be used in one-dimensional systems as well as in two dimensions. For one-dimensional single-file motion (along x) as in Sec. 4.2, the local density of a pedestrian i [45, 95, 120] is given by

$$\rho_i(t) = \frac{2}{d_{i-1,1} + d_{i,i+1}} = \frac{2}{x_{i+1} - x_{i-1}} \tag{C.8}$$

where $d_{i-1,i} = x_i - x_{i-1}$ and $d_{i,i+1} = x_{i+1} - x_i$ is the distance between pedestrian i and the person walking behind, $i-1$, and the distance between i and its predecessor, respectively.

The local (one-dimensional) velocity is defined as the current, individual speed in x-direction

$$v_i(t) = \frac{x_i\left(t + \frac{\Delta t}{2}\right) - x_i\left(t - \frac{\Delta t}{2}\right)}{\Delta t}. \tag{C.9}$$

For the analysis in this work Δt was set to $0.32\,\text{s}$ (corresponds to 8 frames at a frame rate of 25 frames per second) in order to facilitate the comparison to the simulated data.

Evacuation

On the following pages the evacuation time plots investigating the influence of the lower threshold d_S that is used to determine the speed, the restriction of the interaction angle and the introduction of body rotations are shown. For all three adjustments of the model, the evacuation times do not differ significantly, their influence is shown using Voronoi diagrams or screenshots from evacuation runs in Sec. 4.3.
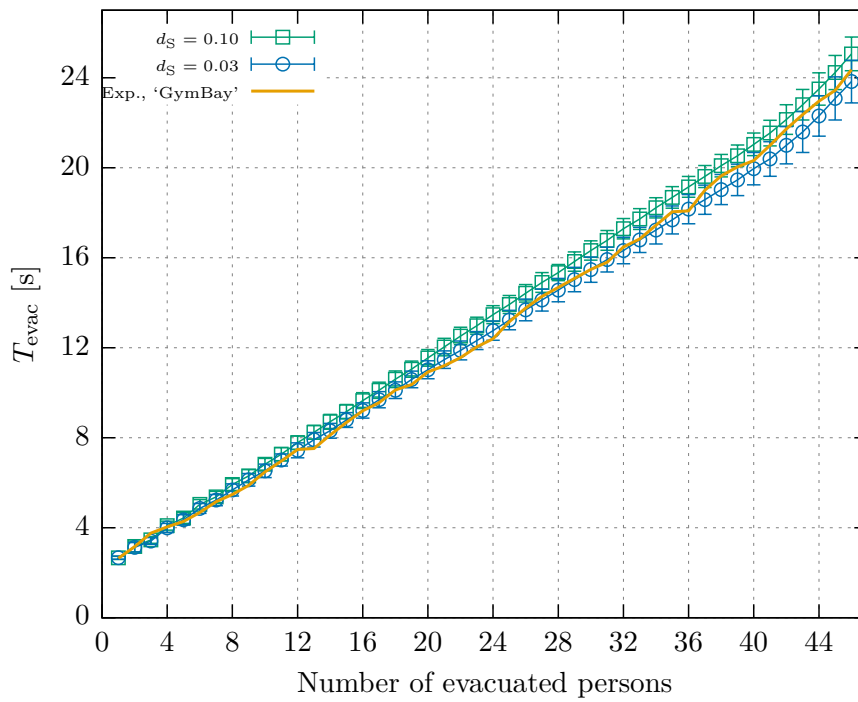
Figure D.1: Decreasing the value for the lower threshold of the velocity-headway relation slightly reduces the evacuation time for larger numbers of evacuated pedestrians.
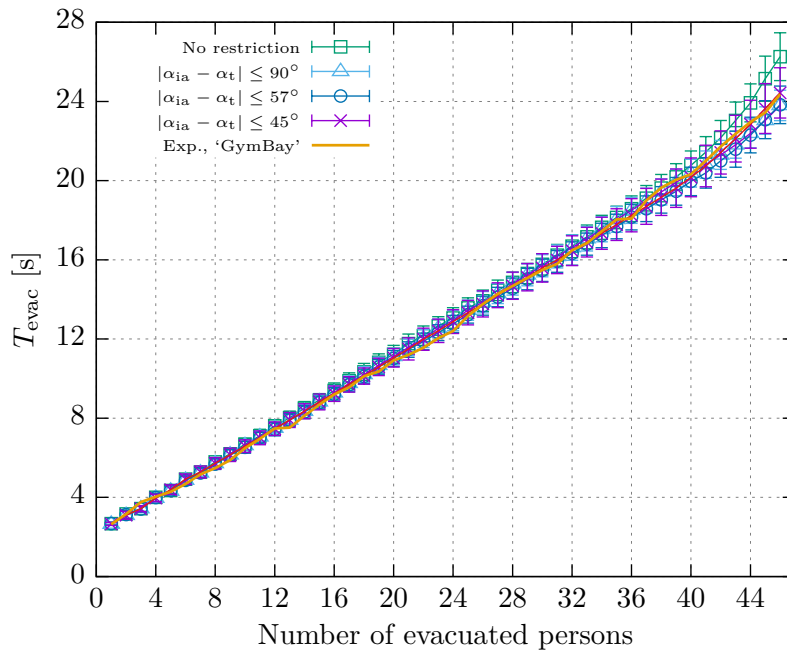
Figure D.2: The choice of the final direction of motion is restricted to directions that do not deviate largely from the target angle in order to prevent the agents from spreading over the room. The evacuation times do not depend on the exact value of the restriction threshold.
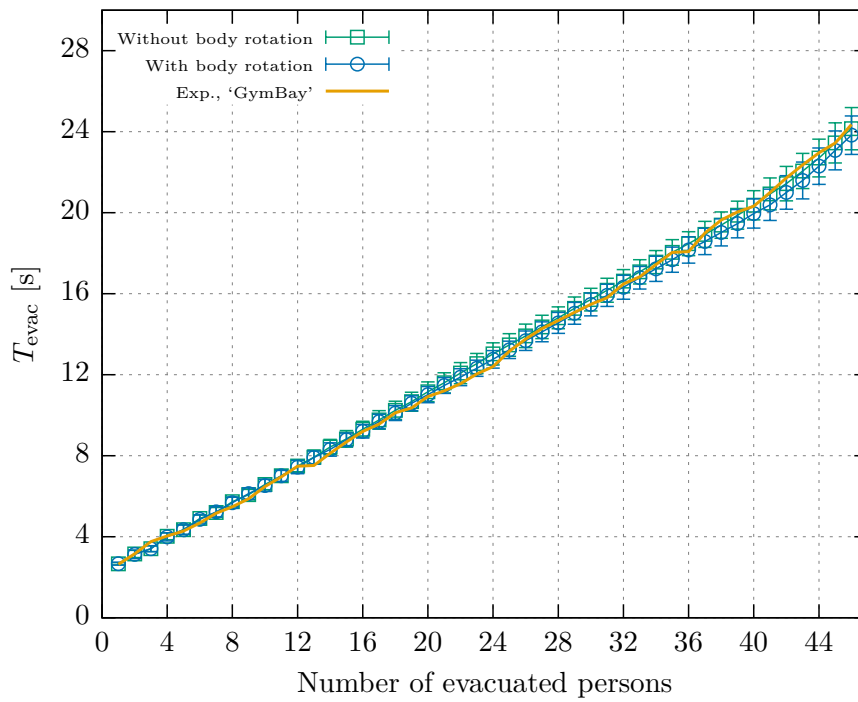
Figure D.3: Body rotations as short-time reductions of a pedestrian's radius are introduced to solve unrealistic conflicts in front of the door more easily and faster. They merely influence the evacuation times.

List of Figures

Danksagung

Erklärung

Ich versichere, dass ich die von mir vorgelegte Dissertation selbständig angefertigt, die benutzten Quellen und Hilfsmittel vollständig angegeben und die Stellen der Arbeit - einschließlich Tabellen, Karten und Abbildungen -, die anderen Werken im Wortlaut oder dem Sinn nach entnommen sind, in jedem Einzelfall als Entlehnung kenntlich gemacht habe; dass diese Dissertation noch keiner anderen Fakultät oder Universität zur Prüfung vorgelegen hat; dass sie - abgesehen von unten angegeben Teilpublikationen - noch nicht veröffentlicht worden ist sowie, dass ich eine solche Veröffentlichung vor Abschluss des Promotionsverfahrens nicht vornehmen werde. Die Bestimmungen der Promotionsordnung sind mir bekannt. Die von mir vorgelegte Dissertation ist von Prof. Dr. Andreas Schadschneider betreut worden.

Teilpublikationen

C. von Krüchten and A. Schadschneider. *Concept of a decision-based pedestrian model.* In: *Proceedings of the 9th International Conference on Pedestrian and Evacuation Dynamics (PED 2018)* (to be published).

Ort, Datum   Unterschrift